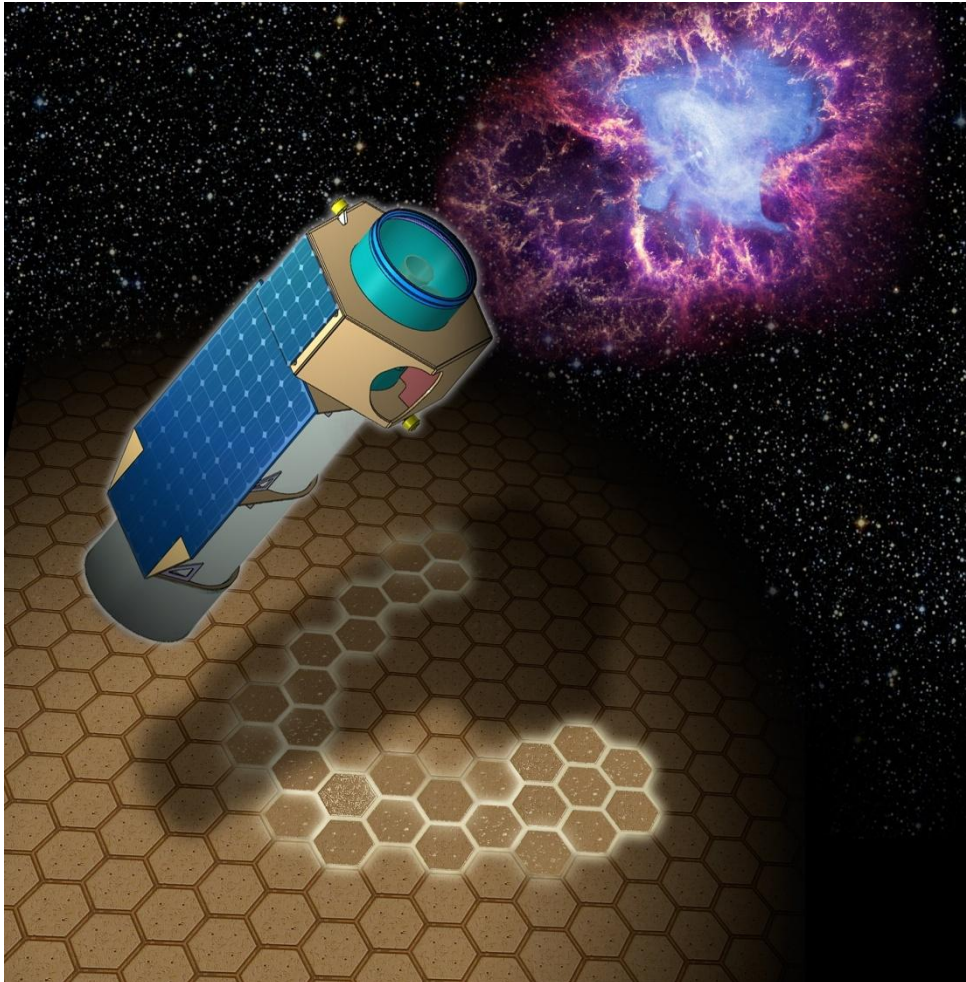


XIPE

The X-ray Imaging Polarimetry Explorer



Lead Proposer: **Paolo Soffitta** (INAF-IAPS, Italy)

Contents

1. Executive summary	3
2. Science case	5
3. Scientific requirements	15
4. Proposed scientific instruments.....	20
5. Proposed mission configuration and profile	35
6. Management scheme.....	45
7. Costing	50
8. Annex	52



XIPE is proposed by:

Soffitta, Paolo	INAF/IAPS	Italy
Bellazzini, Ronaldo	INFN-Pi	Italy
Bozzo, Enrico	Univ. of Geneva/ISDC	Switzerland
Burwitz, Vadim	MPE	Germany
Castro-Tirado, Alberto J.	IAA, CSIC	Spain
Costa, Enrico	INAF/IAPS	Italy
Courvoisier, Thierry J-L.	Univ. of Geneva/ISDC	Switzerland
Feng, Hua	Tsinghua Univ.	China
Gburek, Szymon	Space Research Centre PAS	Poland
Goosmann, René	Observatoire astronomique de Strasbourg	France
Karas, Vladimir	Astronomical Institute of the Academy of Sciences	Czech Republic
Matt, Giorgio	Univ. Roma Tre	Italy
Muleri, Fabio	INAF/IAPS	Italy
Nandra, Kirpal	Max-Planck-Institut für extraterrestrische Physik	Germany
Pearce, Mark	KTH Royal Institute of Technology	Sweden
Poutanen, Juri	Univ. of Turku	Finland
Reglero, Victor	Univ. of Valencia	Spain
Sabau, Maria Dolores	INTA	Spain
Santangelo, Andrea	IAAT Uni Tübingen	Germany
Tagliaferri, Gianpiero	INAF-OAB	Italy
Tenzer, Christoph	IAAT Uni Tübingen	Germany
Weisskopf, Martin C.	NASA-MSFC	USA
Zane, Silvia	MSSL	United Kingdom

Science Team: Agudo, Ivan; Aloisio, Roberto; Amato, Elena; Antonelli, Angelo; Atteia, Jean-Luc; Axelsson, Magnus; Bandiera, Rino; Barcons, Xavier; Bianchi, Stefano; Blasi, Pasquale; Boër, Michel; Bozzo, Enrico; Braga, Joao; Bucciantini, Niccolo'; Burderi, Luciano; Bykov, Andrey; Campana, Sergio; Campana, Riccardo; Cappi, Massimo; Cardillo, Martina; Casella, Piergiorgio; Castro-Tirado, Alberto J.; Chen, Yang; Churazov, Eugene; Connell, Paul; Courvoisier, Thierry; Covino, Stefano; Cui, Wei; Cusumano, Giancarlo; Dadina, Mauro; De Rosa, Alessandra; Del Zanna, Luca; Di Salvo, Tiziana; Donnarumma, Immacolata; Dovciak, Michal; Elsner, Ronald; Eyles, Chris; Fabiani, Sergio; Fan, Yizhong; Feng, Hua; Gburek, Szymon; Gabriele, Goosmann, René W.; Gou, Lijun; Grandi, Paola; Grosso, Nicolas; Hernandez, Margarita; Ho, Luis; Hu, Jian; Huovelin, Juhani; Iaria, Rosario; Jackson, Miranda; Ji, Li; Jorstad, Svetlana; Kaaret, Philip; Karas, Vladimir; Lai, Dong; Larsson, Josefin; Li, Li-Xin; Li, Tipei; Malzac, Julien; Marin, Frédéric; Marscher, Alan; Massaro, Francesco; Matt, Giorgio; Mineo, Teresa; Miniutti, Giovanni; Morlino, Giovanni; Mundell, Carole; Nandra, Kirpal; O'Dell, Steve; Olmi, Barbara; Pacciani, Luigi; Paul, Biswajit; Perna, Rosalba; Petrucci, Pierre-Olivier; Pili, Antonio Graziano; Porquet, Delphine; Poutanen, Juri; Ramsey, Brian; Razzano, Massimiliano; Rea, Nanda; Reglero, Victor; Rosswog, Stephan; Rozanska, Agata; Ryde, Felix; Sabau, Maria Dolores; Salvati, Marco; Silver, Eric; Sunyaev, Rashid; Tamborra, Francesco; Tavecchio, Fabrizio; Taverna, Roberto; Tong, Hao; Turolla, Roberto; Vink, Jacco; Wang, Chen; Weisskopf, Martin C.; Wu, Kinwah; Wu, Xuefeng; Xu, Renxin; Yu, Wenfei; Yuan, Feng; Zane, Silvia; Zdziarski, Andrzej A.; Zhang, Shuangnan; Zhang, Shu.

Instrument Team: Baldini, Luca; Basso, Stefano; Bellazzini, Ronaldo; Bozzo, Enrico; Brez, Alessandro; Burwitz, Vadim; Costa, Enrico; Cui, Wei; de Ruvo, Luca; Del Monte, Ettore; Di Cosimo, Sergio; Di Persio, Giuseppe; Dias, Teresa H. V. T.; Escada, Jose; Evangelista, Yuri; Eyles, Chris; Feng, Hua; Gburek, Szymon; Kiss, Mózsi; Korpela, Seppo; Kowaliski, Miroslaw; Kuss, Michael; Latronico, Luca; Li, Hong; Maia, Jorge; Minuti, Massimo; Muleri, Fabio; Nenonen, Seppo; Omodei, Nicola; Pareschi, Giovanni; Pearce, Mark; Pesce-Rollins, Melissa; Pinchera, Michele; Reglero, Victor; Rubini, Alda; Sabau, Maria Dolores; Santangelo, Andrea; Sgrò, Carmelo; Silva, Rui; Soffitta, Paolo; Spandre, Gloria; Spiga, Daniele; Tagliaferri, Gianpiero; Tenzer, Christoph; Wang, Zhanshan; Winter, Berend; Zane, Silvia.

Participating Institutions: **BR:** INPE; **CH:** ISDC - Univ. of Geneva; **CN:** IHEP, NAOC, NJU, PKU, PMO, Purdue Univ., SHAO, Tongji Univ, Tsinghua Univ., XAO; **CZ:** Astron. Institute of the CAS; **DE:** IAAT Uni Tübingen, MPA, MPE; **ES:** CSIC, CSIC-IAA, CSIC-IEEC, CSIC-INTA, IFCA (CSIC-UC), INTA, Univ. de Valencia; **FI:** Oxford Instruments Analytical Oy, Univ. of Helsinki, Univ. of Turku; **FR:** CNRS/ARTEMIS, IPAG-Univ. of Grenoble/CNRS, IRAP, Obs. Astron. de Strasbourg, **IN:** Raman Research Institute, Bangalore; **IT:** Gran Sasso Science Institute, L'Aquila, INAF/IAPS, INAF/IASF-Bo, INAF/IASF-Pa, INAF-OAA, INAF-OABr, INAF-OAR, INFN-Pi, INFN-Torino, INFN-Ts, Univ of Pisa, Univ. Cagliari, Univ. of Florence, Univ. of Padova, Univ. of Palermo, Univ. Roma Tre, Univ. Torino; **NL:** JIVE, Univ. of Amsterdam; **PL:** Copernicus Astr. Ctr., SRC-PAS; **PT:** LIP/Univ. of Beira-Interior, LIP/Univ. of Coimbra; **RU:** Ioffe Institute, St.Petersburg; **SE:** KTH Royal Institute of Technology. Stockholm Univ.; **UK:** Cardiff Univ., UCL-MSSL, Univ. of Bath; **US:** CFA, Cornell Univ., NASA-MSFC, Stony Brook Univ., Univ. of Iowa, Boston Univ., Institute for Astrophysical Research, Boston Univ., Stanford Univ./KIPAC.

Lead Proposer contact information:

Paolo Soffitta (INAF/IAPS)

paolo.soffitta@iaps.inaf.it

Via del Fosso del Cavaliere, 100, 00133 Roma, Italy

Phone (Office): +39 06 4548 8006

Phone (Mobile): +39 349 38 96 156

The Lead Proposer explicitly states that he will support the study activities of the XIPE mission if selected for the Definition/Study Phase by making available at least 20% of his time throughout the study period.

1. Executive summary

50 years after the first pioneering experiments, X-ray observations are a well-established tool in Astronomy. Enormous progress in instrumentation has allowed for highly performing imaging, spectroscopic and timing experiments. Only one observing technique is still basically missing – polarimetry. Since the infancy of X-ray Astronomy, with the discovery that many X-rays sources were characterized by non-thermal emission processes and/or by radiation transferred in highly asymmetric systems, it was immediately clear that polarimetric observations would be key to understand these sources. In fact, polarimetry adds two more observables, in addition to the position, energy and arrival time of every photon: the degree and angle of polarization. The former gives direct insight in to the emission mechanism and the geometry of the source, while the latter may often provide the only way to measure the orientation of the system. In most models these parameters are free variables: measuring them will make the understanding of the physical processes much more robust. Unfortunately, only recently highly efficient polarimeters, coupled with high throughput focusing X-ray mirrors, became available, so X-ray polarimetry is an undeveloped astrophysical tool. Specifically, only two highly significant measurements exist so far, obtained with non imaging, narrow band Bragg polarimeters, dating from the 70s: a spatially-averaged measurement of the Crab Nebula, and a tight upper limit to the accreting neutron star Sco X-1. The X-ray Imaging Polarimetry Explorer (XIPE) will definitely bring X-ray polarimetry to fruition, and open a new observational window.

Although XIPE has been conceived to address specific scientific goals towards the understanding of the physical nature and geometry of various classes of astrophysical sources, it is very likely that most of the breakthroughs that this mission will deliver are simply unpredictable today. Although this is a general feature of many ambitious space projects, this is more so in the case of XIPE as it will be the very first mission to deliver polarimetry in X-rays.

Among the astrophysical processes for which X-ray polarimetric observations are crucial, particle acceleration has a very prominent role. This is particularly evident in the prototypical cosmic accelerator, the Crab pulsar wind nebula. Comparison of X-ray images with those from lower energies shows that the former bring direct evidence of freshly accelerated particles. As mentioned above, the Crab is the only source for which a strong average X-ray polarization (19%) was measured in the early days. But Chandra images show a complex structure and therefore the net polarization measured 40 years ago should be resolved into contributions of single emitting regions that are to be analyzed separately. XIPE, equipped with spatially resolved polarimetric capabilities, will perform a detailed polarimetric map of the Crab nebula. XIPE's imaging capability is also important for shell like supernova remnants, as it can separate the thermalized plasma from the non-thermal (synchrotron) component and thus locate the site of shock acceleration. This will provide unique direct evidence on the place where cosmic rays are accelerated, and determines how ordered the magnetic field is. XIPE will also study the acceleration processes in jets in both galactic and extragalactic relativistic sources: microquasars, blazars and radiogalaxies. Comparison with polarization at lower frequencies will allow us to understand the magnetic field structure in the jet, while in Inverse Compton-dominated blazars it will solve the long-standing problem of the origin of the seed photons.

High levels of polarization are expected in aspherical geometries. Strong magnetic fields in accreting white dwarfs and neutron stars, funneling the matter along the field lines, provide such geometries. Unique information on the geometry and physics of the accreting column and the magnetosphere can be obtained through X-ray polarimetry. This includes QED vacuum polarization effects predicted almost 80 years ago but yet to be detected. Scattering in aspherical geometries also produces high level of polarization. A case of particular interest is that of molecular clouds around the supermassive black hole in the center of our Galaxy. The polarization degree and angle will determine whether X-ray bright clouds shine because they reflect the past activity of the presently quiet black hole at the Galactic center, and therefore provide uncontroverted proof that a few hundred years ago the center of our Galaxy was $\sim 10^5$ times more active than now. The unknown geometry of the X-ray emitting corona, which in turn is related to its origin, in Active Galactic Nuclei (AGN) and Galactic black holes can also be determined by XIPE. In the latter sources, when in soft state, a continuous change with energy of the polarization angle of the disk thermal emission due to General Relativity (GR) effects is expected. The amplitude of the effect depends on the spin of the black hole, which can therefore be measured.

The above mentioned QED and GR effects are not the only examples of the use of X-ray polarimetry to probe fundamental physics. In fact X-ray polarimetry provides a tool to test theories predicting birefringence effects as a function of energy and distance. Such effects are predicted by the Loop Quantum Gravity and can be tested by observing distant polarized sources like blazars. This kind of observations will also enable the search for Axion-like Particles, one of the most elusive, but of the less exotic, candidates to be the dark matter particle.

In the present scenario, given the long record of missions based on X-ray telescopes, a significant step forward in X-ray imaging and/or spectroscopy requires the high costs associated with the needed cutting edge technological improvements and with a very large collecting area. This is the case of the ESA L2 mission Athena. Conversely, in

the unexplored field of X-ray polarimetry a wealth of discoveries would be achieved with a medium size mission, based on very mature technologies. In particular the technology of imaging focal plane polarimeters, with a suitable energy and time resolution, is available so far only in Europe. A set of X-ray telescopes aboard a dedicated mission, with a photoelectric imaging polarimeter in the focal plane, can provide the large amount of photons needed to achieve the sensitivity to linear polarization of a few % on a large sample and variety of sources, including many extragalactic and many faint galactic sources sampling the wealth of physical phenomena explained before, that can only be elucidated through X-ray polarimetry. The photoelectric imaging polarimeter has already achieved a high readiness level since it was deeply studied and experimentally tested for the XEUS/IXO mission. XIPE will also benefit from a phase A study performed in 2008 for the Italian Space Agency. Thanks to the high sensitivity to polarization in the 2-8 keV band and to the good angular resolution it can resolve extended sources and consequently benefit of a tremendous increase in sensitivity due to the reduction of background to negligible levels. As demonstrated by the study for IXO, the high performances of the ASIC VLSI chip, which is the core of the Gas Pixel Detector, are compatible with a relatively simple, low power electronics.

This was the rationale of the X-ray Imaging Polarimetry Explorer (XIPE), proposed to ESA in 2012 as a small mission, that was very well ranked from the point of view of both science and readiness, but was definitely out of the tight boundaries of cost and complexity for a small mission, as defined by ESA.

The resources allocated for the M4 call, even if definitely lower than those usually allocated for an ESA mission of medium size, are very well matched for a mission capable of addressing the many outstanding scientific goals sketched above, in a good number of representative objects, and -equally important- to provide a large discovery space. Within the cost cap, with the suggested use of a VEGA launcher and within the indicated mass and power budget limits, we can fit a new, enhanced version of XIPE with telescopes of low mass, but good optical quality, based on the same technology developed for e-ROSITA. The good angular resolution of less than 30 arcseconds is such that the flux from the weakest sources is, even in the less favorable cases, dominating over the background. A large total collecting area can be achieved with three telescopes of 3.5 m focal length that can be harbored within the fairing of the VEGA launcher, without any deployable device. The relatively wide field of view (15 arcmin \times 15 arcmin) and the photon by photon handling of data defines mild requirements for the attitude control. Also the low consumption of the electronics is compatible with a fixed array of solar panels. Therefore we do not foresee any moving part except three low mass filter wheels that can be based on a design already tested in space and can be operated independently, to prevent any single point failure. Last but not least, the total low mass excludes the need of a governed re-entry and disposal. The calibration of the XIPE imaging polarimetric detectors will be performed at the existing facility at IAPS, Italy. The calibration of the telescopes, both without and with detectors, will be performed at the PANTER facility of MPE, Germany, with minor modifications to add some additional calibration sources of polarized X-rays. A VEGA launch on an equatorial LEO orbit (although different inclinations or launchers are acceptable), an X-band link with the Malindi base (or Kourou) and the support of the International Scientific Data Center, Switzerland, make XIPE a very standard European X-ray mission. Only a fraction of the data will be devoted to a Core Program to make sure that a minimum set of the already identified scientific objectives will be covered. But, in order to fully exploit the enormous discovery space, following the spirit of ESA scientific missions, all the remaining XIPE observing time will be open to the worldwide community through competitive AO.

The maturity of a mission dedicated to X-ray imaging polarimetry descends from an extended theoretical literature and had been also acknowledged by NASA with the approval of the mission GEMS, subsequently stopped because of programmatic difficulties, by the CNSA study of the future XTP mission and by studies on Polaris in Japan. Largely respecting the tight temporal and budgetary limits of the M4 call, XIPE could place the European Community at the forefront position to open this last remaining observational window in high energy astrophysics. We stress the point that none of the objectives of XIPE can be achieved by any existing or approved mission.

2. Science case

Since the early age of X-ray Astronomy, polarimetry has been recognized as an essential tool for a complete understanding of the physics and geometry of celestial sources. Non-thermal processes giving clear polarization signatures play a major role in many classes of X-ray sources. Moreover, the emission and transfer of radiation in the inner regions of compact sources is based on interaction with matter in highly aspherical geometries. Last but not least the radiation, in its path to the observer, may cross regions of extremely high magnetic fields, where birefringence effects may occur, or of extreme gravitational fields where radiation is strongly affected by General Relativity (GR) effects.

Despite its scientific importance, however, X-ray polarimetry remains poorly developed. The effort of detecting polarization from celestial X-ray sources resulted, with the classical techniques, in the unique positive measurement, by the OSO-8 Bragg polarimeter, of the Crab Nebula, whose degree of polarization was found to be $19.2\% \pm 1.0\%$ (Weisskopf et al. 1976, 1978). The same instrument obtained a tight upper limit to the polarization of Sco X-1 (Long et al. 1979), and coarse upper limits in a handful of other X-ray sources (Hughes et al. 1984). Compton gamma-ray polarimetry has resulted in the very debated measurement of some bright gamma-ray bursts (Coburn & Boggs, 2003; Wigger et al. 2005), and in the measurement of polarization of the Crab (100 keV-1 MeV) and Cyg X-1 using instruments not specifically designed and calibrated for polarimetry on board the INTEGRAL satellite (Dean et al. 2008; Forot et al. 2008). Instead, the most convincing measurement of polarization of a GRB comes from a small dedicated instrument (Yonetoku et al. 2011).

More results are expected in the near future by Soft Gamma Detector (SGD), on-board the Japanese Astro-H. The SGD is based on Compton effect, has a field of view of 0.5° defined by a collimator, and is not imaging. While the sensitivity to polarization is anticipated to be higher than INTEGRAL, the SGD will be operative only in Soft γ -Ray range, (60-400 keV) where the flux from the celestial sources is very low, and in fact will be able to observe only a few brightest galactic sources with a sensitivity which, for the Crab Nebula, is equivalent to that of OSO-8 in the X-rays. Only a small subset of the classes of the high energy sources studied with X-ray observations can be studied with a significant benefit and in most cases the physics involved is quite different.

The development of detectors based on the photoelectric effect, which can measure simultaneously the interaction point, the energy, the arrival time of the photon, together with the emission angle of the photoelectron, opens the possibility to perform spectrally and spatially resolved focal plane polarimetry, with a dramatic jump in sensitivity. XIPE will observe in the classic 2-8 keV range hundreds of sources belonging to most of known classes discovered or studied in 50 years of X-ray Astronomy, image them at sub-arcminute level and measure their polarization. For many of these classes, as we will show below, this will represent a break-through in understanding the physics and the geometry of the studied objects. This totally innovative observing technique it will extend, for the first time, to polarimetry the same revolution performed 38 years ago by Einstein Satellite in the domain of imaging X-ray Astronomy.

2.1. Astrophysics

Significant X-ray polarization degrees are expected in most classes of X-ray sources. Polarization is certainly much more important in X-rays than e.g. in the IR and visible bands, where radiation in the Universe is largely dominated by stellar processes (but where polarimetry nevertheless provided fundamental results, e.g. the AGN unification model, Antonucci 1993). In fact, acceleration phenomena often dominate the energy output of X-ray sources, and strong – or even extreme – magnetic fields significantly affect the emission in many white dwarf and neutron star sources. Moreover, inverse Compton scattering in highly aspherical geometries are widely believed to be the main X-ray emission mechanism from black holes accreting systems, both in Galactic binaries and in AGN.

2.1.1. Acceleration phenomena

Imaging X-ray polarimetry is vital to understand the structure and level of order of the magnetic field in Pulsar Wind Nebulae and Supernova Remnants, without which our understanding of the acceleration mechanisms and matter interactions in these sources – the acceleration site of the all-pervading cosmic rays - is necessarily incomplete. In accreting compact objects, like radiogalaxies and microquasars, X-ray polarimetry will establish the role of jets in the X-ray emission, while in inverse Compton-dominated blazars it will conclusively determine the origin of the seed photons, the major missing piece to complete the puzzle of their Spectral Energy Distribution.

Pulsar Wind Nebulae

The Crab Nebula is the only astronomical source so far with a high-confidence polarimetric measurement in X-rays ($P=19.2\pm 1.0\%$, Weisskopf et al. 1978). Magnetic fields in Pulsar Wind Nebulae (PWN) are rather well ordered, so the emission is locally highly polarized in the radio and optical bands (up to 60%, close to the theoretical limit). The pulsar emission itself is also highly polarized in the same bands. Recent INTEGRAL results (Dean et al. 2008;

Region	σ_{degree} (%)	σ_{angle} (deg)	MDP (%)
1	± 0.60	± 0.96	1.90
2	± 0.41	± 0.65	1.30
3	± 0.68	± 1.10	2.17
4	± 0.86	± 1.39	2.76
5	± 0.61	± 0.97	1.93
6	± 0.46	± 0.75	1.48
7	± 0.44	± 0.70	1.40
8	± 0.44	± 0.71	1.41
9	± 0.46	± 0.74	1.47
10	± 0.60	± 0.97	1.92
11	± 0.52	± 0.83	1.65
12	± 0.53	± 0.85	1.69
13	± 0.59	± 0.95	1.89

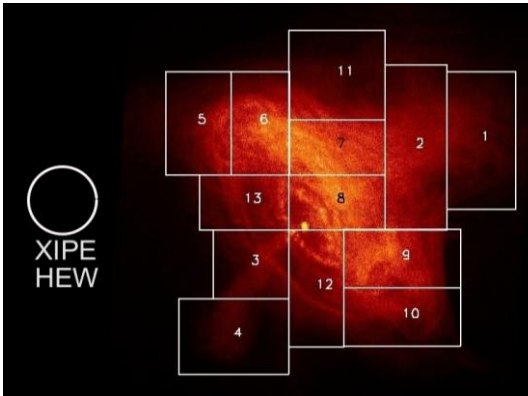


Figure 1 Angular resolution of XIPE, expressed as the Half Energy Width, superimposed on the Crab Nebula image by the Chandra X-ray Observatory (Weisskopf et al. 2000). Assuming conservatively that the polarization degree in each region is that measured by OSO-8 averaging over the entire nebula ($P=19\%$), the error on the measurement carried out with a 20 ks observation of XIPE is reported in the table.

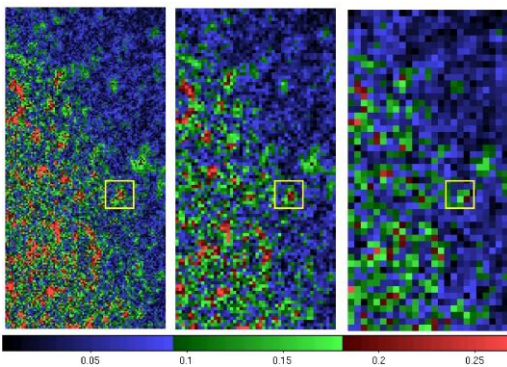


Figure 2 The 5.0 keV synchrotron polarization maps simulated with different pixel sizes for a young SNR. The color bar indicates the degree of polarization. The left one has a pixel size of 9 arcsec, the central of 18 arcsec and the right of 36 arcsec, larger than XIPE. The yellow frame shows a field of view of 2.6×2.6 arcmin². The stochastic magnetic field sample has the r.m.s. value $B = 3 \times 10^{-5}$ G and a flat power-law spectrum of magnetic fluctuations of index $\delta = 1.0$. The simulated SNR shell has a radius of about 0.4 degrees (from Bykov et al. 2009).

Forot et al. 2008) suggest a high level of polarization also in gamma-rays. The X-ray emission of the nebula is highly structured, as shown by Chandra, with a torus plus jet geometry. Since X-ray emitting electrons have a synchrotron lifetime which is far shorter than that of particles which emit at longer wavelengths, X-rays are produced in the regions close to where the electrons are accelerated and therefore provide a much cleaner view of the inner regions than, e.g., optical. Detailed and spatially-resolved measurements by XIPE will allow us to determine the magnetic field orientation in the torus, the jet and at various distances from the pulsar. This is of special interest because, compared to the total synchrotron emission, polarized emission is a more sensitive probe of the plasma dynamics in these nebulae (Bucciantini et al. 2005). It is also the best tool to test the emergent scenarios, based on 3D MHD simulations (Porth et al. 2014), which suggest a paradigm change for PWN dynamics: they invoke the conversion of magnetic energy into particle energy in the radiation region, downstream of the termination shock, rather than upstream. Such scenarios require the growth of turbulence and efficient magnetic field dissipation in a region which can be directly probed by X-ray polarimetric observations. Information on the pulsar wind magnetization and its evolution is essential to clarify the sites and mechanism(s) of particle acceleration in these nebulae, which are among the most efficient accelerators in the Galaxy (Nakamura & Shibata 2007; Volpi et al. 2008). XIPE can measure, in 20 ks, the degree and angle of polarization in many subregions with an accuracy better than 1% in polarization degree and of 1 deg in polarization angle (see Figure 1). Other young and middle-aged PWNe will also be accessible, and similarities and differences with respect to the Crab can be explored. In particular, a subject of current debate is the dichotomy between nebulae characterized by radial (e.g. Vela, see Dodson et al 2003) versus toroidal (e.g. G21.5-0.9, see Zajczyk et al. 2012) field geometry as inferred from radio polarimetry. X-ray polarization, with its enhanced sensitivity to the inner regions can help to determine whether the large scale field geometry is related to the relativistic plasma dynamics or rather induced by the interaction with the surrounding SNR.

Supernovae Remnants

Supernova Remnants (SNRs) are believed to be the acceleration sites of cosmic rays up to very high energies. Diffusive shock acceleration (DSA) is the most popular mechanism of particle acceleration in young supernova remnants. To achieve the observed multi-TeV energies of the accelerated particles in DSA models, the magnetic field must be amplified well above the adiabatic compressed magnitude (e.g. Amato 2014). Moreover, it must be amplified in the shock precursor, most likely by cosmic ray driven instabilities. The amplified magnetic field is likely highly turbulent. Nevertheless, the fluctuating magnetic fields produced by cosmic ray-driven instabilities can be studied with high resolution imaging X-ray polarimetry which may provide unique information or constraints on the magnetic field amplification mechanisms in DSA. In fact, imaging polarimetry is crucial to localize the regions of shock acceleration and to measure the strength and the orientation of the magnetic field at these emission sites (Vink 2012). Probing the regions where thermal or non-thermal plasma is emitting in X-rays is particularly important in small size SNRs like Cas A, Tycho and Kepler (see

e.g. Araya & Cui 2010). The high X-ray polarization degree expected where the synchrotron process is prevalent (e.g. in the filaments usually located on the shell boundaries) should be much reduced where the non-thermal emission is just a fraction of the thermal one. However in the SNR 1006, radio polarization maps (Reynoso et al. 2013) show that where the synchrotron is prevalent (e.g. in the two bright radio and X-ray lobes NE and SW) the measured degree of radio polarization is just 17%, probably due to a partially disordered magnetic field. Instead, in regions where non-thermal emission does not prevail, as in the SE rim, the measured polarization degree is 60% indicating a highly oriented magnetic field. A high degree of polarization is therefore expected also in X-rays whenever the instrument has the capacity of resolving the regions of oriented magnetic fields (see Figure 2); moreover, the XIPE imaging polarimeter will have the capability to reveal polarized emission from the synchrotron stripe structures observed by Chandra in Tycho's SNR (Eriksen et al 2011) for which a high degree of polarization is expected as well (see Figure 3).

Similar considerations can be applied to Cas A for which there is an indication of the presence of a tangential magnetic field at its outer edges (Gotthelf et al. 2001). XIPE can search for a polarized signal in the several regions in which the non-thermal contribution is substantial (about 20% of the total emission in the spectral region between 4 and 6 keV, Bleeker et al. 2001). We show in Figure 4 a simulated view of Cas A: with a 2 Ms observation, we can measure in several spatially resolved regions the degree and the angle of polarization with an error of about 1% and a few degrees, respectively. Based on the Einstein survey (Seward 1990), there are about ten SNRs with a small ($<$ XIPE FoV) size having sufficient flux for X-ray polarimetry while the strategy for a space resolved measurement can be implemented after having analyzed the observation of Cas A. Oppositely large size SNRs ($>$ 30 arcmin) with a clear X-ray synchrotron spectrum in their rims are SN 1006, RX J1713.7–3946, and RX J0852.0–4622, which will be observed in selected regions.

Jets

One of the challenges in high energy astrophysics is to understand how matter is accelerated in jets, and how the mechanism responsible for the emission works both in Galactic and extragalactic sources. At present, about two dozen Galactic X-ray binaries show high velocity, some time superluminal, radio-emitting spots, moving away from a compact core at apparent superluminal speed (Mirabel & Rodriguez 1994). These objects can be extremely bright in X-rays. The high luminosities and high masses indicate that the compact object is a black hole in many of them. Their structure -black hole, accretion disk, and relativistic jet- and their multi-wavelength behavior, including gamma-ray emission (e.g., Abdo et al. 2009, Bulgarelli et al. 2012) and radio and optical polarization (Nagae et al. 2008, and references therein) strongly suggest the sources to be scaled down versions of radio-loud quasars, hence the name

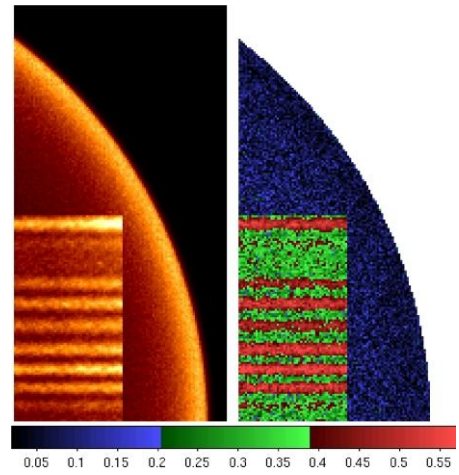


Figure 3 Supernova remnant synchrotron emission images simulated in the NL-DSA model accounting for MFA from a cosmic-ray-current-driven instability. The left panel is the synchrotron X-ray intensity at 5 keV. The degree of polarization of the X-ray emission is shown in the right panel, and the values correspond to the color bar. The relatively high polarization fraction is mainly due to the possible peaked structure of the magnetic fluctuation spectrum and the steepness of the distribution of synchrotron-emitting electrons (from Bykov et al. 2011).

Region	σ_{degree} (%)	σ_{angle} (deg)	MDP (%)
1	± 1.2	± 3.2	3.7
2	± 1.3	± 3.7	4.3
3	± 1.0	± 2.8	3.2
4	± 1.4	± 4.1	4.6
5	± 0.9	± 2.6	3.0
6	± 1.7	± 4.5	5.3
7	± 1.7	± 4.9	5.4

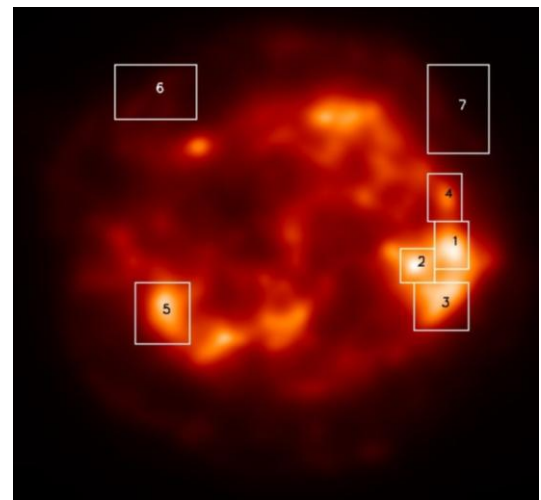


Figure 4 Cas A as it is seen with the XIPE angular resolution. Assuming a polarization degree of 11% for the total (thermal plus non-thermal) emission in the 4-6 keV energy range, the polarization would be measured with the precision reported in the table in each region with an observation of 2 Ms. Regions 4, 6 and 7 are probably dominated by the non-thermal component. The source is largely inside the XIPE field of view (from Fabiani et al. 2014).

microquasars (μ QSO). The study of their time- and energy-dependent X-ray polarization properties (possibly combined with simultaneous radio and optical polarization measurements) can shed light on the still unclear role of jets in the X-ray emission, on their formation and evolution, and their relation to accretion disk emission. These studies may also be applicable to AGN (e.g. Mirabel 2007), but in μ QSO we have the possibility, thanks to the much shorter time scales, to study their behavior over a wide interval of accretion rates. Several different sources, e.g. GRS1915+105, Cyg X-1, Cyg X-3, XTEJ1550-564, etc., have a flux between a hundred mCrab and a few Crab and an MDP (Minimum Detectable Polarization, see 3.1) lower than 1% can be reached in less than 1 day of observation. This will enable time and energy resolved polarization analyses. μ QSO are also good candidates to search for General Relativity effects (see Section 2.2.2).

AGN are customarily divided into two subclasses, radio-loud and radio-quiet AGN, depending on the level of radio (with respect to the optical) emission. In radio-loud AGN, a relativistic, highly collimated jet is present; in the subclass of blazars, it is directed close to the line-of-sight and Special Relativity effects are very important. In particular, due to Doppler boosting, jets dominate the emission at all wavelengths. The spectral energy distribution (SED) of blazars is composed of two peaks, the first one due to synchrotron emission, the second one at higher energies due to inverse Compton Scattering (ICS) of either the synchrotron photons (synchrotron self-Compton, SSC) or external photons, presumably from the accretion disk or from the broad-line region. In some cases, synchrotron emission dominates in X-rays, and strong polarization is therefore expected with a position angle depending on the main emission site (the base of the jet or a downstream shock, Marscher & Gear 1985). In other sources, X-ray emission is instead dominated by ICS, and polarimetry will offer a simple but powerful way to establish if IC is produced by upscattering of either synchrotron or external photons (McNamara et al. 2009). While the polarization angles of synchrotron and SSC emission are expected to be the same, and perpendicular to the magnetic field (Celotti & Matt 1994), those from IC from external photons are related to the jet axis (Begelman & Sikora 1987), and the synchrotron and IC polarization angles need no longer to be the same. In both scenarios (i.e. X-rays from SSC or from IC with seed photons external to the jet), the polarization degree (see Figure 5) is expected to be very high, up to 50% or more unless the electrons responsible for the IC emission are hot (see also Poutanen 1994). Multi-spectral-range polarization monitoring of blazar jets is a powerful tool to locate the emission regions along the spectrum, and therefore to deepen our understanding of their emission mechanisms (e.g. Marscher et al. 2008, Agudo et al. 2011). The polarized millimeter-wave and optical emission often have similar polarization angles and can track each other as they vary, which provides an unambiguous method for locating regions that emit at these wavebands. X-ray polarimetric monitoring of bright blazars with XIPE now brings the opportunity to extend this method up to high energies, which will not only establish the dominant X-ray emission mechanism (SSC or IC, as discussed above), but will also provide unprecedented and robust information about the actual location of the X-ray emission on correlated events along the spectrum. Multi-wavelength polarimetry, with X-rays being at the heart of it, will therefore provide unique information on the emission mechanism, the location of such emission on the jet, and on its structure. XIPE can reach an MDP of a few percent in a few days of observations for some of the brightest blazars. For example, an MDP of $<3\%$ can be reached for Mrk 421 in 10^5 s. In non-blazar radio-loud AGN, the jet is directed away from the line-of-sight, and the jet emission no longer dominates over the disk-related emission. Interestingly, for a few bright sources (most notably the famous bright quasar 3C 273), Grandi and Palumbo (2004; 2007) have suggested, based on spectral deconvolutions, that the two components are of comparable importance in the 2–10 keV band. X-ray polarimetry offers a model-independent way to test this hypothesis: as the two components have different spectra (the jet spectrum being harder), and are polarized with different polarization angles, a rotation of the angle with energy is expected, in accordance with the energy dependent weights of the two components. For a nearby (4.6 Mpc) radio galaxy like Cen A (the X-ray brightest extragalactic source), the imaging capability of XIPE offers the exciting possibility to perform space-resolved polarization, testing the structure of the magnetic field along the jet. An MDP of 5% can be reached in a 200 ks observation.

AGN are customarily divided into two subclasses, radio-loud and radio-quiet AGN, depending on the level of radio (with respect to the optical) emission. In radio-loud AGN, a relativistic, highly collimated jet is present; in the subclass of blazars, it is directed close to the line-of-sight and Special Relativity effects are very important. In particular, due to Doppler boosting, jets dominate the emission at all wavelengths. The spectral energy distribution (SED) of blazars is composed of two peaks, the first one due to synchrotron emission, the second one at higher energies due to inverse Compton Scattering (ICS) of either the synchrotron photons (synchrotron self-Compton, SSC) or external photons, presumably from the accretion disk or from the broad-line region. In some cases, synchrotron emission dominates in X-rays, and strong polarization is therefore expected with a position angle depending on the main emission site (the base of the jet or a downstream shock, Marscher & Gear 1985). In other sources, X-ray emission is instead dominated by ICS, and polarimetry will offer a simple but powerful way to establish if IC is produced by upscattering of either synchrotron or external photons (McNamara et al. 2009). While the polarization angles of synchrotron and SSC emission are expected to be the same, and perpendicular to the magnetic field (Celotti & Matt 1994), those from IC from external photons are related to the jet axis (Begelman & Sikora 1987), and the synchrotron and IC polarization angles need no longer to be the same. In both scenarios (i.e. X-rays from SSC or from IC with seed photons external to the jet), the polarization degree (see Figure 5) is expected to be very high, up to 50% or more unless the electrons responsible for the IC emission are hot (see also Poutanen 1994). Multi-spectral-range polarization monitoring of blazar jets is a powerful tool to locate the emission regions along the spectrum, and therefore to deepen our understanding of their emission mechanisms (e.g. Marscher et al. 2008, Agudo et al. 2011). The polarized millimeter-wave and optical emission often have similar polarization angles and can track each other as they vary, which provides an unambiguous method for locating regions that emit at these wavebands. X-ray polarimetric monitoring of bright blazars with XIPE now brings the opportunity to extend this method up to high energies, which will not only establish the dominant X-ray emission mechanism (SSC or IC, as discussed above), but will also provide unprecedented and robust information about the actual location of the X-ray emission on correlated events along the spectrum. Multi-wavelength polarimetry, with X-rays being at the heart of it, will therefore provide unique information on the emission mechanism, the location of such emission on the jet, and on its structure. XIPE can reach an MDP of a few percent in a few days of observations for some of the brightest blazars. For example, an MDP of $<3\%$ can be reached for Mrk 421 in 10^5 s. In non-blazar radio-loud AGN, the jet is directed away from the line-of-sight, and the jet emission no longer dominates over the disk-related emission. Interestingly, for a few bright sources (most notably the famous bright quasar 3C 273), Grandi and Palumbo (2004; 2007) have suggested, based on spectral deconvolutions, that the two components are of comparable importance in the 2–10 keV band. X-ray polarimetry offers a model-independent way to test this hypothesis: as the two components have different spectra (the jet spectrum being harder), and are polarized with different polarization angles, a rotation of the angle with energy is expected, in accordance with the energy dependent weights of the two components. For a nearby (4.6 Mpc) radio galaxy like Cen A (the X-ray brightest extragalactic source), the imaging capability of XIPE offers the exciting possibility to perform space-resolved polarization, testing the structure of the magnetic field along the jet. An MDP of 5% can be reached in a 200 ks observation.

2.1.2. Emission in strong magnetic fields

Ordered magnetic fields cause radiation to be polarized not only because of synchrotron emission (as in the acceleration phenomena discussed above) but also, if strong enough, because the matter may be channelled along the field lines, resulting in strong asphericities in its distribution. Therefore, X-ray polarimetry can determine the properties of the accretion column in magnetized white dwarfs and neutron stars in binary systems, solving e.g. the

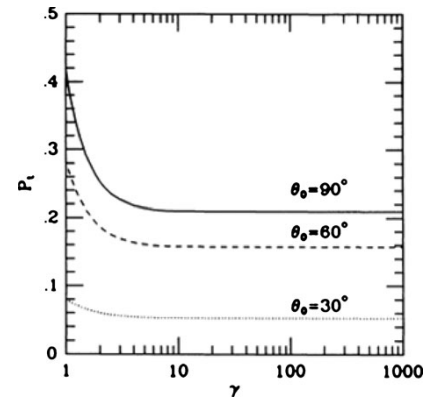


Figure 5 The polarization degree of the SSC emission as a function of the electron Lorentz factor and the angle between the observer and the magnetic field θ_0 (from Celotti & Matt, 1994).

long standing issue of the form (“fan” vs. “pencil”) of the radiation pattern in X-ray pulsars. Moreover, plasma opacity in an intense magnetic field is different in the ordinary and extraordinary modes, leading to strong polarization of the emerging radiation. X-ray polarimetry, therefore, offers a unique opportunity to probe the magnetosphere of magnetars, where the magnetic field reaches extremely high values.

Magnetic cataclysmic variables

Magnetic cataclysmic variables (mCVs), which include polars and intermediate polars, are binaries with a strongly magnetized white dwarf (WD) accreting material from a Roche-lobe filling low-mass star (see Warner 1995 for a comprehensive review). The magnetic field is strong enough (1–100 MGauss) to channel the accretion flow directly to the WD, preventing the formation of an accretion disk in polars and magnetically truncating the disk in intermediate polars. The accreting matter is heated to keV temperatures in a standing shock near the WD surface. The post-shock material is cooled by emitting optical-IR cyclotron radiation and bremsstrahlung in X-rays. The X-rays are in part scattered and reflected by the WD surface, the disk (if present) and the magnetosphere. Scattering opacity in the accretion column need not be negligible for high accretion rates, and the emission may be polarized. The polarization depends on the viewing inclination of the accreting column and it is sensitive to the system configuration. The polarization signal is therefore periodic, with an amplitude reaching 4–8% (Matt 2004; McNamara et al. 2008). Reflection from the WD surface, which is relevant above a few keV, is also expected to be significantly polarized, providing a characteristic energy dependence of the polarization properties (Matt 2004). X-ray polarimetry can therefore help in testing accretion models and determining model parameters. Several bright intermediate polars, and certainly the brightest polar, AM Her, when in high state, can be searched for phase-dependent polarization. In the latter case, an MDP of 2.6% can be reached in 10 phase bins with a 1Ms observation.

Accreting millisecond pulsars

Accretion in close binary systems can spin up the neutron-star rotation, resulting in accretion-powered millisecond pulsars (aMSPs). At present, more than a dozen sources are known, with periods ranging from 1.67 to 5.49 ms. Their spectra consist of a blackbody component, likely originating in a hot spot on the neutron star surface and with typical temperatures of about 1 keV, and a hard power-law component, probably due to Comptonization in a radiative shock surface, with a temperature of 30–60 keV and Thomson optical depths $<1-2$. The observed pulsations indicate that the shock covers only a small part of the neutron-star surface. The scattered radiation should be linearly polarized (see Figure 6), with the polarization degree and angle varying with the phase (Viironen & Poutanen 2004): X-ray polarimetry is essential to test the Comptonization model for the hard component as well as to determine geometrical parameters such as the inclination and the magnetic inclination angles, which are important to constrain the neutron star mass and radius. Millisecond pulsars are usually transient objects. In a 100 ks observation of SAX J1808.4-3658 in outburst, an MDP of 2.1% can be reached in 10 independent phase bins.

Accreting X-ray pulsars

Accreting X-ray pulsars are binary systems in which the compact object is a neutron star with very strong magnetic fields of $10^{12}-10^{13}$ G, as derived from cyclotron lines. In such strong magnetic fields, radiation propagates in two, linearly polarized modes: the ordinary O- and the extraordinary X-mode (parallel and perpendicular to the B-field, respectively). A birefringence effect, due to the different plasma opacity to the ordinary and extraordinary modes, arises, resulting in strong linear polarization of the emerging radiation. Detailed calculations (e.g. Meszaros et al. 1988) show

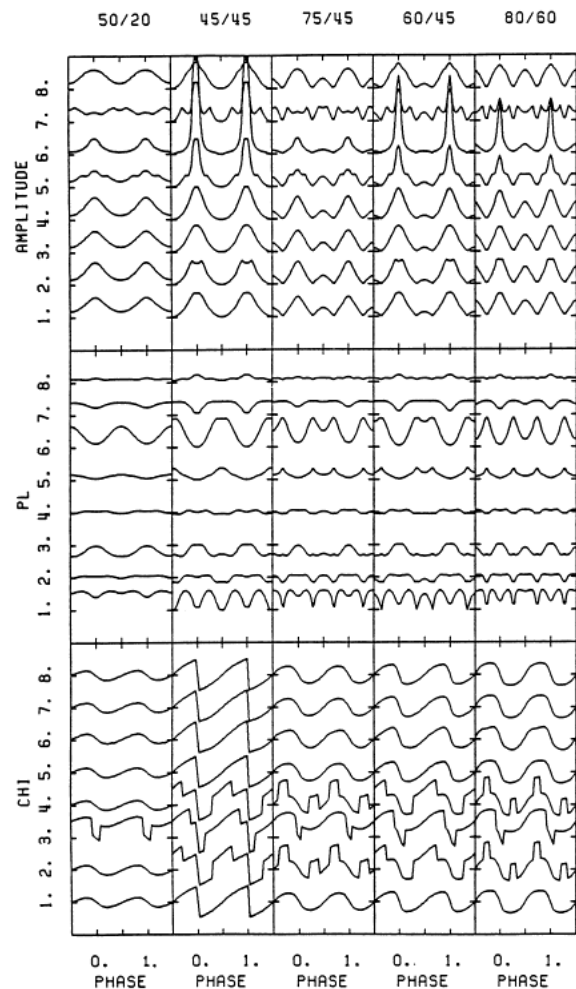


Figure 6 Lightcurves of the flux, polarization degrees and angle in an X-ray pulsar for different sets of the geometrical parameters in the pencil beam model. The energy ranges from 1.6 keV (bottom curve in each panel) to 84.7 keV (top curve) Polarimetry provides two additional observables to constrain the parameters of the model (from Meszaros et al. 1988).

that the linear polarization depends strongly on the geometry of the emission region (accretion column), and varies with energy and pulse phase, reaching very high degrees, up to 70% for favorable orientations at the cyclotron energies. In particular, phase-resolved polarimetry can distinguish between “pencil” and “fan” radiation patterns, a long standing problem still awaiting a firm solution. Because the degree of linear polarization is maximal for emission perpendicular to the magnetic field, the flux and degree of polarization are in-phase for fan beams, but out-of-phase for pencil beams. Both fan and pencil beam components may be present, each component dominating at different energies, resulting in an energy dependence of the polarization angle. The phase swing of polarization angle, instead, is a direct measure of the angle between the rotation and the magnetic dipole axes, usually a free parameter in the models. Many X-ray pulsars are within reach of XIPE: for example, an MDP of 3.0% is achieved in 10 independent phase bins with a 100ks observation of Her X-1.

Magnetars

Soft-Gamma Repeaters (SGRs) and Anomalous X-ray Pulsars (AXPs) are isolated neutron stars which emit strong (10^{38} - 10^{41} erg/s), short (0.1-1 s) bursts of X-/gamma-rays. Their spin periods are in the 2-12 s range and they exhibit relatively high values of the spin-down rates (10^{-13} – 10^{-11} s/s). The inferred values of the magnetic field, 10^{13} - 10^{15} G, are the highest ever measured and provide evidence that these sources host an ultra-magnetized neutron star, a so-called magnetar. This is further supported by their (persistent) luminosity being higher than the rotational energy loss rate, implying that they are powered by their own huge magnetic field. SGRs/AXPs are bright, persistent X-ray sources with luminosity 10^{31} - 10^{36} erg/s (2-10 keV), and a typical thermal plus power-law spectrum. The thermal component is believed to originate from a heated region on the star surface, while the power-law tail results from resonant cyclotron (up-)scattering (RCS) of thermal photons onto magnetospheric electrons/positrons. The different opacity in the two polarization modes implies that the initial polarization state of seed thermal photons may change upon scattering. According to state-of-the-art simulations (Taverna et al. 2014), phase-resolved, polarimetric measurements in bright magnetars (like the AXP 1RXS J1708) are within XIPE capabilities with exposure times of a few hundred ks. They will yield invaluable information on the magnetic field strength and geometry and can, for the first time ever, provide a direct confirmation of QED effects (see Section 2.2.1).

2.1.3. Scattering in aspherical geometries

Scattering is one of the most common way to polarize radiation. X-ray polarimetry is therefore an invaluable tool to study sources in which scattering occurs in aspherical geometries (e.g. accretion disks). For instance, it will determine the geometry (which is related to the origin) of the X-ray emitting, hot corona in X-ray binaries and radio-quiet AGN, and it will proof or reject the hypothesis that the black hole at the center of our own Galaxy is, intermittently, a low luminosity AGN.

X-ray binaries

Even when the magnetic field of the compact object is not strong enough to channel the accreting matter, asphericities are present because the matter usually forms accretion disks. GR effects are expected to be important for the emission originating in the inner regions of the disk, close to the black hole or the neutron star. These effects will be discussed later on. Here we just emphasize that in accretion-disk-fed sources the hard component (which is the dominant one in the 2–10 keV spectrum when the sources are in the so called hard state) is likely due to Comptonization of disk photons in a hot corona, and it is therefore expected to be strongly polarized (e.g. Haardt & Matt 1993; Poutanen & Vilhu 1993). The polarization degree will put constraints on the, so far unknown, geometry of the corona (Schnittman & Krolik 2010, Tamborra et al. in prep.) and on the inclination angle of the disk, a key parameter to robustly determine the mass and spin of the black hole. For the brightest sources, variations of the geometry of the corona with the accretion rate can be searched for by observing the sources in different spectral and flux states, including quiescence. Part of the primary emission is intercepted and reflected by the accretion disk itself, giving rise to the so-called Compton Reflection (CR) component. This component, which becomes relevant above 7 keV, is also highly polarized, the polarization degree depending mainly on the inclination angle of the disk (Matt et al. 1989).

Radio-quiet AGN

It is believed that the innermost regions of radio-quiet AGN are scaled-up versions of those present in galactic black hole systems with the very important difference that here the Comptonization component always dominates, as the disk thermal component is in the UV/Soft X-ray band, due to the $T_{\text{disk}} \sim M_{\text{BH}}^{-1/4}$ relation. For the Comptonization and CR components, the same considerations made in the previous paragraph still hold (but see Section 13 for a test of GR effects based on time/flux variability). An MDP of 3% can be reached with a 100ks observation of the Seyfert galaxy IC4329A. In addition to the accretion disk, other reflecting regions are present in

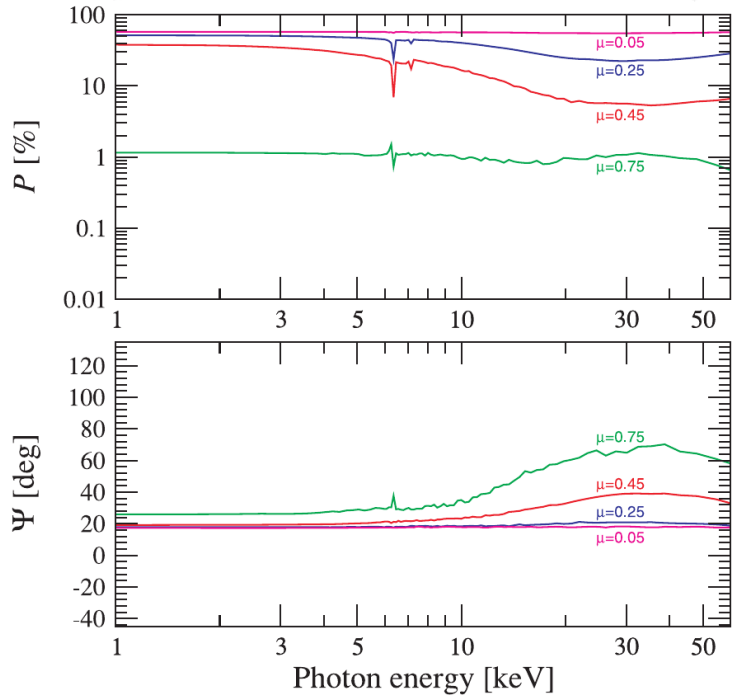
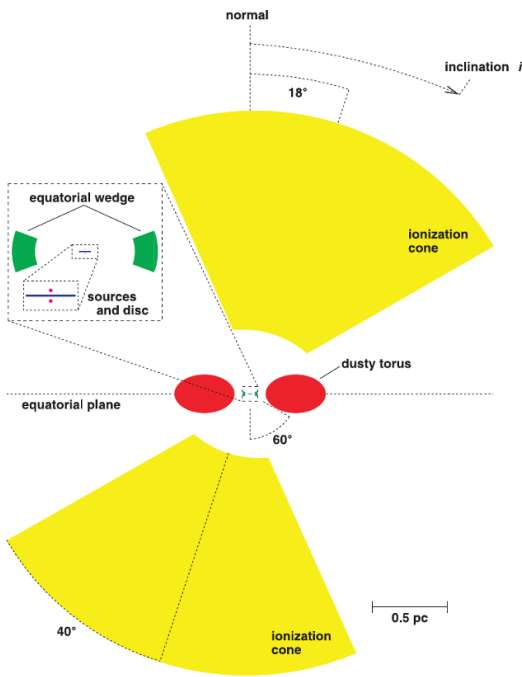


Figure 7 Left: Sketch of the possible geometry of the circumnuclear matter in NGC1068. Note the misalignment of the ionization cone and the torus axis, suggested by IR interferometric observations (Raban et al. 2009). Right: expected polarization degree and angle as a function of energy for different inclination angles of the system ($\mu = \cos(i)$; for NGC1068 μ is likely to be low, Greenhill et al. 1996). From Goosmann & Matt (2011). If the misalignment is real, a non zero value of ψ , the polarization angle measured from the direction perpendicular to the torus axis, should be found.

radio-quiet AGN, first and foremost the so-called dusty torus envisaged in Unification models (Antonucci 1993). Despite the name, the actual geometrical shape of the ‘torus’ is basically unknown, and polarimetric observations can help to solve this issue, as well as to determine its orientation and relation with the optical ionization cones (Goosmann & Matt 2011, see Figure 7). In the case of NGC1068, an MDP of 2% can be reached with a 500ks observation. Investigations of the scattering geometry in AGN will benefit from synergies with polarization studies at longer wavelengths (Marin & Goosmann 2012).

X-ray reflection nebulae

There are a few molecular clouds in the Galactic Center region whose X-ray spectra are well reproduced by a pure Compton Reflection component, indicating that such clouds are reflecting the X-ray radiation produced by an external source (X-ray reflection nebulae, XRN). The most famous example is Sgr B2, but also the X-ray emission from the Sgr C complex was proposed to have the same origin (Murakami et al. 2001). The puzzle here is that there is no X-ray source bright enough in the surroundings. It has therefore been proposed that these clouds reflect past emission by the central black hole source (Sunyaev et al. 1993, Koyama et al. 1996, Ponti et al. 2013), which should therefore have undergone a phase of strong activity about three hundred years ago. If the emission from the nebulae is indeed due to scattering, it should be very highly polarized (Churazov et al. 2002), with a direction of polarization perpendicular to the scattering plane, and therefore to the line connecting the cloud to the illuminating source. The detection of polarized X-ray emission from one or more of these clouds would place a strong limit on the position of the source which illuminated them in the past and, if the polarization plane is indeed perpendicular to the direction towards Sgr A*, it will be proved that not many years ago the Galaxy was a low luminosity AGN. In addition, measurements of the polarization degree will provide unique information on the position of the clouds with respect to Sgr A* along our line of sight. An ambitious campaign (about 3 Ms in total) on the Sgr B and C complexes will be able to prove or reject, once and for all, the fascinating hypothesis that our own Galactic Center is episodically an AGN (see Figure 8).

2.2. Fundamental Physics

High Energy Astrophysics makes natural laboratories of Fundamental Physics accessible, allowing for tests of physical theories which would otherwise be impossible. X-ray polarimetry is a privileged probe to exploit many of them, as explained below. Distinctive signatures on the degree and angle of polarization are expected during photon transfer in strong magnetic or gravitational fields. In particular, it will permit to test a QED effect in extreme magnetic fields which was predicted almost 80 years ago, but is still to be verified; and to measure the black hole

spin in Galactic black hole systems and AGN. Energy dependent rotations of the polarization angle and variations of the polarization degree of the radiation from distant sources may reveal Quantum Gravity effects and allow for the search of axion-like particles.

2.2.1. Matter in Extreme Magnetic Fields: QED effects

As mentioned above, surface emission from neutron stars (NSs) should be highly polarized because the opacity of the atmosphere to photons polarized perpendicular to the magnetic field (X-mode) is smaller than that for parallel polarized radiation (O-mode) (Lodenqual et al. 1974). Although this basic result holds in general, the polarization properties of the NS thermal emission crucially depend on the still poorly known conditions of the outermost stellar layers. For very large magnetic fields, the surface may be in a condensed state, or, if a phase transition does not occur, it could be covered by a gaseous atmosphere (e.g. Medin & Lai, 2006). Regardless of the polarization state of thermal radiation, X-ray polarimetry of NS emission gives the opportunity to observe a genuine quantum-electrodynamics (QED) effect (Heyl & Shaviv 2000), that is the vacuum polarization induced by a strong magnetic field, predicted nearly 80 years ago (Heisenberg & Euler 1936) but still to be verified experimentally. In the presence of ultra-strong magnetic fields (as in magnetars), the components of the vacuum dielectric and magnetic permeability tensor depend on the magnetic field intensity. This effect influences the propagation of the photons: the typical scale length along which the properties of the wave electric field evolve is proportional to B^{-2} (Fernandez & Davis 2011, Taverna et al. 2014). Near the stellar surface, where the magnetic field is stronger, the direction of the wave electric field is strongly coupled to that of the local magnetic field, and the photons' polarization mode does not change (adiabatic propagation). In the external region, however, where the local magnetic field intensity has sufficiently dropped, the local magnetic field direction changes more rapidly than what the photon electric field can do. As a result, the electric field direction freezes and the polarization modes begin to change. Theoretical models (Taverna et al. 2014, and references therein) show that vacuum polarization affects both polarization angle and polarization degree (see Figure 9). X-ray polarimetry can confirm the occurrence of vacuum polarization effects and also provide a proof of the presence of ultra-strong magnetic fields in these sources (currently such a magnetic field was estimated only in SGR 0418+5729, Tiengo et al. 2013).

Should an atmosphere be present, detailed calculations (van Adelsberg & Lai 2006) have shown that a resonance, occurring when the contribution to the dielectric tensor of the plasma and of the vacuum compensate each other, would produce a transition between the two photon modes analogous to the Mikheyev-Smirnov-Wolfenstein mechanism for neutrino oscillation (Lai & Ho 2003). For not-too-strong field regimes ($<7 \times 10^{13}$ G, when the occurrence of an atmosphere is most likely), the resonance lies outside the photospheres of the two photon modes and the total emission is dominated by one mode or the other depending on the energy. The net effect is a rapid 90 degree shift of the angle of polarization which, for typical atmosphere parameters, occurs at a few keV. Instead, for stronger magnetic fields, as expected in magnetars, the polarization angle should not flip between low and high energy photons because the resonance occurs inside the O-mode photosphere.

Phase-resolved polarimetry allows us to probe the geometry of the source, i.e. the angles that the line-of-sight and the magnetic axis make with the spin axis (Fernandez & Davis 2011, Taverna et al. 2014). Furthermore, when modes are coupled again at a distance which is large with respect to the radius of the NS, the local magnetic field is almost parallel and therefore photons coming from different regions of the NS surface add coherently. Since the modes of lower energy radiation couple first, but in the meanwhile the magnetosphere rotates with the NS, an observable prediction of the presence of vacuum birefringence effects is that the angle of polarization at low energy should lag behind higher energy photons (Heyl & Shaviv 2000).

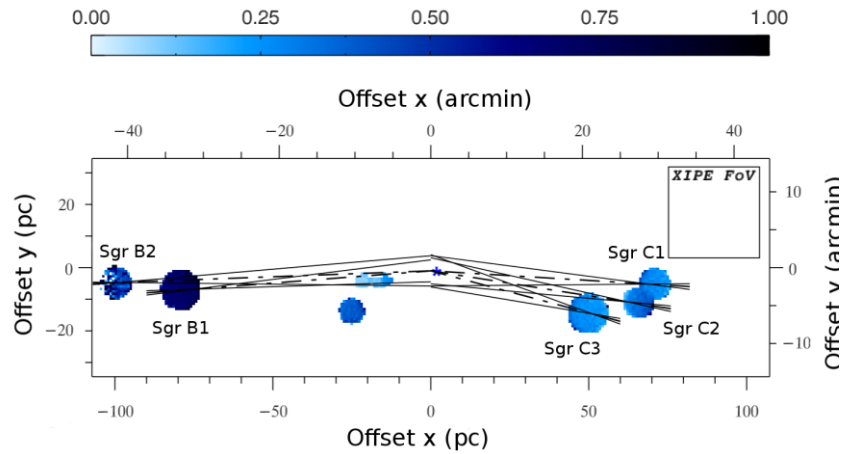


Figure 8 Observation of the molecular clouds in the Galactic center with XIPE. The angle of polarization will be orthogonal to the line, showed in the figure, connecting each molecular cloud to the source which illuminated it in the past. With an observation 1 Ms and 2 Ms long of the Sgr B and Sgr C complexes, respectively, the combined angular constraints from the different clouds will be tight, unambiguously determining if the illuminating source was actually Sgr A*. The fluxes from the XRNe change with time; our estimates are based on recent Suzaku observations (Ryu et al. 2009 and 2013) and take into account the contribution from the diffuse (unpolarized) thermal emission in the Galactic center. The color represents the polarization degree of the emission (from Marin et al., submitted).

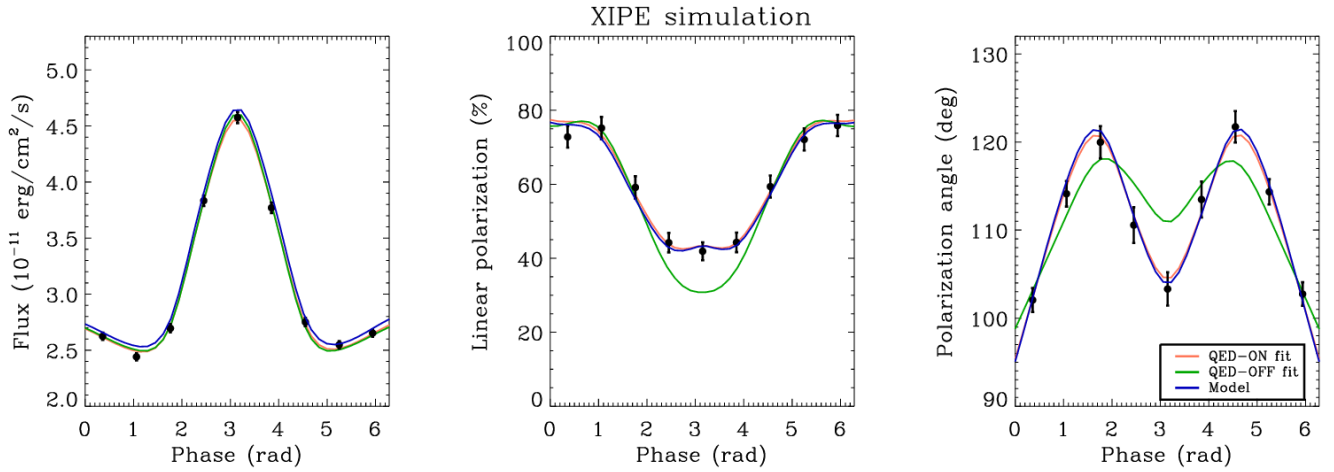


Figure 9 Light curve, degree and angle of polarization expected in case of the ‘twisted magnetosphere’ model with parameters similar to those derived for the AXP 1RXS J170849.0–400910. Points are generated assuming a 250 ks observation of the source and following the blue line, which represents the model including vacuum polarization. Points are fitted with models including (red line) or not (green line) such an effect; the latter is excluded with high confidence (from Taverna et al. 2014).

2.2.2. Matter in Extreme Gravitational Fields: GR effects

Galactic Black Hole systems

When black hole binaries are in high state, the dominant component in the 2-10 keV band is the thermal emission from the accretion disk. The innermost regions of the disk are very close to the black hole, where GR effects are very strong. These effects cause a rotation of the polarization angle of the radiation emitted from the disk, the amount of rotation depending on the azimuthal angle and the radius of the emitting point. Even after averaging over the azimuthal angle, a net rotation remains. The closer to the black hole the emitting point is, the larger the rotation. Because the emission is locally a thermal one, and because the temperature decreases with the disk radius, what is eventually observed is a rotation of the polarization angle with energy (Stark and Connors 1977, Connors et al. 1980, Dovciak et al. 2008, Li et al. 2008, Schnittman and Krolik 2009). The measurement of this effect will be a powerful probe of General Relativity effects in the strong field regime. Moreover, it will provide an independent estimate of the spin of the black hole to be compared with those obtained by other techniques (i.e. continuum fitting and Fe line spectroscopy). Such a comparison on a large sample will hopefully help us to reduce the systematic uncertainties that currently limit BH spin measurements.

The best but not the only source to search for this effect is GRS1915+105 (see Figure 10), a bright microquasar whose 2-8 keV emission is, when in high state, dominated by thermal emission. Moreover, the source is highly inclined (70 degrees, Mirabel & Rodriguez 1994), and therefore the polarization degree is expected to be high. Other less inclined sources may show lower polarization levels, which however could still be easily detected in a relatively short exposure time (a few days). In addition, about 6 transient BH binaries are expected during 3 years of

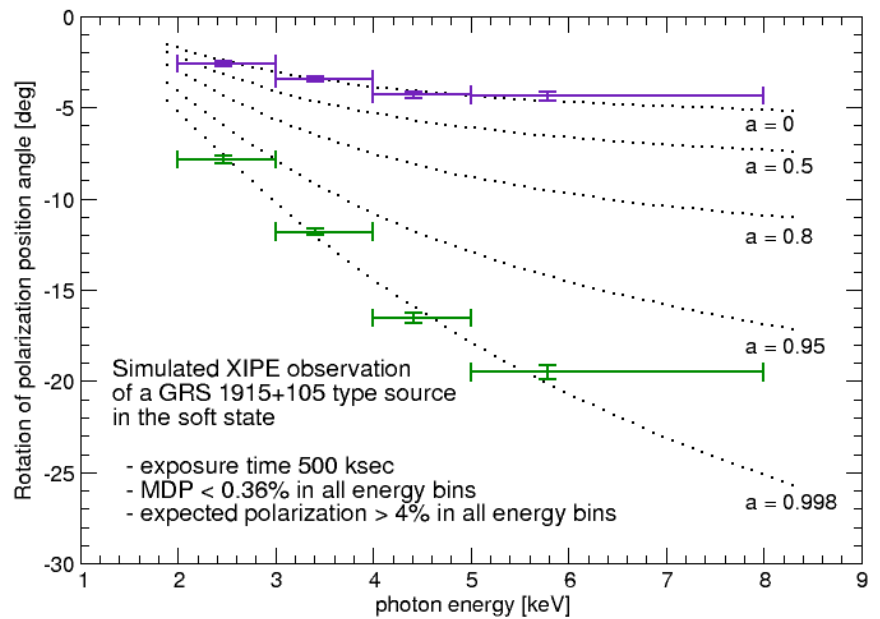


Figure 10 Simulated 500 ks observation with XIPE of GRS 1915+105 in the soft state for two angular momenta of the black hole: the Schwarzschild case (indigo, $a = 0$) and the extreme Kerr case (green, $a = 0.998$). The figure shows the polarization position angle as a function of photon energy. The obtained MDP is smaller than 0.36%, whereas the expected polarization fraction exceeds 4% in all energy bins and for both cases of black hole rotation. The models were adopted from Dovciak et al. (2008).

XIPE operation which may be other good sources to search for GR effects.

Active Galactic Nuclei

In AGN, the disk thermal emission is outside the working band of XIPE. However, GR effects may manifest themselves through a time-dependent, rather than energy-dependent, change of the polarization degree and angle. In fact, there is increasing evidence that the X-ray emitting corona is very compact (Reis & Miller 2013, Emmanoulopoulos et al. 2014), with a mean height varying with time (e.g. Miniutti & Fabian 2004, Fabian et al. 2012, Parker et al. 2014). The polarization degree and angle of the reflected radiation must vary accordingly (Dovciak et al. 2011), in a way that depends on the spin of the black hole. Polarimetry can therefore provide a further and powerful probe of radiative transfer in a strong gravity field as well as an estimate of the black hole spin. In MCG-6-30-15, the archetypal source with a relativistic iron line, an MDP of about 4.1% can be reached with XIPE in 100 ks. A long look (1 Ms or more) at this source may then provide a first test of the model.

It is worthwhile to remark that the relativistic interpretation for MCG-6-30-15 and other sources has been challenged because the broad iron K line could also be modeled as a non-relativistic feature arising from partial covering (Miller et al. 2009). Partial absorption in a clumpy outflow intercepting the line of sight generally induces low polarization and always produces a polarization position angle that is constant across the iron line band. On the contrary, in the reflection case the polarization is large and its position angle varies systematically across the iron line (Marin et al. 2012b).

2.2.3. Quantum Gravity

One of the most ambitious efforts of modern physics is to develop a theory that unifies Gravity with the other three fundamental forces within a single theoretical framework. Different approaches to Quantum Gravity are pursued (Loop, String, non commutative space-times) all sharing the general problem of finding good observational tests (Amelino-Camelia 2004). One of few such tests can be made with polarimetry. Loop Quantum Gravity predicts that, at the Planck scale, a small vacuum birefringence effect is present which violates Lorentz invariance and, for linearly polarized radiation, results in a rotation of the polarization angle along the photon path (Gambini & Pullin 1999). This rotation is proportional to the distance of the source, and to the square of the energy of the photon, via a dimensionless factor of proportionality, η . Previous UV and X-ray polarization measurements (the latter performed on the Crab Nebula, the only source for which there is a solid positive detection so far) have already constrained η to be less than about 10^{-4} in the case the effect is linear with energy (Gleiser & Kozameh 2001; Kaaret 2004) with claims as low as a few times 10^{-7} based on optical/UV measurements of a gamma-ray burst afterglow (Fan et al. 2007). Even tighter constraints to η of the order of 9×10^{-10} were put forward by Maccione et al. (2008) comparing the polarization measurement of the Crab pulsar in soft gamma-rays by INTEGRAL with the optical observations. The most recent results based on the INTEGRAL polarization detection of GRBs put this limit down to 10^{-16} (Götz et al. 2014).

Although all of these measurements seem to exclude any birefringence at a high confidence level, they were performed exploiting extemporaneous measurements and instruments not dedicated to X-ray polarimetry. A tighter test of the theory would require, on the one hand, measuring (or putting upper limits to) values of η as small as possible to constrain also theories other than linear; on the other hand, to check results against e.g. possible errors due to intrinsic polarization angle variability by looking to different sources at different distances. With an observation of 2×10^5 s, values of η down to 3×10^{-10} can be measured with XIPE using e.g. the known blazar 1ES1101+232, at $z=0.186$, with a clear synchrotron spectrum and high optical polarization, assuming it has a 10% polarization degree in the X-ray band. Several bright enough blazars at different distances, which will be observed also to pursue other scientific objectives, are available to put the result on a firm statistical basis.

2.2.4. Search for axion-like particles

Axion-like particles (ALPs) are spin-zero bosons predicted by many extensions of the Standard Model of particle physics, like four-dimensional models, compactified Kaluza-Klein and superstring theories. Depending on the actual values of their mass and on the $\alpha\gamma\gamma$ photon coupling constant, ALPs can play an important role in cosmology, either as cold dark matter particles responsible for the formation of structures in the Universe or as quintessential dark energy that presumably drives the present accelerated cosmic expansion. In a magnetic field, the mixing between photons and ALPs produces both a photon-ALP conversion and, if a transverse component is present, a change of the photon polarization. In particular, linearly polarized photons acquire, as they travel in the magnetic field, an elliptical polarization with the major axis rotated with respect to the initial polarization. A detection of the latter effect employing a laser beam by the PVLAS collaboration was claimed, but subsequently withdrawn (Zavattini et al. 2006, 2008). While laboratory experiments devised to search for ALP-induced photon polarization changes suffer from the intrinsic limitations due to the inevitably short baseline, systematic astrophysical observations of distant X-ray sources offer the opportunity to overcome this limitation. Bassan et al.

(2010) suggested that in the case of very light ALP, photon-ALP mixing in intergalactic, intracluster and Galactic magnetic fields may significantly affect the polarization of radiation emitted by distant sources, inducing either a linear polarization on initially unpolarized photons or a dispersion of the degree of polarization of initially linearly polarized ones (see Figure 8). Moreover, ALPs signatures should strongly depend on energy and on the projected position of the object on the sky because of the different magnetic field morphology in different

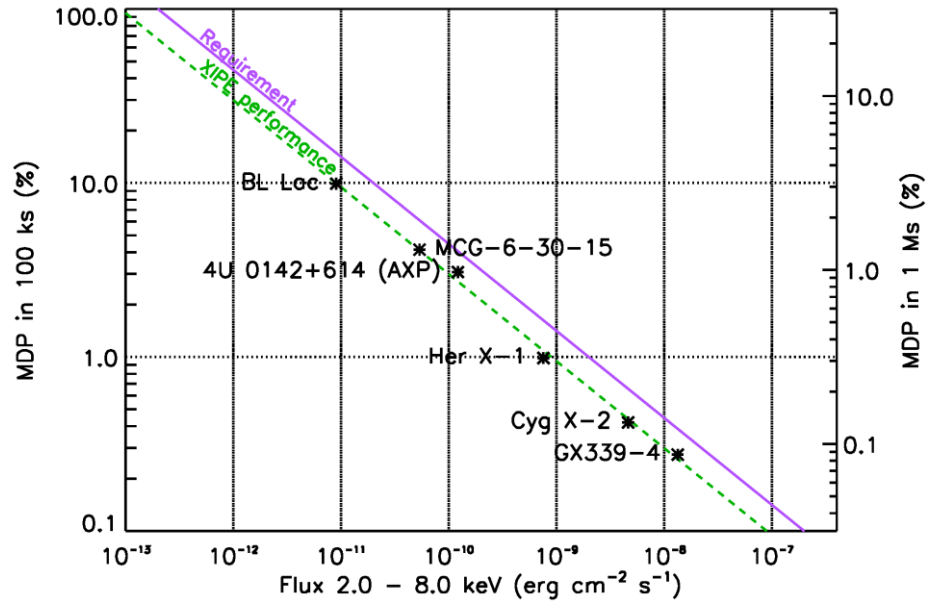


Figure 11 Scientific requirement of the polarimetric sensitivity and XIPE performance.

directions of observation. Natural candidates for these studies are the blazars which will be observed by XIPE also to achieve other scientific objectives, but ALP-induced effect can be searched also in the correlation between the polarization of galactic sources and the viewing direction. Similarly, it has been suggested that axion-photon conversion may leave a characteristic signature, a rotation of the plane of polarization, also in the polarization of the emission from neutron stars (Perna et al. 2014). Also in this case, these objects will be observed as a part of the XIPE core science program and therefore the speculative yet potentially highly rewarding activity of searching for axion-like particles will be carried out without putting additional constraints on the mission.

3. Scientific requirements

The scientific requirements described in this Section are summarized in Table 1, together with the high level mission requirements discussed in details in Section 5. We stress the point that the performance in some topics of the proposed baseline configuration is significantly better than these requirements.

3.1. Polarimetric performance

The capability to measure the degree and the angle of polarization can be expressed in terms of the Minimum Detectable Polarization (MDP). The MDP represents, at the 99% confidence level, the maximum degree of polarization which can be attributed solely to statistical fluctuations in the instrumental response. In fact, polarization is a positive definite quantity and therefore it is always measured to some extent. Only a detection greater than the MDP is statistically significant and, as a matter of fact, to reach a 3- σ measurement of a certain level of polarization an integration time 2.25 times longer than that corresponding to the same MDP is required (Weisskopf et al. 2010).

If the level of background is negligible with respect to the counts from the source, the MDP is expressed as

$$MDP = \frac{4.29}{\mu\sqrt{S}} \frac{1}{\sqrt{T}}$$

where S is the source count rate, T the observation time and μ the modulation factor of the instrument. From this equation, it follows that the MDP scales as $1/\sqrt{T}$. The sensitivity to the polarization angle is tightly related to the MDP so that the latter parameter is the synthetic parameter describing the performance of an X-ray polarimeter. A measurement at 3- σ on the polarization degree allows for a 1- σ confidence interval on the position angle of about 17 degrees (Weisskopf et al. 2010).

The requirement on polarimetric sensitivity to achieve the scientific objectives described above is that an MDP of 10% must be reached with an observation of 100 ks for a source with flux of 2×10^{-11} erg/s/cm² (corresponding to 1 mCrab) in the 2-8 keV band (**Req-Sci-010**, see Figure 11). Such a requirement scales with the flux of the source and with the observation time as discussed above and it is sufficient to, e.g.:

- measure a spatially averaged polarization as low as 6% in 100 ks for the Vela PWN, to look for analogies and differences with the Crab nebula;
- resolve spatially half a dozen PWNe in several regions, reaching an MDP<10% in each region;

Table 1 Summary of XIPE scientific requirements.

Parameter	Quantity	Scientific driver	Name
Scientific requirements			
Polarimetric sensitivity	MDP<10% for 100ks observation of source with flux 2×10^{-11} erg/s/cm ² (1 mCrab) in the 2-8 keV band	NGC1068, GC, ...	Req-Sci-010
Spurious polarization	<0.5%	GRS1915, Cyg X-1	Req-Sci-011
Angular resolution	<30 arcsec	Crab, jet in CenA, SNR, GC, ...	Req-Sci-020
Field of View	>10 arcmin	PWNe, SNRs, ...	Req-Sci-030
Spectral resolution	<20% at 5.9 keV	Black hole spin	Req-Sci-040
Timing resolution	8 μ s	Accreting millisecond pulsars	Req-Sci-050
Timing synchronization with the Universal Time	10 μ s	Accreting millisecond pulsars	Req-Sci-051
Dead time for one telescope	<100 μ s	Crab Nebula, Cyg X-1, ...	Req-Sci-052
Mission duration	3 yr	Core program and population studies	Req-Sci-060
TOO	Repointing <12 hr during working hours	Bursts	Req-Sci-070
Sky accessibility	1/3 of the sky accessible at any time	Observation of galactic and extragalactic sources	Req-Sci-080
Forbidden directions	None over one year	Core program and population studies	Req-Sci-081
Payload requirements			
Total collecting area	>1100 cm ² at 3 keV	See Req-Sci-010	Req-Pay-010
Modulation factor	>30% at 3 keV	See Req-Sci-010	Req-Pay-020
Detector efficiency	>10% at 3 keV	See Req-Sci-010	Req-Pay-030
High Level Mission Requirements			
Orbit	LEO, altitude<600 km, inclination<6°	Background for GC	Req-Mis-010
Absolute Pointing Error (APE)	≤ 1 arcmin	SNR, PWNe, ...	Req-Mis-020
Absolute Pointing Drift (APD)	≤ 1 arcmin	SNR, PWNe, ...	Req-Mis-030
Relative Pointing Error (RPE)	≤ 1 arcmin	SNR, PWNe, ...	Req-Mis-040
Absolute Measurement Accuracy (AMA)	≤ 10 arcsec/5 Hz	SNR, PWNe, ...	Req-Mis-050
Observation length	5 ks – 2 Ms	Crab – GC	Req-Mis-060
Number of pointings	150/year	Population studies	Req-Mis-070
Telescope optical axis mutual alignment	<3 arcmin	SNR, PWNe, ...	Req-Mis-080
Telescope optical axis alignment to the boresight	<2 arcmin	SNR, PWNe, ...	Req-Mis-090
Focal plane distance error	<1 mm	SNR, PWNe, ...	Req-Mis-100

- detect a polarization higher than 10% in 10 regions for 4 SNRs (Cas A, Tycho, IC443, MSH11-54) with 1000 ks observations;
- measure, in 2 Ms of observing time, the polarization degree and angle in selected regions of Cas A with an error better than 2%/5 degrees respectively, to map the level of order of the magnetic field (see Figure 4);
- reach an MDP of order 5% in 100 ks in half a dozen blazars, enough to distinguish between Synchrotron Self-Compton and External Compton models;
- measure a polarization degree as low as 3% in 10 phase bins in a 1000 ks observation of the magnetic Cataclysmic Variable AM Herculis, to probe the physical conditions of the accretion column;
- reach, in a 100 ks observation, an MDP of about 3% in 10 phase bins of the accreting millisecond pulsar SAX J1808-3658, to test the Comptonization scenario;
- reach, in a 100 ks observation, an MDP of about 3.0% in 10 phase bins of the X-ray pulsars Hercules X-1, to distinguish between “fan” and “pencil” radiation patterns;
- understand the emission mechanism in the quiescent state of Galactic black hole candidates by e.g. measuring, in a 500 ks observation, a polarization degree as low as 3% in GX 339-4 when in quiescence;
- measure, in a 500 ks observation, a polarization degree as low as 3% and the angle of polarization with an error of 2.5 degrees in the archetypal Seyfert 2 galaxy NGC1068, to probe the geometry of the “torus” (10% polarization expected);
- verify the hypothesis that our own Galactic Center is an intermittent low-luminosity AGN by measuring, with an accuracy of ± 5 degrees in a 1 Ms observation, the polarization angle of the Sgr B2 molecular cloud;
- observe, for the first time, the vacuum polarization QED effect by distinguishing, in a 250 ks observation of the AXP 1RXS J170849.0-400910, between models with and without this effect included;
- measure, in a 500 ks observation of the μ QSO GRS1915+105, the polarization angle in 4 spectral bins with a precision of 1 degree to estimate the black hole spin;
- reach in 200 ks an MDP<5% for 25 blazars (8 FSRQs, 17 BL Lac) at different redshifts and 7 radio galaxies to search for (or put tight constraints on) the birefringence effect predicted in the Loop Quantum Gravity theory, and to search for Axion-Like Particles.

This sensitivity will allow population studies for several classes of objects. For instance, we can reach an MDP of 3% with observing times per source between 100 and 500 ks in about a dozen radio-quiet AGN. This will allow us to distinguish between different geometries (and therefore origin) of the X-ray emitting corona and, if the geometry will turn out to be highly asymmetric (e.g. a slab above the accretion disk), to measure the inclination angle distribution, with important consequences on the AGN unification model.

The polarization sensitivity requirement described above can be met only if the instrument is characterized by a spurious polarization lower than the polarization degree to measure. This implies that the spurious polarization must be <0.5% (**Req-Sci-011**).

3.2. Imaging Performance and Field of View

Imaging capability is necessary for two reasons:

- to single out the target source from the others in the Field of View (FoV) and to reduce the underlying background, and
- to perform spatially resolved polarimetry of extended sources (e.g. Pulsar Wind Nebulae, Supernova Remnants, the Galactic Center molecular clouds).

The minimum requirement on the imaging capabilities is that angular resolved polarimetry must be performed with an angular resolution better than 30 arcsec to separate the emission from the torus and the jet in the Crab Nebula (**Req-Sci-020**). The FoV must be larger than 6x6 arcminutes square to image the Crab Nebula with a single pointing, including spacecraft pointing error (**Req-Sci-030**). This requirement is adequate for the other extended sources of interest. In particular, for SNRs, a better spatial resolution would not be of much use, as it would result in heavily photon starved spatial bins. For the Galactic Center molecular clouds, it is sufficient to single out the most important clouds from the very crowded region.

3.3. Spectral Performance

A moderate energy resolution of 30% is sufficient to disentangle the dependency on energy of polarimetric information and of instrumental response, e.g. the modulation factor and the efficiency. However, many scientific cases (e.g. the measurement of black hole spin) require energy-dependent polarimetry. An energy resolution of <20% is required to have at least 4 independent energy bins over the working band (**Req-Sci-040**), to unambiguously distinguish between a static and a maximally rotating black hole in GRS1915+105 (see Figure 10).

3.4. Timing Performance

XIPE scientific goals require a timing resolution of 8 μs (**Req-Sci-050**) and a synchronization of the on board time with the Universal Time at the 10 μs level (**Req-Sci-051**), mainly driven by the necessity to resolve in phase the emission of rapidly spinning millisecond pulsars. The dead time must be $<100 \mu\text{s}$ to observe bright sources like the Crab Nebula or Cyg X-1.

3.5. Operative requirements

Other requirements are those of a typical X-ray astrophysical mission:

- The expected duration of the mission is 3 years to complete the core program and the population studies (**Req-Sci-060**). No parts of the payload are consumable.
- Re-pointing ($<12 \text{ hr}$) within working-hours to perform Target of Opportunity observations is highly desirable to observe bursts from a number of source classes (**Req-Sci-070**)
- At any time, 1/3 of the sky must be accessible (**Req-Sci-080**), with no forbidden directions over one year (**Req-Sci-081**), to observe both galactic and extragalactic sources.

3.6. Other requirements

The scientific requirements discussed above put some basic requirements on the payload instruments:

- Total collecting area $>1100 \text{ cm}^2$ at 3 keV (**Req-Pay-010**);
- Modulation factor $>30\%$ at 3 keV (**Req-Pay-020**);
- Detector efficiency $>10\%$ at 3 keV (**Req-Pay-030**);

Other high level mission requirements, discussed in more details in Section 5, are:

- Orbit: nearly equatorial ($<6^\circ$), altitude $<600 \text{ km}$ for having a low background and successfully observe faint sources (**Req-Mis-010**);

Attitude Control Systems requirements

- An Absolute Pointing Error (APE) $<1 \text{ arcmin}$ is required to image large extended sources with only one pointing (**Req-Mis-020**);
- An Absolute Pointing Drift (APD) $<1 \text{ arcmin}$ is required to avoid large extended sources to exit the field of view during the observation (**Req-Mis-030**);
- A Relative Pointing Error (RPE) $<1 \text{ arcmin}$ is required to not spoil the imaging capabilities of the instrument (**Req-Mis-040**);
- An Absolute Measurement Accuracy (AMA) $<10 \text{ arcsec}/5 \text{ Hz}$ is required to superimpose the instrument images with those of other observatories without spoiling the imaging capabilities (**Req-Mis-050**).
- The duration of an observation of a single source will last from 5 ks to 2 Ms to reach good sensitivity even for faint sources (**Req-Mis-060**).
- The number of pointings will be 150/year (**Req-Mis-070**).

Alignment requirements

- the optical axis of the telescopes must be mutually aligned within 3 arcmin to contemporaneously image a large extended source (**Req-Mis-080**)
- the optical axis of the telescopes must be aligned with the boresight within $\pm 2 \text{ arcmin}$ to center the requested source (**Req-Mis-090**).
- the focal plane distance error must be the $<1 \text{ mm}$ to not spoil the imaging capabilities (**Req-Mis-10**).

3.7. Observing Plan

The three years of life of XIPE correspond, assuming an observing efficiency of about 50% as appropriate for a satellite in Low Earth Orbit, to a total observing time of 45 Ms. Assuming a mean observing time per pointing of $\sim 300 \text{ ks}$, and foreseeing that a number of sources will be observed more than once to search for variations in the polarimetric properties, we can estimate that a total of about 100-150 sources will be observed over the mission lifetime. Therefore, the brightest sources for each class of interest will be studied to individuate population properties and guarantee the achievement of the scientific objectives listed above. On the other hand, there will be enough room to readjust the observing plan, should any new and unexpected result arrive (it is worth emphasizing that we are going to open a new observing window, so the discovery space is enormous).

We plan to have a three months Science Verification Phase (SVP). The remaining observing time will be divided between a Core Program (CP, three months each year) and a Guest Observer (GO) program for the rest of the time,

Table 2 A possible observing plan for the first six months of XIPE. ΔP is the error on the polarization degree; $\Delta\phi$ is the error on the angle of polarization.

Object	Class	$F_{2-8 \text{ keV}}$ (10^{-11} cgs)	T_{exp} (ks)	MDP (%) or $\Delta P/\Delta\phi$	Expected Polarization	Science goal
Crab Nebula	PWN	1950	20	$\Delta P < 1\%$ and $\Delta\phi < 1\text{deg}$	$> 19\%$ (Weisskopf et al. 1978, Volpi et al. 2008)	Map of the Nebula
Vela PWN	PWN	6.0	100	MDP=6.0%	$> 10\%$ (Volpi et al. 2008)	Mean polarization
Cas A	SNR	116	1000	MDP=3-5%	$> 10\%$ in selected regions (Bykov et al. 2009, Fabiani et al. 2014)	Map of the remnant
Cyg X-1	μ QSO	1000	170	MDP=0.5%	$< 5\%$ @2.6 keV (Weisskopf et al. 1977)	Jet, corona
Mrk 421	Blazar	27	100	MDP=3%	$> 10\text{-}20\%$ (Poutanen 1994, Celotti & Matt 1994)	Jet
Cen A (jet)	Radiogalaxy	4	200	MDP=5%	$> 10\text{-}20\%$ (Poutanen 1994, Celotti & Matt 1994)	Jet (spatially resolved)
Am Her	MCV	10	1000	MDP=3.0% /10 phase bins	5-10% (Matt 2004)	Accretion column
SAXJ1808	AMP	100	100	MDP=3.0% /10 phase bins	$> 5\text{-}10\%$ (Viironen & Putanen 2004)	Scattering corona
Her X-1	LMXRB/ Pulsator	90	100	MDP=3.0% /10 phase bins	$> 10\%$ (Meszaros et al. 1988)	Fan vs. Pencil beam
1RXS J1708	Magnetar	4	250	MDP=9.3% /10 phase bins	$> 50\%$ (Taverna et al. 2014, Van Adelsberg & Lai 2006)	Vacuum polarization
GX339-4 (outburst)	XRBB	500	100	MDP=0.6%	$> \text{a few } \%$ (Schnittman & Krolik 2010)	Corona
GX339-4 (quiescence)	XRBB	4	1000	MDP=2.2%	Unknown	Corona
NGC1068	AGN	0.5	1000	MDP=4%	10% (Goosmann & Matt 2011)	Torus geometry
IC4329A	AGN	10	100	MDP=3%	$> \text{a few } \%$ (Schnittman & Krolik 2010)	Corona
SGR B complex	Molecular cloud	0.3	1000	$\Delta P < 4\%$, $\Delta\phi < 3^\circ$	$> 40\%$ (Churazov et al. 2002, Marin et al. submitted)	Past activity of SgrA*
GRS1915+10 5	μ QSO	1300	500	$\Delta P < 0.5\%$ and $\Delta\phi < 1 \text{ deg}$	$> 5\%$ (Dovciak et al. 2008, Schnittman et al. 2009)	BH spin
MCG-6-30-15	AGN	4	1000	MDP=1.3%	5% (Dovciak et al. 2011)	BH spin

The CP will be planned by the mission team to guarantee that observations, crucial to the achievement of the main scientific goals, will be performed, including a number of very time consuming, but potentially highly rewarding, observations (e.g. the Galactic Center). The data from the CP will be made public as soon as the on-flight calibrations will be released, to get the community engaged and help the perspective participants to the GO program to optimize their own proposals. The fact that 2/3 of the observing time will be assigned through a GO program will ensure the involvement of a large community and will guarantee that new, bright ideas will be duly considered.

A tentative observing plan for the first six months is given in Table 2.

4. Proposed scientific instruments

The XIPE proposal takes advantage of previous studies, and in particular: (i) the assessment study of XEUS/IXO by ESA/NASA/JAXA; (ii) the successful phase A study of POLARIX, a mission proposed in response to a call by the Italian Space Agency (ASI) - the program was discontinued due to financial problems; (iii) the study of NHXM, a mission proposed to ESA M3 call.

The XIPE scientific payload is divided in three main parts (see Figure 12): the Mirror Assembly (MA), the Focal Plane Assembly (FPA) and the Control Electronics (CE). In the proposal, we will assume that the MA and the Telescope Support Structure (TSS, see Figure 13) will be ESA-procured with the scientific support of the XIPE consortium, whereas the responsibility of the FPA and of the CE will be on the XIPE consortium and will be financed by the Member State Agencies (MSAs).

4.1. Mirror Assembly

The Mirror Assembly comprises three identical Telescope Units (TUs), which are mounted together on a Mirror Mounting Structure (MMS, see Figure 14). The MMS is also the interface to mount the MA on the Telescope Supporting Structure and then on the Service Vehicle Module through the Thrust cylinder (see Figure 13). Each TU

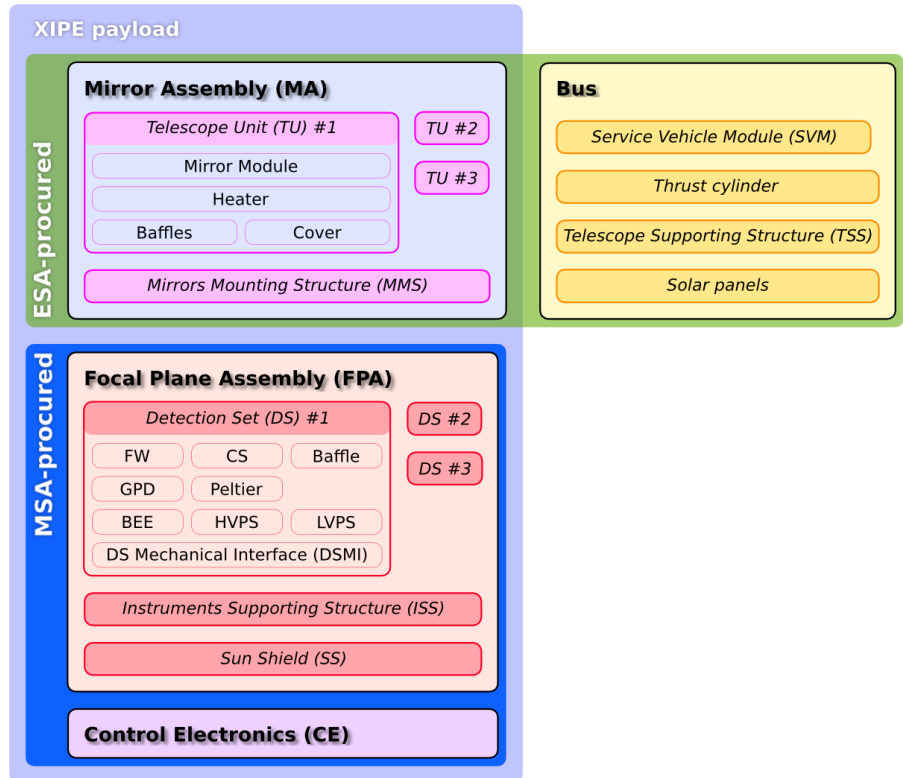


Figure 12 Block diagram of the XIPE scientific payload.

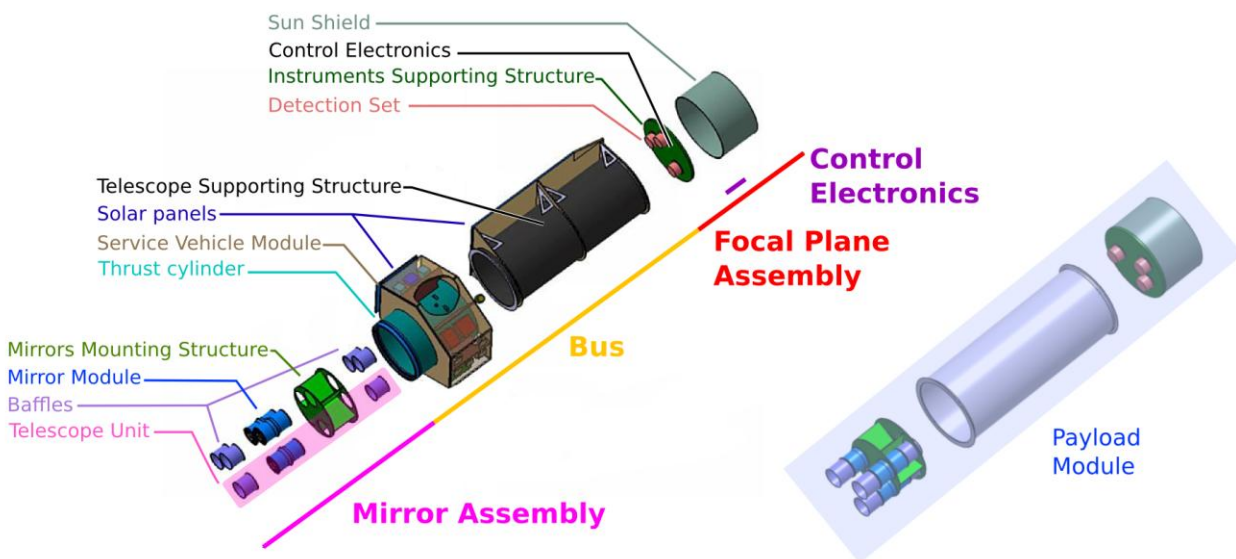


Figure 13 Main components of the XIPE spacecraft (payload+bus). The Payload Module (PM) comprises the MA, the FPA and the TSS.

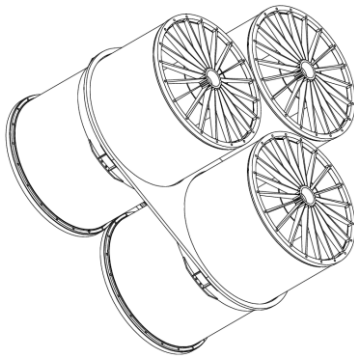


Figure 14 Mirror Modules assembled in the Mirror Support Structure.

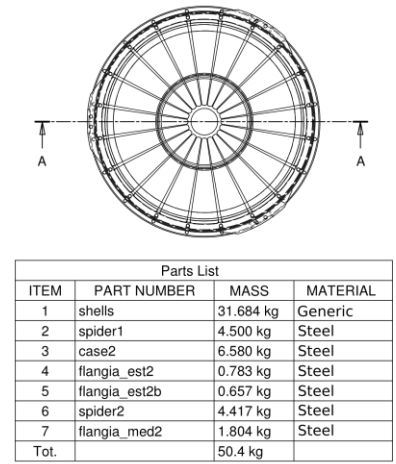
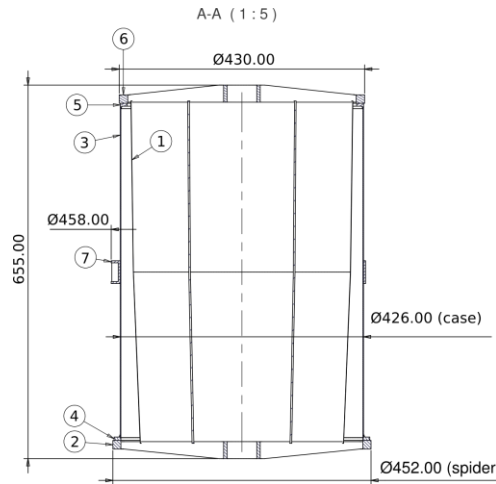


Figure 15 Technical drawing of the XIPE MM. The weight is 50.4 kg (without margins).

comprises: (i) a cover to remove after launch (ii) two baffles, used as sun and thermal shield, (iii) heaters to control the stability of the temperature and (iv) a group of nested shells, with its own support structure (Mirror Module, MM), which focuses X-rays in a grazing incidence configuration. This is a very well-established technique with an extensive flight heritage. Although the MA will be procured by ESA, we have already identified a design which satisfies all of the requirements discussed above and therefore it is used also for evaluating the budget and the sensitivity of the XIPE mission. This design has been developed by INAF Brera Observatory, one of the leading members of the XIPE consortium, in collaboration with Media Lario Technologies. They have already designed, manufactured and calibrated successfully the telescopes for JET-X/Swift, BeppoSAX, XMM-Newton, and eRosita. An offer by the Media Lario Technologies for the manufacturing of the EQM and flight models is attached as an Annex to this proposal.

Each XIPE MM comprises 27 mirror shells with diameters from 380 mm to 180 mm, each of them featuring a double-cone approximation of the Wolter-I profile with 300 mm of parabolic segment plus 300 mm of hyperbolic segment. The focal length is 3.5 m and it is chosen so that XIPE can fit in the fairing of the Vega launcher. In fact, three telescopes with a focal length of 3.5 m, that is, equivalent to those proposed for XIPE, was proved to fit in the fairing of this launcher by the POLARIX phase A study led by Thales-Alenia Space (Costa et al. 2010). The thickness of each shell is determined on the basis of the thin and light design studied for the NHXM mission, for which an angular resolution of 15-20 arcsec has been proven with fully integrated prototype mirrors (Spiga et al. 2010). With electroformed Nickel mirrors, given a fixed initial mandrel quality of a few arcsec, the geometric angular resolution of the mirror mostly depends on the thickness/diameter ratio (τ/R , assumed constant throughout the module). This parameter increases with the mirror stiffness but, at the same time, the mass/geometric area ratio of the telescope also increases, with the result that better quality mirrors require a larger mass keeping the effective area constant (Basso et al. 2008). For JET-X, which had an angular resolution of 13 arcsec, the value was $\tau/R = 7 \times 10^{-3}$, while for XMM this value was decreased by a factor of 2. In the NHXM project, we have been able to decrease τ/R by a further factor of 2.5, without affecting the mirror mechanical properties, owing to the adoption of an *ad hoc* integration concept (Basso et al. 2011). Assuming for the shells a minimum thickness of 0.2 mm (the smaller value tested for the shells in the NHXM project), the total weight of the MM, including a structure, is of 50.4 kg without margins (see Figure 15).

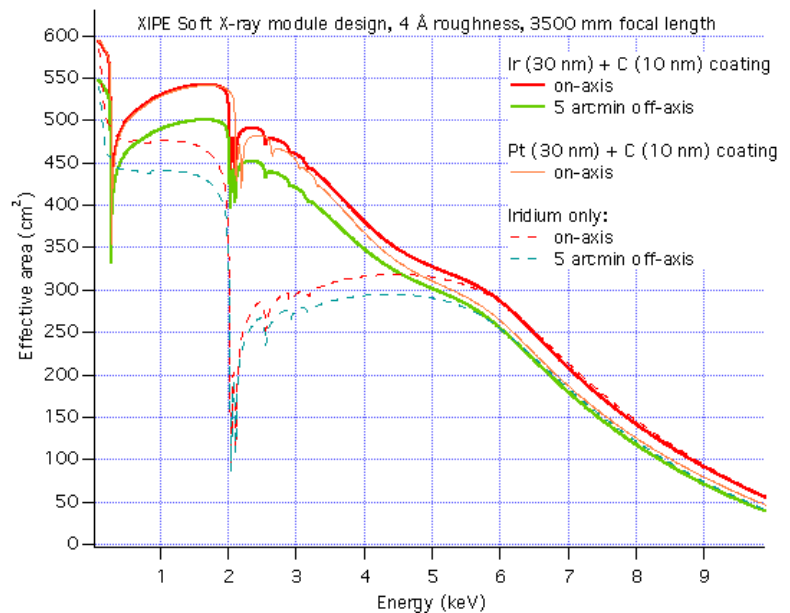


Figure 16 Effective area of a single XIPE mirror module, on-axis (red lines) and 5 arcmin off-axis (green lines). The computations without the Carbon over-coating are shown as dashed lines, and return a much lower effective area. The computed effective area assuming a Pt +C coating (yellow line) differs only a little from the Ir+C coating.

In soft X-rays, a simple high-Z coating is sufficient to guarantee high reflectivity, and Iridium (or Platinum) is a viable solution. Near the atomic energy edges, however, the reflectivity drops because of the photoelectric absorption. Fortunately, over-coating with a low-Z layer greatly improves the reflectivity at energies below 5 keV (Pareschi et al. 2004; Cotroneo et al. 2007). We have computed analytically the effective area of the XIPE telescope on-axis and 5 arcmin off-axis using analytical formulae (Spiga 2011), and the results are shown in Figure 16. We have assumed a reasonable value of 4 Å rms for the surface roughness (the effect is almost irrelevant at these energies). The importance of the Carbon over-coating is apparent; with a simple Iridium layer (dashed line), the total effective area is 300 cm²

at 3 keV, whereas there is an increase of about 50% by adding an amorphous Carbon over-coating, so that the effective area on-axis at 3 keV is 450 cm². The effective area at 5 arcmin off-axis is lower than on-axis by less than 10%; the field of view, corresponding to the region where the collecting area is larger than 50% of the on-axis value, is about 30 arcmin, that is, much larger than that accessible by the focal plane instrument. The optimal value for the Carbon over-coating is 10 nm, while the thickness of the Iridium layer is much less critical and can be set to 30 nm, a value sufficient to guarantee high reflectivity and at the same time to avoid problematic stress and roughness in the coating. Changing the Ir+C to Pt+C slightly decreases the effective area, but the difference is very small. In all these calculations, 10% of the effective area is assumed to be obstructed by the spider (the dependence of the spider obstruction on the off-axis angle can be neglected). The analytical calculations presented above were checked with accurate ray-tracing computations, which provided consistent values of the effective area.

The thermal environment for the mirror modules must be such that the HEW is not degraded by more than 10 arcsec which implies that the mirror units should have a thermal gradient of less than 2°C. The stabilization of the temperature of the mirrors has already been studied during the POLARIX phase A for similar telescopes and it is positively actuated on the mirror flying on-board the Swift satellite. The rate of change of mirror temperature, in any phase, operational or non-operational, must not exceed 10°C per hour with a maximum thermal gradient on the mirror being 2.0°C (longitudinal) and 1.0°C (azimuthal). There is no power requirement from the MMs other than that needed to power the thermal heaters. Cleanness requirements for the MMs are discussed in Section 4.5. The characteristics of the XIPE MM are summarized in the Table 3.

Table 3 XIPE MM characteristics.

Geometrical profile	Wolter I
Focal length	3.5 m
Mirror length	60 cm
Max/min shell diam.	380-180 mm
# of spiders	2
# of spokes per spider	20
Spiders & case material	Steel
# of shells per module	27
Wall material	Electroformed NiCo
Wall thickness	0.33-0.20 mm
Coating	Ir (30 nm)+C (10 nm) bilayer
Weight (without margins)	50.4 kg
Power (without margins)	<16 W

4.2. Focal Plane Assembly

The Focal Plane Assembly will be the responsibility of the XIPE Consortium and it is based on three identical photoelectric X-ray polarimeters exploiting the Gas Pixel Detector design (GPD, Costa et al. 2001; Bellazzini et al. 2006, 2007). This instrument was already studied in the same configuration proposed for XIPE during the phase A study of POLARIX (by the Italian Space Agency) and of XEUS/IXO (by ESA/NASA/JAXA).

4.2.1. Detection principle

The GPD is able to measure the linear polarization of photoabsorbed photons by reconstructing the emission direction of the ejected photoelectrons. It comprises a gas cell with a thin 50 μm Beryllium entrance window, an absorption/drift gap, a charge amplification stage and a multi-anode read-out which is the pixelated top metal layer of a CMOS ASIC analog chip (see Figure 17, Costa et al. 2001). The ASIC has 105600 pixels at 50 μm pitch, and it is at its third generation of development (see Figure 18, Bellazzini et al.

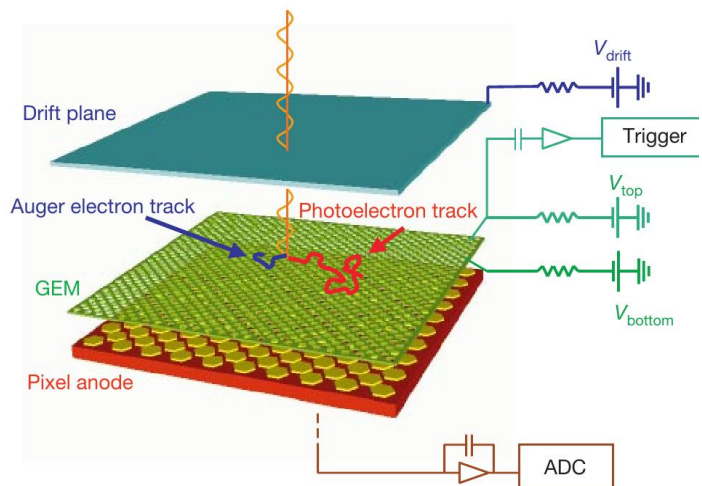


Figure 17 Principle of operation of the GPD (Costa et al. 2001).

2006). The GPD ASIC was produced under design of Pisa INFN and is available at this institute in a number that is widely redundant to any need of the XIPE program. When the X-ray photon is absorbed in the gas gap the ejected photoelectron produces an ionization pattern in the gas (track, see Figure 19). The track is drifted by a uniform electric field to the Gas Electron Multiplier (GEM) where the charge is amplified without changing the track shape (Costa et al. 2001). Below the GEM, at a distance smaller than a few hundred micron, the top layer of the multilayer ASIC is covered by metal pads with a high filling factor distributed on a hexagonal pattern. Each pad is connected underneath to its own independent analog electronic channel, whose average noise is only 50 e⁻ rms; with a moderate gain of 500, single electrons produced in the gas cell can be detected. The system has self-triggering capability and it can autonomously determine a window (called ROIs, Regions of Interest) which contains the pixels which triggered, plus a margin. Only the charges of the pixels included in the ROI are read-out from a common output and analog-to-digital converted in real-time. The size of the ROI typically ranges between 600 to 800 pixels; notwithstanding, the large part of these pixels does not contain any charge and they can be suppressed after the analog-to-digital conversion. The image of the track which has to be eventually analysed contains only 50-60 hit pixels on average.

The track is analysed by an algorithm which provides a measurement of the absorption point and of the photoelectron emission direction. The former is used to image the source and the measured spatial resolution for a pencil beam is 92 μm Half Energy Width (HEW, see top panel in Figure 20). This allows to oversample the Point Spread Function (PSF) of typical X-ray telescopes and then to add a negligible contribution to

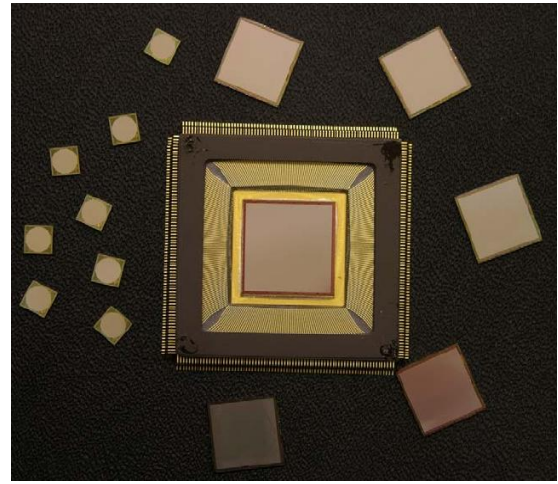


Figure 18 The three ASIC generations, with increasing pixel number and decreasing pixel size, at the basis of the Gas Pixel Detector (Bellazzini et al. 2006).

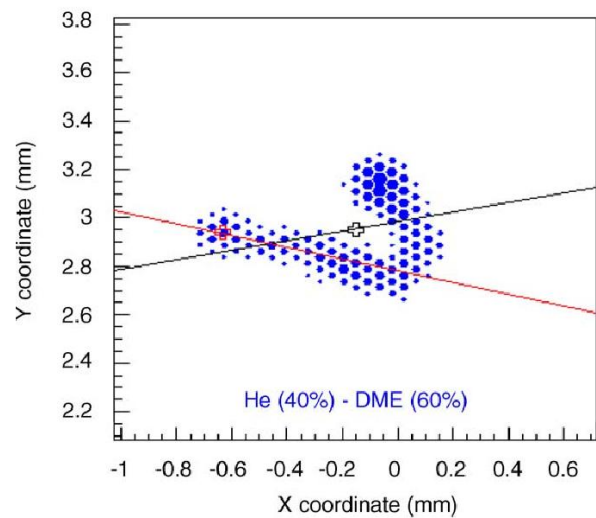


Figure 19 An example of a real photoelectron track at 5.9 keV (Bellazzini et al. 2006).

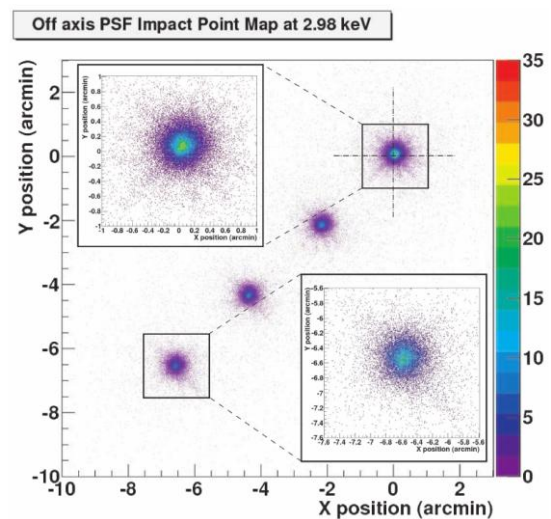
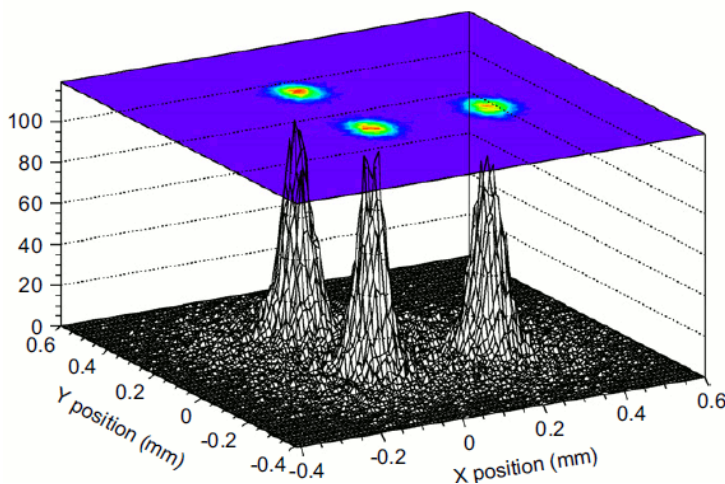


Figure 20 (Left) Image of three 4.5 keV pencil beams (spot size of a few tens of microns) shifted by 300 μm in the X and Y directions. The measured HEW is 92 μm (from Soffitta et al. 2013, Fabiani et al. 2014). (Right) Point Spread Function of the GPD in the focus of a JET-X mirror module at 2.98 keV (Fabiani et al. 2014).

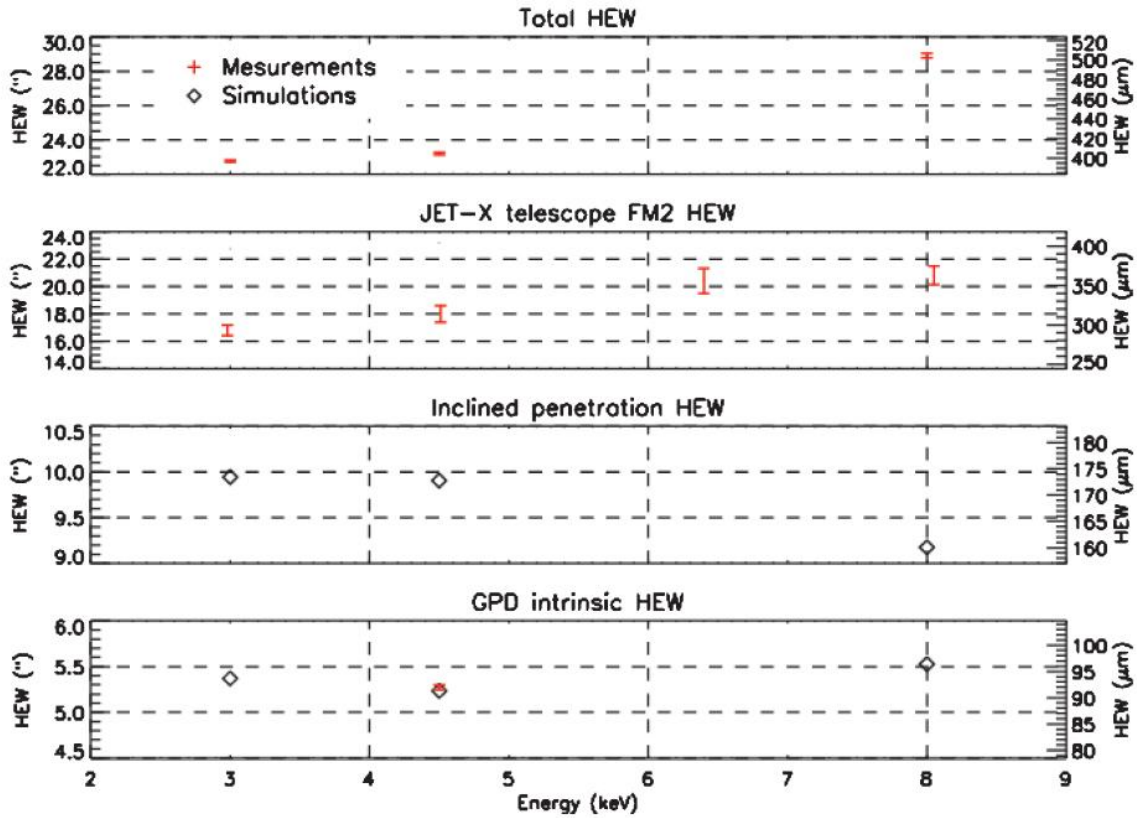


Figure 21 HEW measured at the PANTER X-ray testing facility for the GPD + JET-X assembly, with breakdown of the single contributions. From top to bottom: (i) the measured value for the assembly; (ii) the HEW of the mirror measured by substituting the GPD with a CCD (Charge-Coupled Device) imager; (iii) the contribution, derived by a Monte Carlo, due to the inclined penetration of the focused X-ray photons in the GPD gas cell; (iv) the HEW of the GPD for a pencil beam orthogonal to the detector (Fabiani et al. 2014).

the final angular resolution of the system. In fact, we tested the GPD imaging capabilities with a real X-ray telescope of good quality, that is, one of the JET-X modules which has a HEW equal to 16.8 ± 0.4 arcsec at 2.98 keV (Spiga et al. 2014). We measured for the telescope+GPD assembly a HEW of 22.7 ± 0.1 arcsec (Fabiani et al. 2014, see Figure 21); the HEW for XIPE is evaluated by rescaling properly the inclined penetration from this value. The $15 \times 15 \text{ mm}^2$ active area of the ASIC allows for a FoV of 15×15 square arc minutes with a focal length of 3.5 m assumed as a baseline for XIPE.

The emission direction is used to measure the polarization because the photoelectron is preferentially ejected in the direction of the absorbed photon electric field. In case of polarized photons, the histogram of the azimuthal emission directions, called modulation curve, shows a \cos^2 modulation whose amplitude is proportional to the degree of polarization, and the maximum points in the polarization direction (see the left panel in Figure 22). On

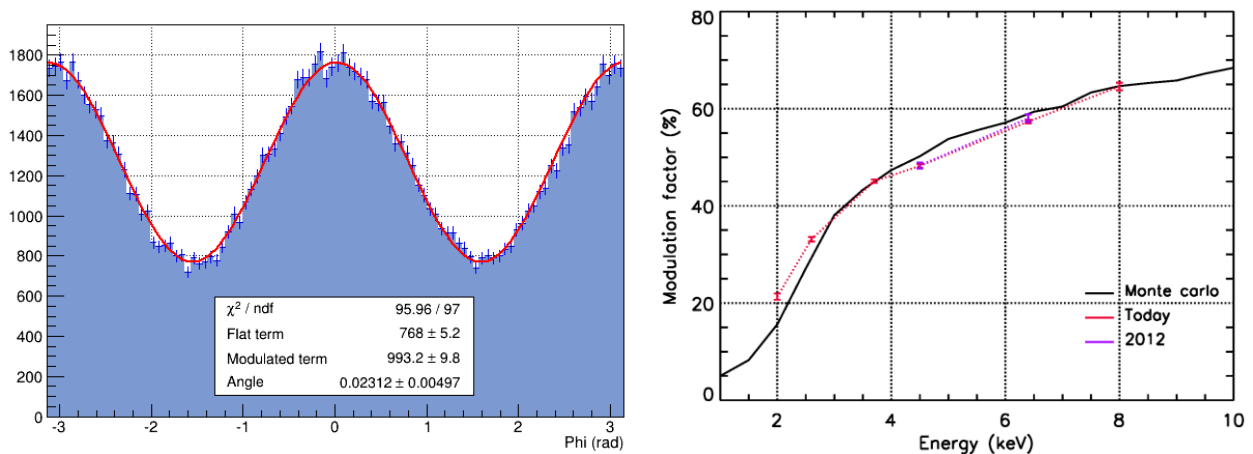


Figure 22 (Left) Modulation curve at 3.7 keV. The measured modulation factor is 41% even without any data selection. (Right) Modulation factor measured for the GPD as a function of the energy, assuming a cut of 20% of data selected on the basis of the elongation of the track. The measurements carried out in 2012 are consistent with those performed two years later. The measurements are also compared with the result of a Monte Carlo.

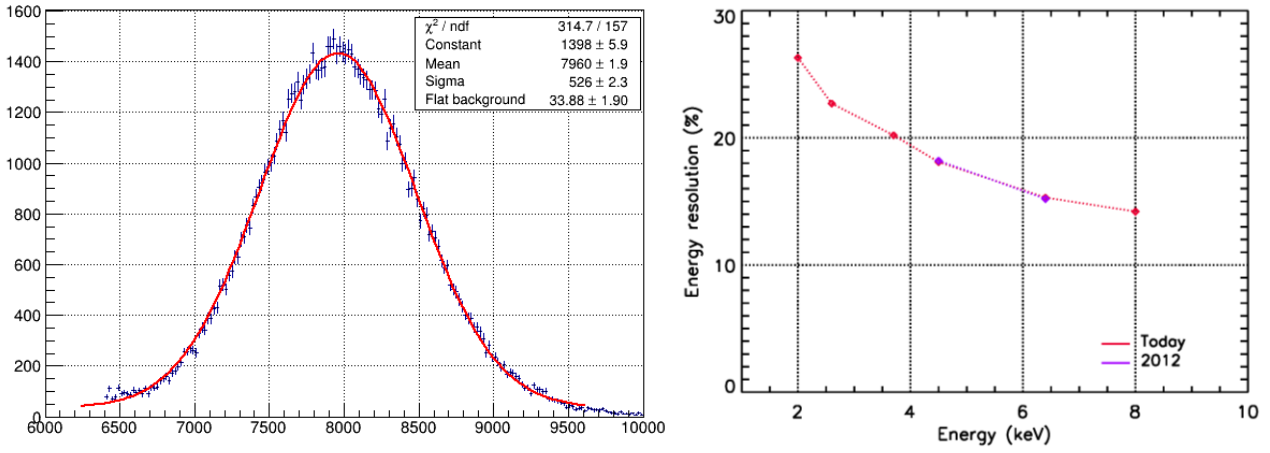


Figure 23 (Left) Spectrum of 6.4 keV photons. The measured energy resolution is 15.5%. (Right) Energy resolution as a function of the energy measured for the GPD in 2012 and today.

the contrary, if the absorbed photons are unpolarized, the modulation curve is -statistically speaking- flat. The probability of correctly reconstructing the initial direction of the photon depends on the track length and then on the energy; it is quantified by the amplitude of the modulation for completely polarized radiation, called modulation factor μ . The modulation factor of the GPD has been extensively studied (Muleri et al. 2008, Muleri et al. 2010) and it will be periodically verified on-orbit, as discussed in Section 4.4. Its dependence on energy is reported in the right panel of Figure 22; the values are calculated assuming a cut of 20% of data, selected on the basis of the elongation of the track. Such a cut, despite the reduction of the efficiency, allows for a net increase of the sensitivity to polarization (Muleri et al. 2008). The measured values of the modulation factor are consistent with those expected from a Monte Carlo code, which was specifically developed to accurately describe the propagation of low energy electrons in the gas cell. Moreover, the value of the modulation factor has remained constant since the manufacturing of the detector; we will discuss more on the stability of the GPD performance in Section 4.2.2. The spurious polarization, that is, the polarization measured in case of unpolarized radiation because of small non-uniformities in the azimuthal response of the detector, was measured to be less than 0.5% (Bellazzini et al. 2010). The sum of the charge contained in all of the track pixels provides a measurement of the photon energy. The energy resolution measured at different energies is reported in the right panel of Figure 23 and, like the modulation factor, it has remained constant since the manufacturing of the GPD. It is 16% at 5.9 keV.

The drift time of the charges in the gas cell is $<1 \mu\text{s}$. We report in Figure 24 the timing of the sequence which is performed internally by the ASIC to capture an event. When a charge above threshold is collected by any of the ASIC pixels, a trigger is set within a time $T_{\text{th}} < 2 \mu\text{s}$. The charge signals of all of the pixels are independently shaped with a shaping time of typically $4 \mu\text{s}$, and the signal *DataReady* is set high after that the search for the peak, lasting a time $T_{\text{pd}} < 15 \mu\text{s}$, is finished. Then, the ROI is identified and the signals of the pixels in it are read-out line-by-line. The trigger tags the time of the arrival of the photon within a few (<3) microseconds, including the drift time.

We summarise the performance of the GPDs on-board XIPE in the Table 4. The expected performance, based on actual measurements of the modulation factor and of the efficiency, is also compared with the scientific requirements discussed in Section 3. The GPDs will be filled as a baseline with a mixture 20% He - 80% DME at 1 atm to be sensitive in the 2-8 keV energy range with a gas mixture absorption/drift thickness of 10 mm, but an activity of fine-tuning is foreseen during the Definition/Study Phase. The high voltages required for collecting and multiplying the charge with the GEM are: $V_{\text{drift}} = -2 \div -3.5 \text{ kV}$; $V_{\text{top GEM}} = -0.5 \div -1 \text{ kV}$; $V_{\text{bottom GEM}} = -100 \div -500 \text{ V}$. The GEM, as any multiplication device, is

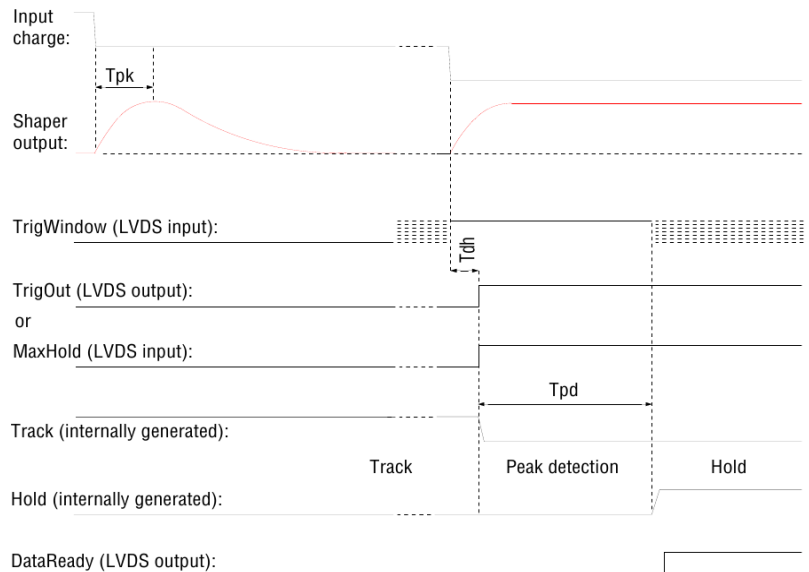


Figure 24 ASIC internal sequence for the capture of an event.

Table 4 Summary of the performance of the XIPE GPDs.

Performance		Note
Polarimetric sensitivity	6.7% (goal: 5%) for 1 mCrab in 100 ks	Compliant with Req-Sci-010
Spurious polarization	<0.5 % (goal: <0.1%)	Compliant with Req-Sci-011
Angular resolution	<26 arcsec (goal: <24 arcsec)	Compliant with Req-Sci-020
Field of View	15x15 arcmin ²	Compliant with Req-Sci-030
Spectral resolution	16% @ 5.9 keV	Compliant with Req-Sci-040
Timing	Resolution <8 μ s	Compliant with Req-Sci-050
	Dead time 60 μ s	Compliant with Req-Sci-052
Stability	>3 yr	Compliant with Req-Sci-060
Other characteristics		
Mixture	20%He-80%DME 1 atm 1 cm	Baseline
Window	50 μ m Be	
Energy range	2-8 keV	
Background	2×10^{-6} c/s or 4 nCrab	Negligible for all observations
High Voltages	$V_{\text{drift}} = -2 \div -3.5$ kV; $V_{\text{top GEM}} = -0.5 \div -1$ kV; $V_{\text{bottom GEM}} = -0.1 \div -0.5$ kV	
Operating Temperature	+5 \div +20 $^{\circ}$ C, stability $\pm 2^{\circ}$ C	For gain stability

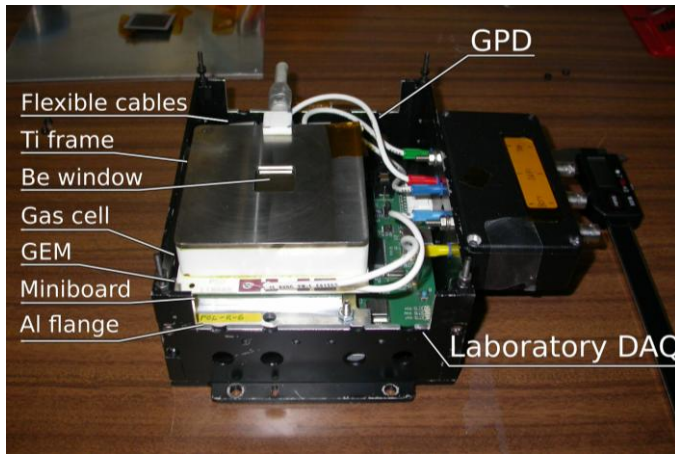


Figure 25 The current version of the GPD, together with the BEE (Laboratory DAQ) used in the laboratory.

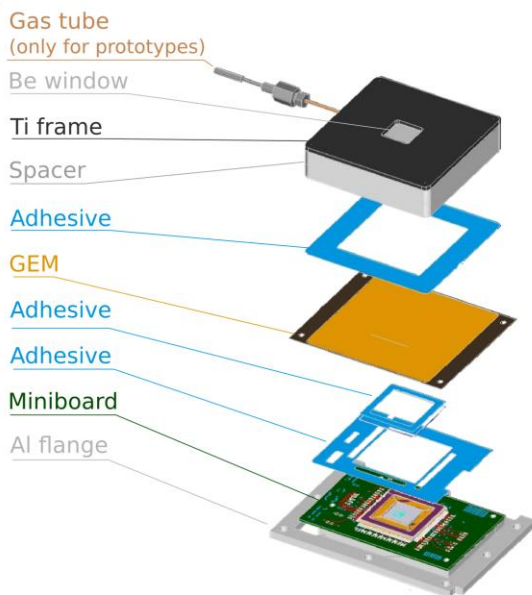


Figure 26 Exploded view of the GPD.

sensitive to temperature variations. Although the GPD laboratory prototypes have proved to work properly without any temperature stabilisation (see Section 4.2.2), we conservatively foresee the use of a Peltier cooler on-board XIPE.

A picture of the current GPD prototype is shown in Figure 25. The ASIC is bonded into a Kyocera package, which is soldered and glued on a miniboard. The miniboard is connected to the read-out electronics by flexible cables and is supported on an Aluminum flange. The gas cell, enclosed in a ceramic package made of MACOR, is much larger than the ASIC 15×15 mm² active area. The GEM has a surface of 88×88 mm², but only the central 18×18 mm² is active. Such a large GEM creates a drift region of uniform electric field (Muleri et al. 2012). Moreover, the peripheral region of the gas cell can be exploited as anticoincidence to reduce the background induced by low energy secondary particles produced in the gas cell walls (Soffitta et al. 2012). A study of the GPD background, including background rejection methods and possibly tests, will be performed during the Definition/Study Phase. The inclusion of a light anti-coincidence will also be considered. The Be window is 20×20 mm² and it is glued on a Ti frame (see Figure 26).

4.2.2. Detector heritage and environmental tests

The GPD is manufactured, evacuated, filled with a clean gas mixture and sealed by Oxford Instruments Finland oy, under the control of Pisa INFN team and of the Finnish

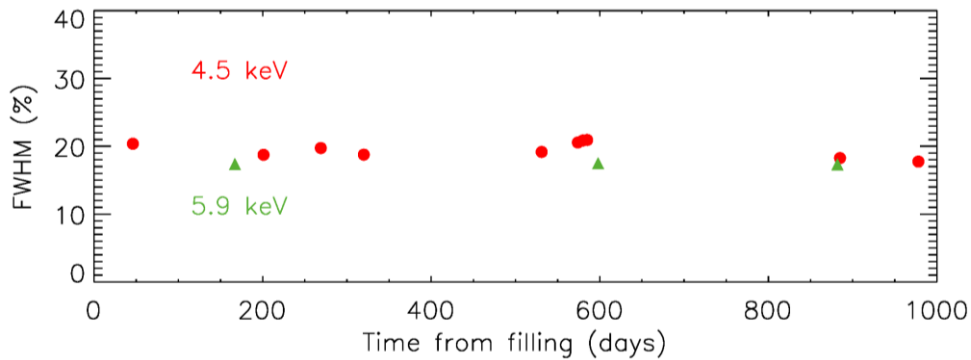


Figure 27 Energy resolution of the GPD FOR nearly 3 years at different energies (Soffitta et al., submitted).

team of XIPE. The procedures and the materials of the detector are basically already flight-proven. The company has a long heritage of sealed gas detectors with beryllium windows for space missions (SXR/SGR, PCA/XTE, NEAR, JEM-X/INTEGRAL, HETE-2, MOXE), and has so far produced all the prototypes of GPDs. FEM (Finite Element Method) analysis and actual tests carried out during IXO Assessment Phase (IXO-XPOL-TN-004-01) proved that the Be window can sustain at least 1.6 bar differential pressure, to be compared with 1 bar (operative pressure), with a safety factor that exceed GEVS (General Environmental Verification and Standard). X-ray gas detector with Beryllium windows has flown in space for 50 years.

The GPD has been extensively tested in the configuration and in the energy range proposed for XIPE. Calibration measurements in the whole energy range were performed for the baseline mixture (Muleri et al. 2008; see also Figure 22) and for other mixtures, working in the same energy range (Muleri et al. 2010) or not (Fabiani et al. 2012). The measured performance is very stable; a prototype, filled and sealed on 4th November 2011, has showed an energy resolution variation $<1.2 \cdot 10^{-3} \%$ /day over nearly three years (see Figure 27; Soffitta et al., submitted). During the same period, the modulation factor changed $<2.5 \cdot 10^{-3} \%$ /day.

The GPD passed thermal and mechanical tests. It was operated in high vacuum between $+10^{\circ}\text{C}$ and $+20^{\circ}\text{C}$, and underwent cycles (in non-operative conditions) between -15°C and $+45^{\circ}\text{C}$ (see the left panel Figure 28). The gain of the detector was stable within 1% in the operating temperature range. The GPD was also vibrated along three axes with random (NASA-GSFC-STD700A, GEVS STANDARD) and sinusoidal solicitations (see the right panel in Figure 28). No resonances were found at frequencies lower than 2 kHz.

The GPD was also operated in high vacuum ($P \approx 6 \cdot 10^{-6}$ mbar) at the PANTER X-ray testing facility of the Max-Planck-Institut für extraterrestrische Physik of Garching (Germany), during the imaging measurements with a flight-spares model of the JET-X telescope (Fabiani et al. 2014, see Figure 29). This is the same facility where the end-to-end calibrations of XIPE will be performed (see Section 4.4) and allowed us to verify that the angular resolution of the GPD with an X-ray telescope is dominated by the quality of the latter, as anticipated by Monte Carlo simulations (Lazzarotto et al. 2010).

A slow proton or a nucleus from cosmic rays can produce a large amount of ionization, able to trigger a temporary short circuit in the GEM holes. If the GEM is operated at a too high gain, the consequent spark can damage the

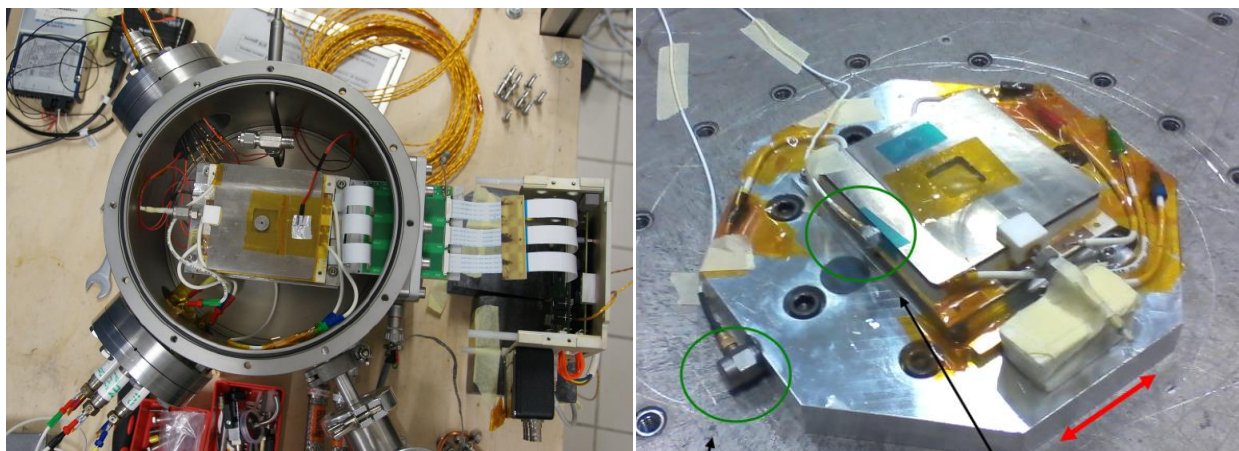


Figure 28 (Left) The GPD inside the vessel for thermal-vacuum tests. It was operated between $+10^{\circ}\text{C}$ and $+20^{\circ}\text{C}$, with thermal cycles between -15°C and $+45^{\circ}\text{C}$. An ^{55}Fe radioactive source is in front the detector to verify the GPD operation during the test. The 3 white, flat cables connect the detector to its read-out electronics, visible on the right side of the picture. The high-voltage feed-through are visible at the bottom-left of the picture while the heaters and temperature monitor feed-through are on the top-left. (Right) Setup for vibration tests.

GEM. In order to test the sensitivity of the GPD to the radiation environment in Space, we irradiated the GPD with heavy ions in the 500-MeV/nucleon Fe beam at the Heavy Ions Medical Accelerator in Chiba (HIMAC), Japan (Bellazzini et al. 2010). The total exposure was 1.7×10^4 Fe ions, which corresponds to 42 years in space in a LEO orbit. During the irradiation the GPD was powered on, at the nominal voltage levels. A single event acquired during the test by the online monitor is shown in Figure 30. The event saturates the electronics and several secondary delta rays are also visible. We did not register any damage or performance loss in the detector (Bellazzini et al. 2010). This was expected because the GPD ASIC is based on $0.18 \mu\text{m}$ VLSI technology, which is known to sustain high level of radiation. The other radiation-sensitive component of the GPD is the Gas Electron Multiplier (GEM). The current version is based on a GEM produced by Scienergy Japan in cooperation with Riken, based on a liquid crystal polymer $50 \mu\text{m}$ thick dry etched with laser. This is by far the best GEM for space applications, showing an excellent stability when irradiated with high Z particles, above the most pessimistic scenarios in a LEO (Tamagawa et al. 2009). The high voltage power supplies are very standard devices, moreover the currents expected are very low ($<10 \mu\text{A}$).

4.2.3. FPA design

The focal plane assembly of XIPE will host three identical GPDs; each detector, together with the components necessary to operate and calibrate it, forms a **Detection Set (DS)**. In particular, each DS comprises (see Figure 12):

- a GPD;
- a Filter Wheel (FW), which is used to put Calibrations Sources (CSs) or filters in front of the detector. The FW is similar to that on-board XMM-Newton;
- a baffle, which shields the detector from the diffuse X-ray photons not coming from the observed cosmic source. An electrostatic grid at +28V (such as the one flown on-board the Beppo-SAX satellite), will be located on top of the baffle to avoid ions to impinge on the detector window, which is polarized at $-2 \div -3 \text{ kV}$;
- Back End Electronics (BEE), which power and manage the DS.

The DS is organized in two boxes, one for the detector and the FW and one for the BEE, mounted on the Detection Set Mechanical Interface (see Figure 31). The three DSs are mounted on the Instruments Supporting Structure (ISS) and a Sun Shield (SS) allows for the dissipation of the thermal load from the DSs (see Figure 32).

The FW will have 7 positions:

1. open slot for standard observations;
2. slot with a Be absorber to reduce the flux of exceptionally bright sources (rate $>500 \text{ c/s}$ on each DS);
3. slot with a diaphragm to observe faint sources close to a bright source;
4. slot with a ^{55}Fe unpolarized calibration source;
5. slot with a Cu unpolarized fluorescence source;
6. slot with a polarized X-ray source;
7. closed slot for the launch and the study of the internal background.

The polarized X-ray source will be based on Bragg diffraction at nearly 45 deg. A baseline design is described by Muleri et al. (2007) and it can provide nearly 100% polarized and monochromatic photons at 2.6 and 5.9 keV with a reasonable flux for the entire duration of the mission, and requires a ^{55}Fe 10 mCi source. As an alternative, we

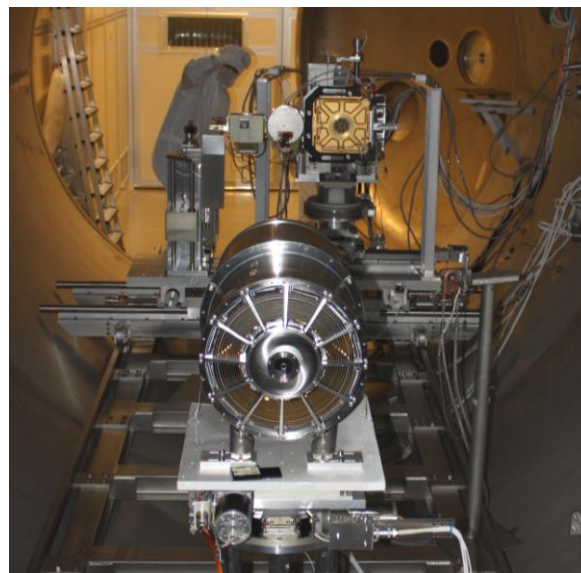


Figure 29 The GPD inside the vacuum chamber (on the left in the background) at the PANTER X-ray testing facility with the flight spare model of the JET-X telescope.

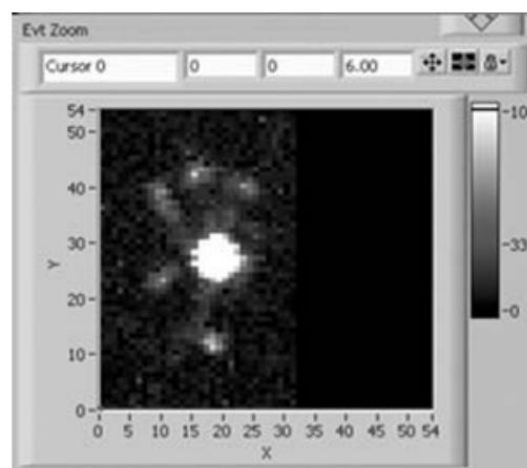


Figure 30 Track generated by a Fe ion with an energy of 500 MeV/nucleon shown by the online monitor during the irradiation test. The dimension of each pixel is $50 \mu\text{m}$. The event saturates the electronics in a 5 pixels radius. Several delta rays are also visible (Bellazzini et al. 2010).

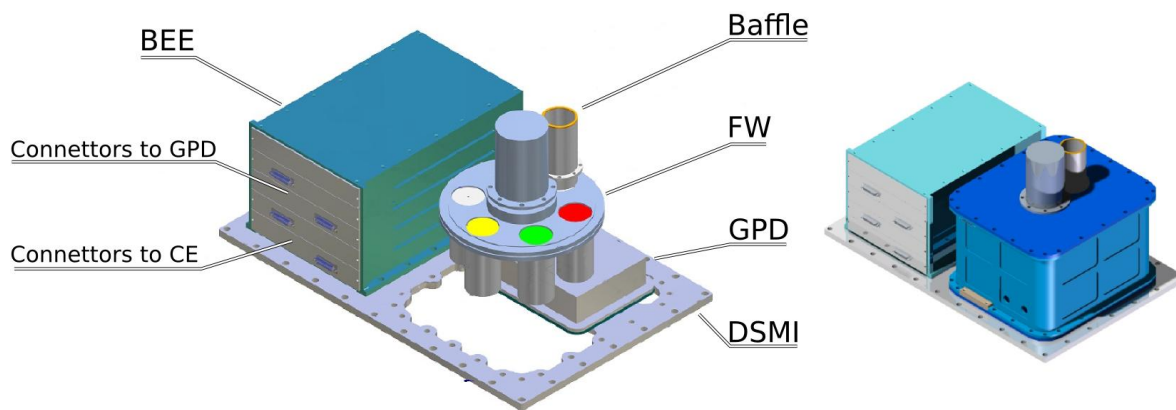


Figure 31 Sketch of the Detection Set.

will study a similar source based on photodiodes, similar to that devised for Astro-H, which does not require any radioactive material (Modulated X-ray Source, MXS, de Vries et al. 2012).

The BEE will comprise 4 electronic boards dedicated to:

- distribute and filter the Low Voltage Power Supplies (LVPSs) required for the ASIC operation;
- generate and filter the High Voltage Power Supplies (HVPSs) required for the detector operation. Each GPD requires three high voltages in the range 0÷-3.5 kV. The values will be programmable with a 10 bit DAC.
- program and manage the ASIC;
- digitally convert the analog output of the ASIC;
- store auxiliary information related to each event (e.g. X,Y coordinates of the ROI corner);
- tag the event with the differential time with respect to the previous event with at least 8μs resolution;
- digitally perform some basic processing (pedestal calculation, suppression of the pixels in the ROI which were not-hit). An event ROI of, on average, 600-800 pixels is zero suppressed by the BEE to about 50-60 pixels.
- temporarily storing the converted data from the ASIC;
- integrate some House Keeping (HK) and Science Ratemeters related to the detector activity (e.g. good event, rejected events, ...);
- interface the Peltier driver for the detector temperature control;
- transmit to the Control Electronics (CE, see below) the science data to be processed;
- provide instrument HK to the CE for active monitoring and telemetries purposes.

A laboratory BEE is routinely used in the laboratory; an eventual flight model foresees the use of a Rad-Tolerant (200 krad dose) ACTEL FPGA RTAX2000S chip running at 40 MHz, a 20 MHz sample/s 14-bit High-Reliability ADC and a SPARC Leon-3FT processor. For analog signal integrity reasons, the BEE should be placed close to the detector, at a distance <20cm.

The three independent DSs interface with the spacecraft through the Control Electronics, described in the next Section. A functional diagram of the FPA is reported in Figure 33.

4.3. Control electronics

The Control Electronics (CE) are a data processing box which also controls the three DSs, interfacing them and the spacecraft. The CE:

- manage three serial interfaces with the three instrument to:
 - configure the corresponding BEE;
 - manage the digital HK periodic acquisition;
 - retrieve and format the science data;
- convert the differential time tag of the event in Universal Time (UT) with 10μs accuracy. The on-

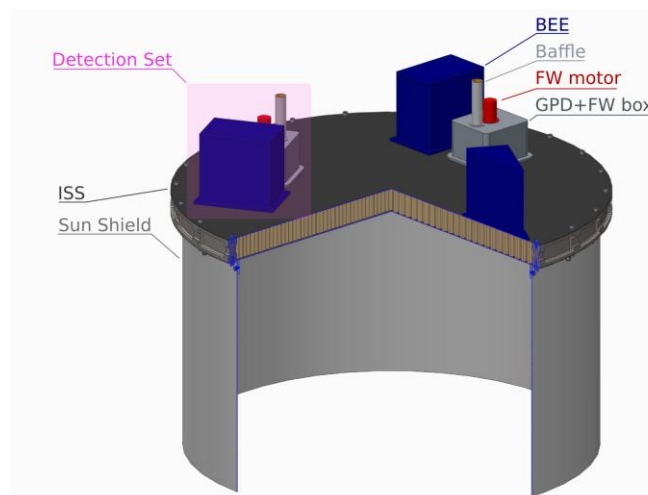


Figure 32 Accommodation of the DSs on the FPA.

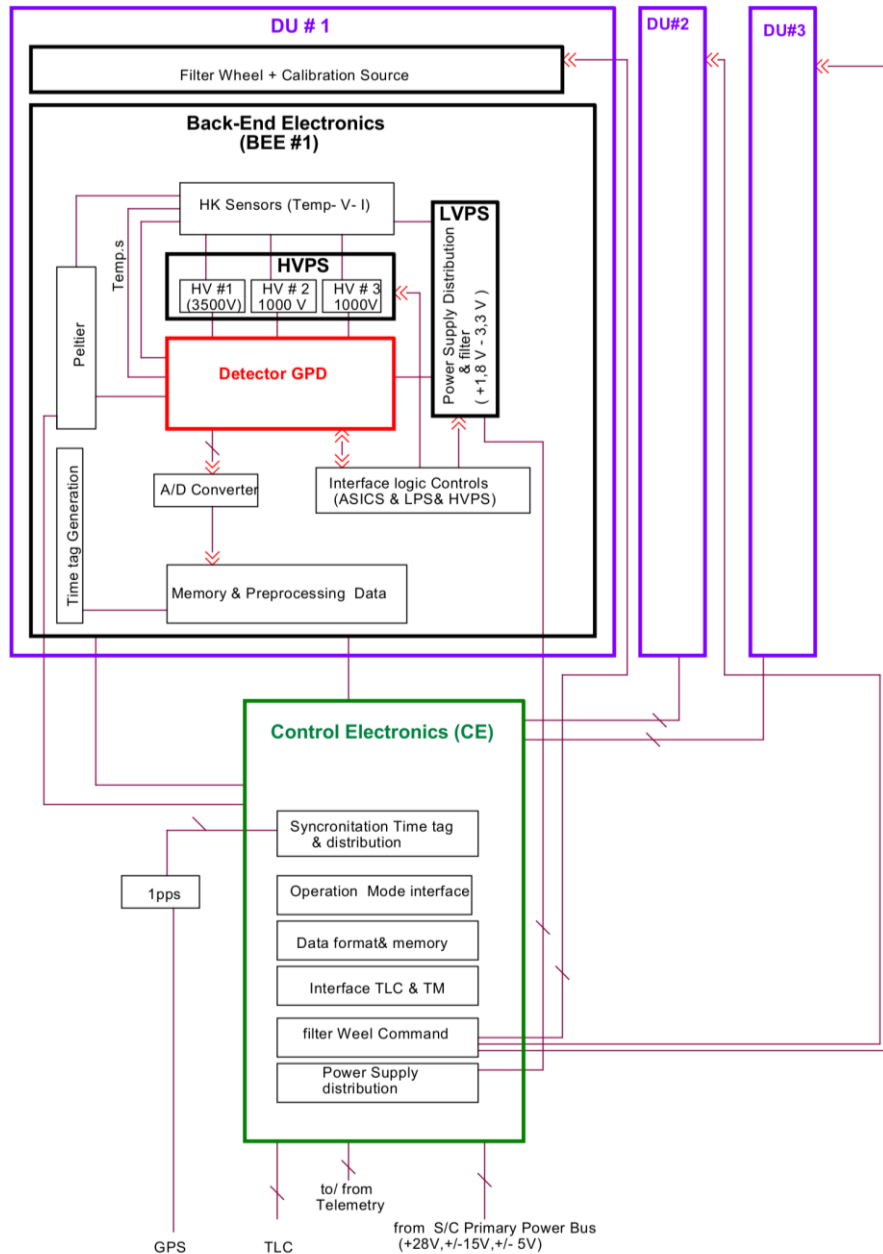


Figure 33 Functional diagram of the FPA and of the CE.

board time and the UT will be synchronized with a Pulse Per Second (PPS) synchronization signal, provided by the GPS in the bus.

- in case of high science data rates, store this data into a Payload Mass Memory of 8 Gbyte, before sending them to the on-board data handling for the downlink. This is the worst case, corresponding to the storage of 20 ks of Crab Nebula observation if only the S-band (no X-band) is available for the downlink.
- manage one filter wheel for each detector;
- drive one Peltier driver for each instrument, to implement the detector thermal controls with an accuracy of $\pm 2^{\circ}\text{C}$;
- manage the DS Operative Modes, which are:
 - “OBSERVATION”, devoted to the acquisition from celestial sources.
 - “PHYSICAL CALIBRATION”, to acquire X-ray data from the calibration source of the filter wheel. The format of the data are as in the “OBSERVATION” mode.
 - “SAA”, devoted to the passage in the South Atlantic Anomaly. We foresee to lower the top GEM voltage to have no gain from the GEM. HKs are acquired.
 - “DIAGNOSTIC” mode to make a diagnostic of the ASIC addressing the single pixel or a group of pixels.

- “TEST”, where the payload parameters (e.g. thresholds or other parameter of the ASIC and HVs) can be changed by telecommands and the performance is evaluated by acquiring X-rays from celestial source, filter wheel or with an electrical stimulus.
- In each operative mode the nominal set of parameters for each DSs is defined by a fixed telecommands stream uploaded in the “IDLE” mode.
- manage three dedicated interrupt lines to trigger the science data retrieval of the already pre-processed data from the BEE;
- manage one multiplexed differential analog line to periodically acquire the analog HK of each instrument (voltages, currents, temperatures,...). We assume to acquire up to 16 analog values (already conditioned inside the BEE);
- manage the non regulated primary power bus in order to carry out all the secondary voltages needed by the unit;
- manage one MIL-1553 A&B data interface with the spacecraft. This link is used to get TC from the Spacecraft and to send both Science and HK telemetry packets.

From the functional point of view, the CE shall also:

- parse and execute the TCs coming from the Bus;
- generate scientific and HK telemetries;
- generate messages, warnings and error reports;
- implement the detector thermal control algorithms;
- control the positioning of the three Filter Wheels;
- A to D convert all the Payload analog HK lines both for thermal control, position control and HK purposes;
- perform the Instrument Control Function, i.e. the active monitoring of some Payload safety critical parameters in order to implement a nearly real-time reaction to avoid damage.

In our baseline, the CE (see Figure 34) is mounted on the ISS, on the same side with respect to the DSs. This choice allows to simplify the AIV (Assembly Integration and Verification) phase, because the FPA and the CE can be integrated on a common interface (the ISS) before the delivery for system integration. Notwithstanding, the CE can be mounted anywhere in the SVM if requested for, e.g., simplifying the thermal control of the FPA. In fact, the communication between the CE and the DSs is through digital signals which can be transmitted for meter-long distances without degradation.

4.4. Ground and in-orbit calibration

The XIPE payload is highly modular and therefore the most sensitive parts, the three MMs and the three GPDs, will first be calibrated separately on-ground; only subsequently will they be paired to perform an end-to-end calibration.

The stand-alone GPD calibration will be performed with polarized and unpolarized X-rays at INAF-IAPS, where a test facility has already been built and routinely used for the calibration of the GPD (see Figure 35, Muleri et al. 2007). Such calibrations will be dedicated to measure the energy resolution, modulation factor, efficiency and spurious polarization at different energies and in different positions of the sensitive area.

The MMs will be calibrated at the PANTER X-ray testing facility of the Max-Planck-Institut für extraterrestrische Physik of Garching (Germany). This facility, used in the past for the calibration of previous experiments such as Exosat, ROSAT, Chandra (LETG), BeppoSAX, SOHO (CDS), XMM-Newton, ABRIXAS, Swift (XRT) and

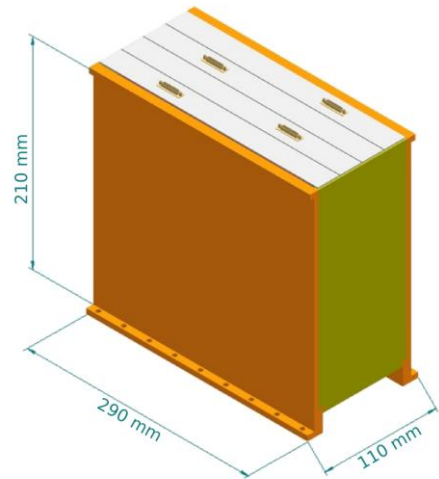


Figure 34 Sketch of the CE with its dimensions.

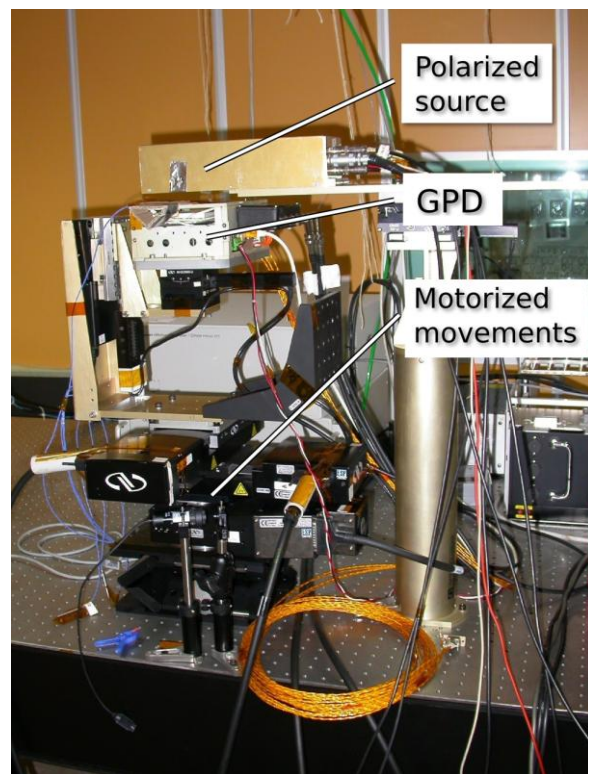


Figure 35 The GPD in the test facility at INAF-IAPS.

eROSITA, is already perfectly equipped to calibrate the XIPE MMs. In stand-alone calibration, a CCD detector and unpolarized photons will be used to measure the PSF at different energies and in different off-axis positions. The end-to-end calibrations, involving an MM and a DS at a time, will be performed again at the PANTER X-ray testing facility but, in this case, we will use both unpolarized and polarized X-ray sources. In the facility there is already available a double crystal monochromator with Silicon and graphite crystals which provides polarized and monochromatic X-ray photons in the 2-3 keV energy range, where the GPD has the maximum sensitivity. The consortium will provide the PANTER with additional crystals for adding more polarized-photon energies. The measurements will be dedicated to: (i) the characterization of the PSF of the assembly at different energies, on and off-axis, with polarized and unpolarized radiation; (ii) the measurement of the modulation factor at different energies in different on and off-axis positions; (iii) study the spurious polarization in different on and off-axis positions.

In-orbit calibrations will be performed using both calibration sources and the few celestial sources with known X-ray polarization. Each DS hosts a filter wheel with three calibrations sources, which can provides monochromatic photons and polarized/unpolarized photons at two energies. These will allow to check the modulation factor, the presence of a spurious polarization signal, the energy resolution and the gain of each detector periodically. Calibration observations will last <100 ks and will be repeated at least twice per year; alternatively, calibration measurements will be performed during the Earth occultation when the observed source is not bright (to not overload the telemetry). In addition to the calibration sources, whose polarization is known with very good accuracy, XIPE will be also calibrated with celestial sources. The average polarization of the Crab nebula is known with good precision ($P=19.2\pm 1.0\%$, Weisskopf et al. 1978) and therefore this source will be periodically (once per month) observed for a short time (10 ks) with XIPE. Similarly, periodic (twice per year) 100 ks observations of Sco X-1, whose emission is polarized below 1.0% (Long et al. 1979), or Capella, whose X-ray emission is thermal, will be used to verify the absence of a spurious polarization signal. Imaging capabilities will be verified during the Science Verification Phase with a long pointing (500 ks) on Cas A.

4.5. Cleanness requirements

Mirrors are the payload component most susceptible to cleanness, therefore requirements of the mirror during all phase of the mission is given. The cleanness requirements on the mirror are less than 300Å molecular surface contamination at EOL, less than 200Å on the ground, and less than 100Å in orbit; less than 4% particulate obscuration at launch. The cleanness of the other items are not critical and a clean-room class 100.000 is sufficient for the other payload items on ground.

4.6. Payload resources

4.6.1. Telemetry

The scientific data generated by the GPD are the image of the photoelectron track, together with the time of arrival and the energy of the absorbed photons. Therefore, for each event, the telemetry must encode information on:

- the address and the charge content of each fired pixel into the ROI;
- the time tag, the energy and the absolute coordinates of one of the ROI vertex.

Such information can be encoded with different formats, which have been already identified during the IXO Assessment study and require about 1 kbit per track. In particular, the most efficient one is organized as follows:

- the sole energy content for all consecutive fired-pixels separated by the address of the last pixel belonging to a sequence of non-fired pixels (transition);
- the time tag, the total energy and the absolute coordinates of the ROI vertex.

The number of bits required for each field is shown in Table 5. The formatting of the science telemetry is in charge of the CE.

A bright source like the Crab Nebula will produce between 1 and 10 keV about 1000 c/s on the three detectors; therefore, the telemetry generated will be 903 kbit/s. If the downlink will not allow to download all the data orbit per orbit, they will be temporarily saved on the CE mass memory and downloaded after the observation, when a fainter sources is observed and therefore the telemetry load is less massive. We report the typical examples for typical source fluxes in Table 6.

Table 5 Telemetry budget. The total is calculated assuming an average of 50 fired-pixels and 15 transitions.

For each photon						For each fired pixel	TOT	
Time	Energy	ROI vertex coord.		ROI XY length		TOT	Energy or coord. (+1 bit marker)	
18	8	9	9	6	6	58	13	903

Table 6 XIPE payload telemetry load for different typical sources.

Bright source (Crab Nebula, flux= 1950×10^{-11} erg/cm ² s)	903 kbit/s for 20 ks
Typical source (Her X-1, flux= 90×10^{-11} erg/cm ² s)	42 kbit/s for 200 ks
Faint source (Sgr B2, flux= 0.3×10^{-11} erg/cm ² s)	0.1 kbit/s for 1 Ms
Housekeeping	<4 kbit/s

4.6.2. Payload mass budget

PAYLOAD MASS BUDGET								
	Component	No.	Unit Mass (kg)	Total Mass (kg)	Design maturity margin	Design Maturity Margin (DMM) (kg)	Mass with DMM (kg)	Note
MA	MMs	3	50.4	151.2	20%	30.2	181.4	
	Heater+Baffle+Cover	3	4.3	13.0	20%	2.6	15.6	
	MMS	1	10.0	10.0	20%	2.0	12.0	
	Harness	1	1.0	1.0	20%	0.2	1.2	Heaters only
	MA TOT:			175.2	MA TOT with DMM:		210.2	
FPA	GPD (incl. Peltier)	3	0.6	1.8	20%	0.4	2.2	XPOL/IXO
	GPD cover box	3	1.3	5.4	20%	1.1	6.5	XPOL/IXO
	BEE (incl. HVPS, LVPS, #4 cPCI cards)	3	1.6	4.8	20%	1.0	5.8	XPOL/IXO
	FW+CS+Baffle	3	1.55	4.7	20%	0.9	5.6	XPOL/IXO
	DSMI	3	0.5	1.5	20%	0.3	1.8	XPOL/IXO
	ISS	1	9.0	9.0	20%	1.8	10.8	
	Sun Shield	1	9.0	9.0	20%	1.8	10.8	
	FPA harness	1	3.0	3.0	20%	0.6	3.6	8% FPA mass
	FPA TOT:			39.2	FPA TOT with DMM:		47.1	
CE	CE	1	5.5	5.5	20%	1.1	6.6	
	Harness	1	1.0	1.0	20%	0.2	1.2	10% CE mass
	CE TOT:			6.5	CE TOT with DMM:		7.8	
PAYLOAD TOT:				220.9	PAYLOAD TOT with		265.1	kg

4.6.3. Payload power budget

PAYLOAD POWER BUDGET								
	Component	No.	Design Maturity Margin (DMM)	Unit power Avg with DMM (W)	Unit power Max with DMM (W)	Power Avg with DMM (W)	Power Max with DMM (W)	Note
MA	Heater	3	20%	20	20	60	60	SAX, XMM
	MA TOT with DMM:						60	60
FPA	GPD	3	20%	0.6	2.0	1.8	6.0	XPOL/IXO
	Peltier	3	20%	1.4	2.0	4.2	6.0	XPOL/IXO
	BEE (excl. HV)	3	20%	5.0	5.0	15	15	XPOL/IXO
	HV	3	20%	0.6	1.8	1.8	5.4	XPOL/IXO
	FW	3	20%	0.0	6.0	0.0	6.0	Only one operative at a time
	FPA TOT with DMM:						22.8	38.4
CE	CE	1	20%	31.2	31.2	31.2	31.2	XPOL/IXO
	CE TOT with DMM:						31.2	31.2
PAYLOAD TOT with DMM:						114.0	129.6	W

4.6.4. Volume of the main payload elements

PAYLOAD VOLUME				
	Component	No.	Volume	Note
MA	MM	3	Ø458 mm, h=600 mm	See Figure 15
	MMS	1	Ø930 mm, h=20mm	
	Baffle	6	h= 400 mm	
FPA	GPD+FW+Baffle	3	170x190x180 mm ³	XPOL/IXO heritage
	BEE	3	140x190x100 mm ³	XPOL/IXO heritage
	ISS	1	Ø900 mm, h=20mm	POLARIX heritage
	Sun Shield	1	h= 900 mm	POLARIX heritage
CE	CE	1	290x110x200 mm ³	XPOL/IXO heritage, see Figure 34

4.7. Payload TRL

Item	Mission Funding Agency	TRL (ISO SCALE)	Rationale
Mirror Modules	ESA	6	The mirror modules are produced by a well proven thin foil Ni-replica technique. Mirror of this kind were produced for NHXM (proposed for ESA M3) and a complete assembly of 7 telescopes for eRosita.
Mirrors Mounting Structure	ESA	6	To be designed and produced. Based on the previous integration experience of JET-X/SGR and XRT/Swift and on the heritage study performed for POLARIX, SIMBOL-X, NHXM (then proposed for ESA/M3) and eROSITA.
MM thermal system	ESA	6	To be designed and produced based on SAX and XMM implementation and ASI accomplished Phase A for POLARIX.
MM optical/thermal baffles	ESA	6	Already developed for JET-X/Spectrum X-Gamma, two new thermal baffles fabricated and flying on the XRT/Swift.
GPD+BEE	ASI/IT TEKES/Fi CNSA/China	6+5	Heritage is about 15 years for prototyping/tests/calibration included thermal/thermal vacuum, vibration up to 11.2 g and Fe ions irradiation equivalent to 40 years in LEO orbit, performance tests, including successfully accomplished phase A for POLARIX and XEUS/IXO with a TRL 6 (ISO SCALE) assigned by ESA.
HVPS/LVPS	SRC-PAS/PL	6	DIOGENESS, RESIK and RF-15I spectrometers used gaseous detectors and were equipped with HVPS build at SRC-PAS.
Control Electronics & EGSE	DRL/DE	6	Based on a long-standing heritage of such devices already flown and operated successfully on the high-energy experiment HEXE on-board the MIR space station, ROSAT, the FUV-EUV telescope ORFEUS on-board ASTRO-SPAS, the instrument IBIS on INTEGRAL, the EPIC-pn camera on XMM-Newton as well as the failed mission ABRIXAS. Recent developments include prototypes for successful studies performed for MIRAX, SIMBOL-X and the HTRS on-board IXO.
BACKG. Issue/Antic.	SNSB/SE	8	The anticoincidence relies on a simple thin plastic scintillator slab placed below the GPD, with therefore a very high TRL.
Filter Wheel	UKSA/UK ASI/IT NSO/NL CNSA/China	9	MSSL has produced filter wheels for both space instruments (XMM/OM, Swift/UVOT, Beagle II/WAC, ExoMars/WAC ISO/LWS) as well as a ground based calibration system for JWST/NIRSPEC. Only small modifications are required for XIPE.
ISS	CDTI/ES	6	Payload structure is based on well proven and simple concept. Based on the heritage of INTEGRAL.

Telescope Supporting Structure	ESA	6	Heritage: XMM, XRT/Swift. The TSS is considered a part of the bus.
BUS	ESA Proc.	7	A possible Bus for XIPE is Prima Science studied for ASI phase A study of POLARIX which hosted an analogous payload.

5. Proposed mission configuration and profile

5.1. Proposed launch vehicle

The mission concept is based on an injection into a circular, low equatorial orbit by the VEGA Launcher. The considered orbit for XIPE is of LEO type, and has the following characteristics:

Table 7 Characteristics of the XIPE orbit.

Altitude	(550 +/- 16) km for 3-year mission and un- controlled re-entry.
Inclination	5°+/-1°
Eclipse duration	36 minutes max
Ground Station	Malindi
Ground station visibility	8 - 11 min

The typical VEGA mission includes a three stage sub-orbital ascent (Vega User's Manual, Issue 4/ Revision 0, April 2014). The satellite will benefit from the VEGA capability to deliver it directly into its circular orbit:

- a first AVUM (Attitude and Vernier Upper Module) burn for transfer to the intermediate elliptical orbit with an altitude of apogee equal to the target value;
- a second AVUM burn for orbit circularization, and
- a third AVUM burn for de-orbit or orbit disposal maneuver.

VEGA performance data for circular orbit missions with different inclination and altitudes are presented in Figure 36. The mass at launch of XIPE (see Section 5.22.2) is more than a factor 2.2 smaller than the performance of the VEGA.

The VEGA Launch Vehicle can be launched at any day of the year and any time of the day. The inaccuracy of the planned launch is less than one second, by taking into account the dispersions in the launch sequence and start/ignition processes. The launch window and its impact on performance are calculated as part of the launcher mission analysis. The launch vehicle attitude control systems are able to orient the satellite to the desired attitude, including maneuvers for thermal control and Sun-angle pointing constraints.

The payload adapter's separation systems are designed to deliver a minimum relative velocity of 0.5 m/sec. Nevertheless, for each mission, Arianespace will verify that the distances between separated spacecraft and launch vehicle are sufficient to avoid any risk of collision and, if necessary, the separation system will be adequately tuned. According to a defined launch trajectory and timeline, the LEOP (Launch and Early Orbit Operations) and injection will be visible from defined G/S (Ground Station).

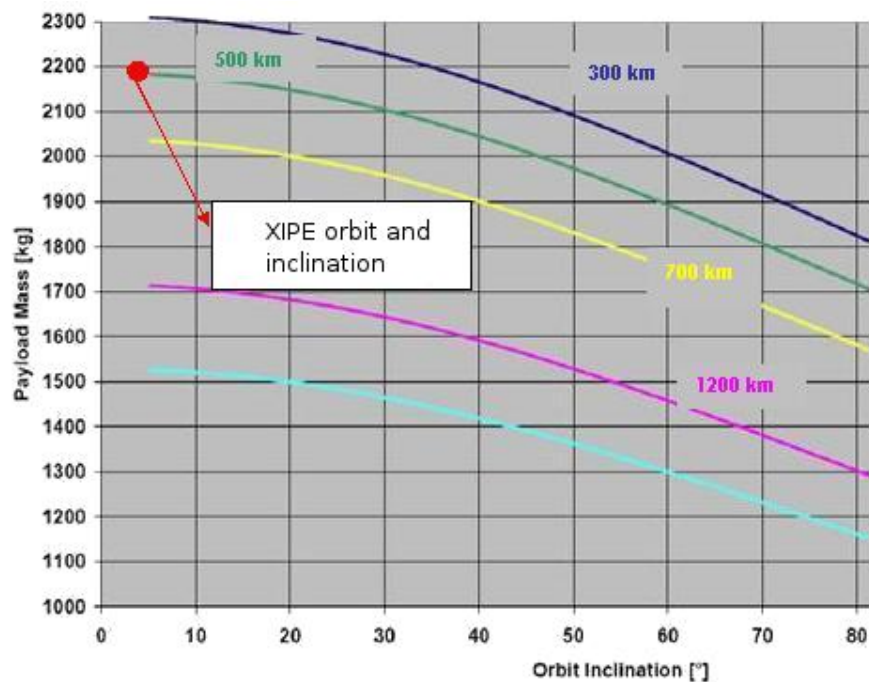


Figure 36 LV (Launch Vehicle) performance for the nearly circular orbits of XIPE. The XIPE dry mass (including margins) is 877 kg (see Section 5.22.2).

5.2. Mission overview

The nominal mission duration is three years including 1 months for commissioning, 3 months for the Science Verification Phase (SVP), and 1 month for decommissioning.

For the low orbit inclination foreseen, every orbit has an eclipse from the Earth of about half an hour, with a small seasonal change up to 36 minutes. From the eclipse point of view, every day of the year is equivalent for launching. By assuming launch in 2025, XIPE will be put in orbit at about the maximum of the solar activity phase (see Figure 37). The consequence is a

quicker altitude decay in the first years of the mission. Even the solar flares, very castigating events for a LEO altitude, are more frequent and strong around the solar maxima. If the launch is delayed, a period of decreasing solar flux is met and then the decay lasts longer if the same altitudes are adopted.

Considering such a mission profile, the XIPE spacecraft (S/C) can be designed considering the guidelines reported hereafter.

5.3. Satellite controlled re-entry

Having a mass smaller than 1000 kg (see Section 5.22.2), **controlled re-entry is not necessary**; however the height of the satellite is chosen in order to have a re-entry with spacecraft main resources still operational.

5.4. Propulsion

The spacecraft propulsion can be sized considering that it must allow to:

- modify the orbit elements at injection, in order to cover initial orbit dispersion due to the launcher;
- cover orbit collision maneuvers.

No orbit maintenance maneuvers are planned because the natural orbit decay is well inside the mission duration period. A preliminary ΔV budget is shown in the budget section (see Section 5.22.1).

5.5. Ground station

XIPE must be supported by one dedicated low latitude ground station at least, like Malindi, which has the following co-ordinates and minimum elevation:

Table 8 Malindi G/S characteristics.

Ground station	East longitude[°]	Geocentric Latitude[°]	Minimum elevation [°]
Malindi	40.2092	-2.9165	5

The Malindi ground station is optimally located for the near-equatorial XIPE satellite orbit. The coverage pattern (see Table 9) for this LEO altitude is a regular sequence of contacts, 15-16 per day, once per orbit, each one followed by a gap of about 85 min. The passage duration decreases with time due to altitude decrease and consequent orbital velocity increase.

Malindi represents the baseline Ground Station upon availability of X-band, the alternative is Kourou in French Guiana where X-band antenna are available.

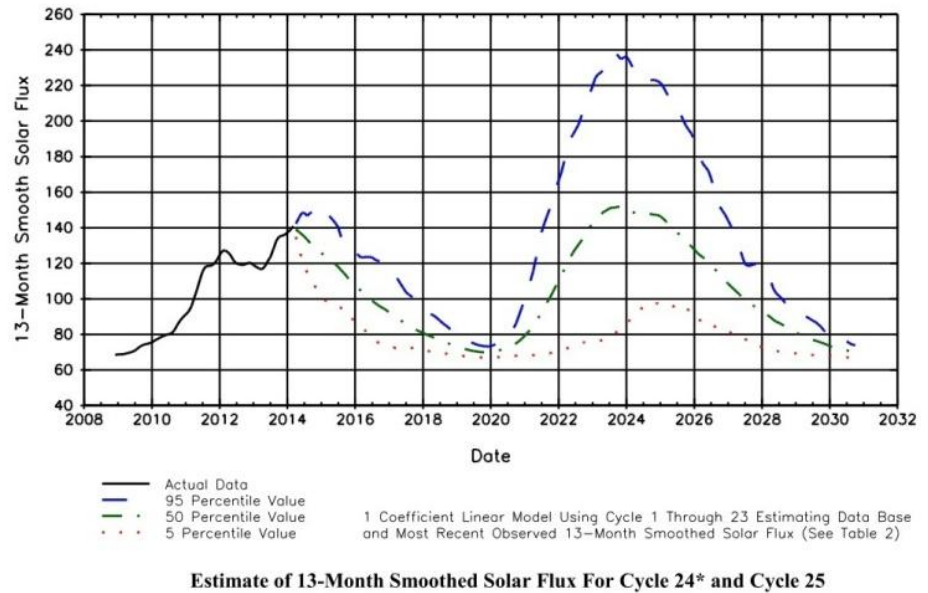


Figure 37 Plot of (October 2014 Bulletin) Monthly Mean and 13-Month Smoothed Solar Flux (max 95%).

5.6. Observation strategy

Table 9 Malindi G/S coverage, values at beginning of Mission.

The use of X-band allows for downloading data at a maximum rate of 10 Mbit/s including coding. Our observation strategy will be to observe a bright source interleaved by an

Average Duration [min]	8 (worst case initial altitude)
Average daily duration [min]	120.5
Access per day (Average)	15

observation of dim sources to allow for downloading all the data of the former. In case of an observation of 20 ks of the Crab nebula, about 3 orbits are needed for downloading the data; such an observation will likely be followed by an observation of an AGN, a magnetar or a molecular cloud which can last days with a negligible memory occupation and downloading time.

5.7. South Atlantic Anomaly interference

When the satellite approaches the meridian at 45° West, it's in the closest position to the South Atlantic Anomaly (SAA or Brazilian anomaly, latitude 25 °S), that presents a regional decrease of the Earth magnetic field intensity. It extends over an area of several thousand square km, under the nearby portion of the Van Allen belt. This causes a reduction of the background proton flux shielding. Satellites crossing this region of space are bombarded by energetic protons at a rate of some thousands hits per square centimeter per second. Nonetheless, if the satellite orbit inclination is low, the SAA influence is the weakest possible: the total radiation dose remains limited to 2-3 krad, and is therefore very limited and not considered a concern for XIPE. The conservative case corresponds to a satellite position close to the meridian of the SAA at the lowest latitude that is a periodic event due to the node drift. As an example, past simulations performed over 100 orbits at altitude 600 km (worst case height for radiation) showed that during 5- 6 orbits the proton flux is $> 10 \text{ cm}^{-2} \text{ sec}^{-1}$ for time intervals up to 6-7 min; a period of 8-9 orbits follows where the proton flux does not exceed this threshold. The GPD was successfully tested in operation when irradiated by 500 MeV/nucleon Fe ion (see Section 4.2.2) so it is not necessary to switch off the detector. However a further caution is possible by just lowering the “top” GEM voltage to prevent the multiplication of the charge released in the drift region.

5.8. Phases Definition

Mission phases can be divided as follows: (1) LEOP (Launch and Early Orbit Operations) (2) COP (Commissioning Phase) (3) POP (Payload Calibration) (4) MOP (Measurement Phase). (5) EOP (End of Mission Phase)

5.9. Ground Contact

The Malindi ground station is optimally located for the near-equatorial XIPE-Satellite orbit. The coverage pattern for this LEO altitude is a regular sequence of contacts; it is foreseen to have 15 contacts a day with an average duration of 8 minutes each and an average contact period of 120.5 minutes a day. Assuming this contact time and a TM data rate of 10 Mbit/s (X-Band with Reed-Solomon coding), the data downloadable volume is 72 Gbit/day. Based on the fact that it is not requested to send TC during the pass, uplink set-up is not needed and this avoids time consumption in a very short duration contact with ground.

Regarding the downlink, since it is not possible to leave the transmitter powered during the entire orbit period, the transponder transmitter shall be switched on by MTL (Mission TimeLine) before each contact and switched off after the data transmission by MTL as well. The most demanding observation in terms of data collection is the observation of the Crab Nebula. For this source 20 ks of observation will be downloaded in about 3 Ground Station links by using X-band.

5.10. S/C Modes

The SpaceCraft (S/C) modes define the S/C configurations at different conditions during the mission. Modes are however not identical to mission phases (see Figure 38). There is not always a fixed set of telecommands implemented to initiate transitions among these modes. This is because the modes, such as failure mode or safe mode, are not entered or left at unique conditions. Nevertheless, such system modes facilitate the operations because they can be used to define conditions for the execution of operational procedures. Whenever possible, information on the kind of transition is given, for example if it is triggered by ground command or by an autonomous onboard action

- **OFF Mode.** The OFF Mode is used during Ground Storage, transportation, payload integration, installation of the satellite on the launcher, or in the frame of mechanical assembly / disassembly activities and also for vibration testing. The satellite is not powered.

- **Pre-Launch Mode.** The Pre-Launch Mode will be used during final preparation and check-out activities on the launch pad. It is automatically entered when the satellite is switched on. In this way it will be used also during all ground testing.

- **Launch Mode.** The satellite is in the Launch Mode from removal of the umbilical connector until separation. In this phase the platform equipment receives power from the battery. The Satellite Management Unit (SMU) is active and the XIPE On Board software executes. The ACS (Attitude Control Subsystem) remains fit in Stand-By Mode to assure that no actuators are commanded. The SMU observes the separation switches continuously. TM packets generated are stored in a mass memory and can be dumped later to ground. The telecommand and telemetry link is interrupted.

- **Acquisition Mode.** The Acquisition Mode is used to bring the platform from the coarse pointing attitude to a fine pointing attitude and after this in the drag free status. The Acquisition Mode is entered autonomously upon detection of the separation of the platform from the launcher. The platform starts autonomously rate damping and acquisition of a stable Sun orientation.

The thermal control is active and ensures that thermal stable conditions are maintained. Transmitters are switched on and telecommands from ground can be received and executed. After transmitter switch on, the ground will receive cyclic housekeeping telemetry collected and formatted by the platform application software. In addition, High priority telemetry (HPTM) is collected by the SMU telemetry module and provided as formatted TM packets. HPTM generation is a pure hardware-based function and allows the ground to monitor essential housekeeping parameters without involvement of the platform application software. The platform remains in Acquisition Mode until the ground commands the transition to the Calibration Mode.

- **Calibration Mode.** The Calibration Mode is used to collect all necessary data to calibrate by ground calculations the whole satellite in order to achieve the required performance.

- **Science Mode.** The Science Mode is the ultimate mission mode, i.e. to collect the scientific measurement data from the payload while the Drag Free and Altitude Control (DFAC) maintain the platform in its drag free state. The platform remains in Science Mode for the complete mission phases measurement (potentially interrupted by further calibration phases).

- **Survival Mode.** The platform enters autonomously in the Survival Mode upon detection of one of following four major system failures. - Sun aspect angle anomaly - Attitude rate anomaly - Battery anomaly (low voltage) - SMU reboot or switch-over. In Survival mode, the P/L is switched off. The thermal control is operated at lower temperatures than nominal for power saving reasons. The platform design foresees to exit from Survival Mode only by appropriate sequences of ground commands.

- **Re-entry Mode.** The Re-entry mode is the final phase of the mission, during which no scientific activity is performed, but during which the satellite will be monitored.

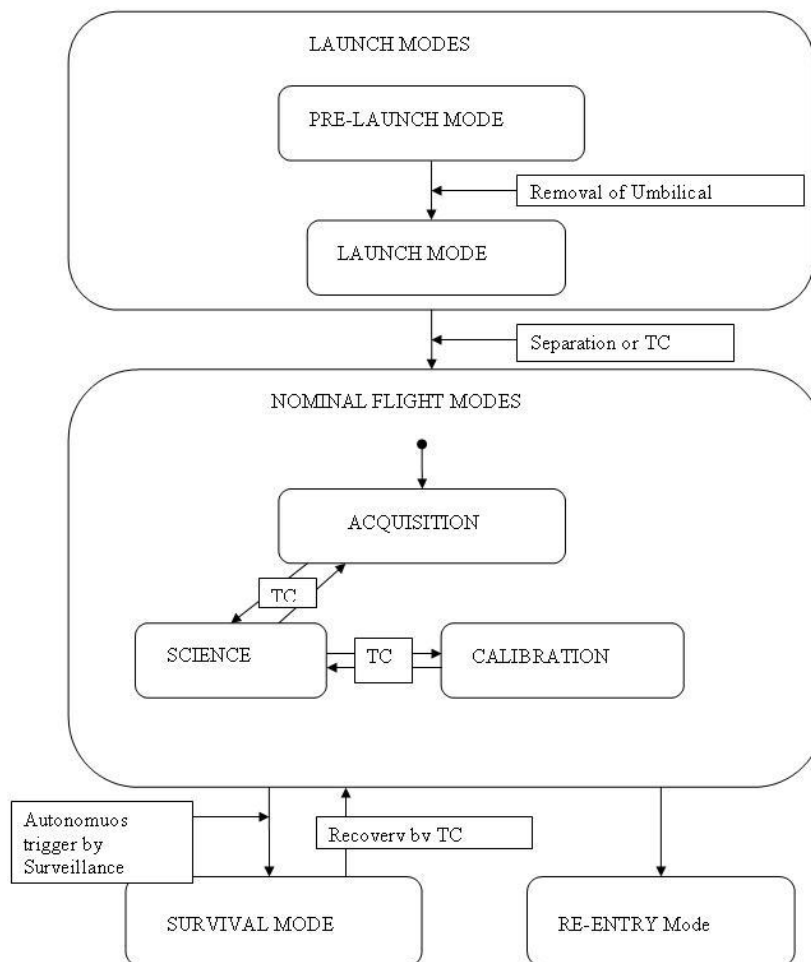


Figure 38 XIPE operative modes.

5.11. Mission Control Concept

A high level of system autonomy is the main design driver to allow achievement of the mission objectives. XIPE on-board autonomies have the twofold function of executing S/C operations when there is no Ground Station visibility and of recovering S/C nominal operation, when malfunctions are detected on board. The satellite control

concept will be essentially based on “non-real-time” operations planning. The main XIPE mission autonomy requirements are recalled hereafter:

- The XIPE spacecraft shall perform autonomously nominal operations when ground intervention is not possible.
- The XIPE spacecraft shall remain safe for a period of at least a few days without ground intervention.
- The satellite shall respond to on-board failures by switching, independently of ground control, to redundant functional path. Where this can be accomplished without risk to satellite safety, such a switching shall enable the continuity of the mission timeline and performance. In the event that alternative redundant paths do not exist or that the failure effect is too complex to allow autonomous recovery, the satellite shall enter Survival Mode.

Mission operations requiring a reaction within a few hours (critical operations) shall be clearly identified by the available telemetry transmitted to ground. They shall be reduced to a minimum and limited to specific mission phases (e.g. LEOP).

In order to cope with the ground station visibility constraints and autonomous control concept, the design of the subsystems and instrument operating modes has to be done having in mind the reduction to a minimum of the number of commands required for nominal operations in absence of anomalies.

In addition, the following on-board functions will be implemented, in order to increase the overall autonomy:

- **On-board Mission TimeLine (MTL):** this facility contains the commands needed for control and execution of all the routine operations.
- **On Board Monitoring Function (OBMF)** this facility is capable of monitoring ground selected parameters during the non-visibility periods. Such monitoring is checked against limits or range verification. Specific action (i.e. events generation and command execution) can be programmed in case of out of limit/range is detected by the on board monitoring function.

The S/C nominal commanding will be executed via the on-board MTL independently of whether the satellite will be in visibility from ground or not.

Anomaly messages will be generated as a consequence of failure occurrences and stored on-board in the System Log. Periodical housekeeping telemetry will be generated as well. Anomaly, on-event messages and periodic telemetry retrieval will be performed during ground contacts, in order to reconstruct on ground S/C nominal and contingency actions taken during non-visibility periods.

Fault Detection Isolation and Recovery (FDIR) functionalities will be implemented on-board in a hierarchical manner. In order to prevent S/C permanent degradation or loss of the mission and to guarantee satellite safety in any operational circumstance, every failure recovery action will be taken at lowest possible level. In principle, the first attempt will go in the direction of minimizing the S/C reconfigurations needed to recover the malfunction, maintaining the measurement production.

Mission operations are mainly performed autonomously (contact periods are very short compared to the orbit duration). Therefore, if predefined fault conditions will be detected, the S/C will be able to autonomously react to recover and continue the nominal operations. Any failure or anomaly occurrence will be notified via dedicated anomaly packets, anyhow. When in Survival Mode, all the essential on-board functions but FDIR provisions will be maintained available.

5.12. Spacecraft Design

The XIPE mission is based on a concept design inherited from both old (BeppoSAX) and in-house ASI Phase A studies experiences (SIMBOL-X, POLARIX, NHXM) in the field of X-ray missions. The satellite can be designed and manufactured with large use of standard equipment. No new development is required for any aspect of the S/C. In some cases the effort has been concentrated on the optimization of the performance, reducing the complexity of the mission and the associated costs.

The main components of the S/C are:

- the Service Vehicle Module (SVM), which provides all the necessary functions to the operation of the scientific instrumentation (Thermal Control, Structure, On Board Data Handling, Telecommunications with ground, Attitude and Orbit Control, Electrical Power generation and distribution, interface with the launch system) and accommodates the Mirror Assembly (MA).
- the 3.5 m Telescope Supporting Structure (TSS), which realizes the distance between the Focal Plane Assembly (FPA) and the MA along their main axis, provides interfaces with the FPA while upholding alignment between each detector and the corresponding Mirror Module.

The main elements belonging to the Scientific Payload (P/L, see Figure 11) are:

- the MA, which includes the three Mirror Modules (MMs);
- the FPA, accommodating the 3 detectors;

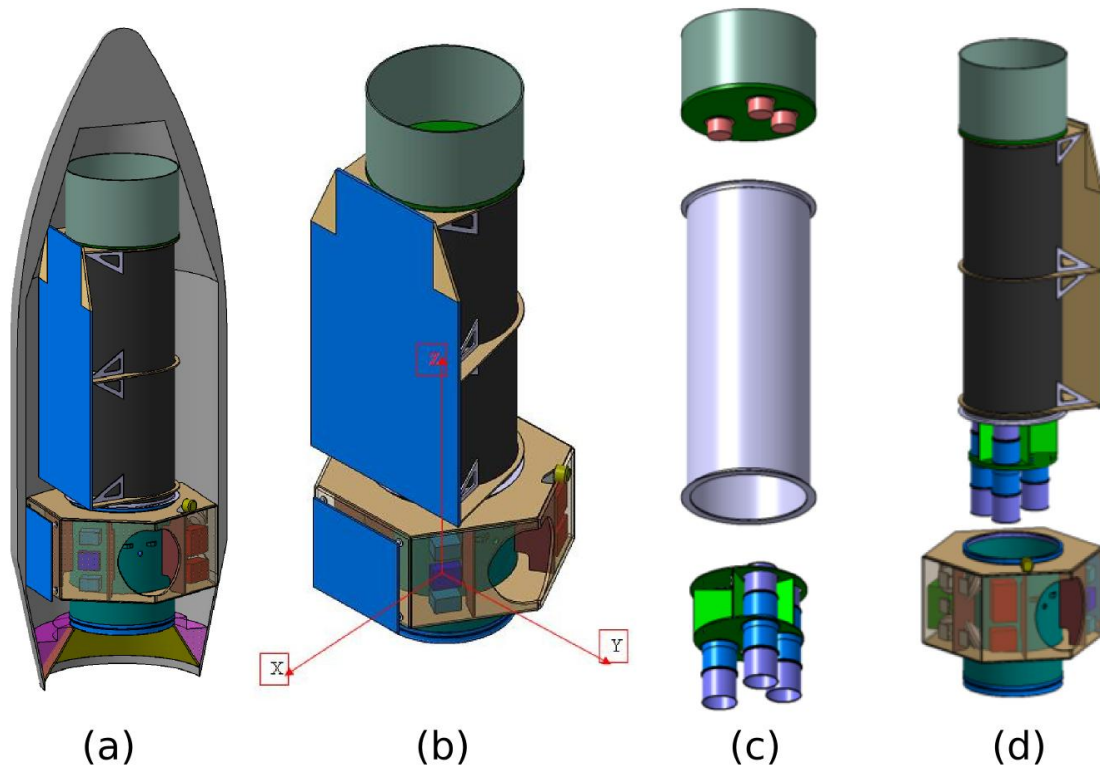


Figure 39 (a) XIPE in the Vega fairing. (b) The complete spacecraft with fixed solar panels. (c) The three main elements of XIPE (Focal plane assembly, the telescope supporting structure and the mirror assembly (the control electronics are hidden from view). (d) The plug&play approach with SVM (below) and P/L and telescope supporting structure (above).

- the Control Electronics (CE).

The S/C configuration concept is based on strong hardware modularity. The interface between P/L and S/C shall be agreed on both P/L and S/C sides. This concept will be better illustrated in the next paragraphs.

Besides the characteristics of commonalities mentioned above, this S/C concept has noteworthy advantages on the development schedule, thanks to the modularity of the concept. The development of the P/L (the MA and the FPA) can follow a parallel development plan, and their integration can be done in a direct ‘plug-and play’ approach. The S/C main characteristics can be summarized as follows: (1) MMs are accommodated inside the cylindrical thrust structure (2) the TSS rigidly keeps aligned the MA with the detectors on the FPA and the Payload Module with the LOS (Line Of Sight) (3) MMs are shielded against contamination and Sun incidence by thermal blankets (4) **Solar Panels (SP, see Figure 39) are fixed** and they have been sized for the power budget, on the basis of eclipses duration (eclipses are brief, up to 36 min, but many cycles occur during mission lifetime) (5) TT&C has been configured for the ground link requirements, with a limited number of antennas (1+1), providing hemispheric coverage (6) Thermal Control has been based on a passive concept (7) OBDH architecture has been outlined on an in-house-product-based concept.

The SVM (Figure 40) consists of a hexagonal assembly obtained by sandwich panels with Al core. In detail the structure is composed by a central cylindrical tube, joined with six shear panels and two platforms at the lower and upper faces (see Figure 40). This assembly is laterally enclosed by six panels (four hollowed and two integral panels).

The Thrust Cylinder has to withstand the loads experienced by the SVM and by the Telescope Supporting Structure, transferring it to the launcher interface and guaranteeing adequate stiffness to the Service Vehicle Module in order that the entire satellite assembly satisfies the launcher frequency requirements. Its main components are: (1) The lower ring, obtained by a forging plate of 7075-T651 AL-Alloy, (2) The upper ring, which provides the interfaces with the Payload via continuous interface ring, is obtained by a forging plate of 7075-T651 AL-Alloy. The preliminary evaluation of the major resources needed for the XIPE S/C places it in the 1000kg class, well within in the VEGA launcher capability, also from the point of view of purely geometrical sizing, as can be seen in Figure 39. The selected Thrust Cylinder is the 937 mm diameter one (interface with the launcher).

5.13. Thermal Control Design

The thermal control shall be able to meet the following thermal requirements during the entire mission phases and in the different operational modes: (1) Mirror Modules: $20\text{ }^{\circ}\text{C} \pm 2^{\circ}\text{C}$; (2) detectors: $5\text{--}20\text{ }^{\circ}\text{C} \pm 2^{\circ}\text{C}$. For the other units, values assumed are reported in Table 10.

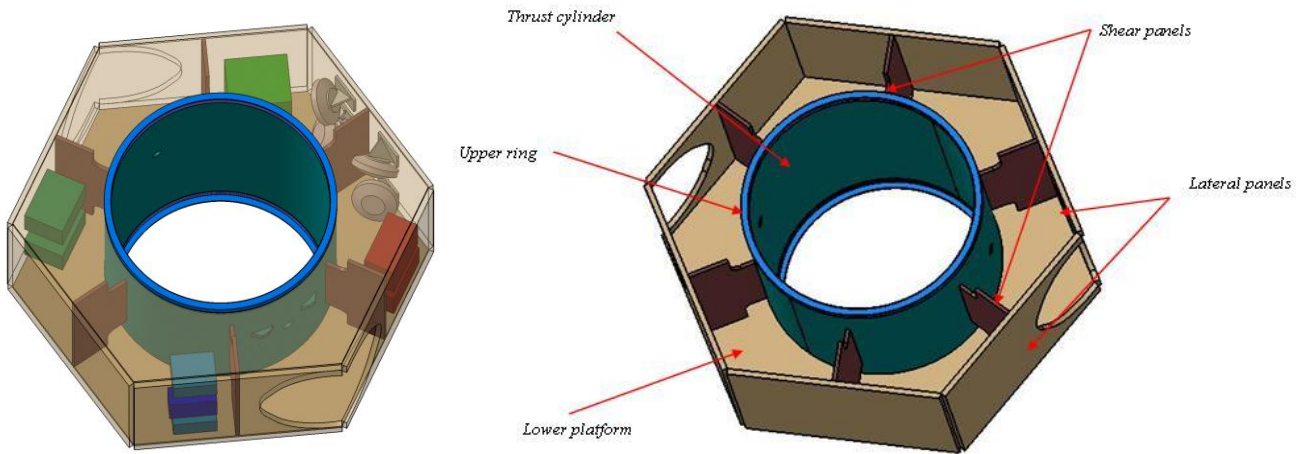


Figure 40 (Left) Overview of the SVM internal configuration. (Right) the SVM structure assembly without top panel.

The thermal control of XIPE can be realized by quite classical approaches and means (see Figure 41). Control of the detectors can be obtained by means of heaters and a radiator, the latter protected from a solar shield (Sun Shield baffle) to avoid direct flows from external environment. The radiator of the Focal Plane has to be always shaded. The solution to avoid exposure to Sun or Earth is the adoption of a cylindrical Sun Shield. For the MMs of XIPE a radiative thermal control approach like SAX and XMM can be adopted. The thermal control is based on the concept to create a hot environment that radiatively controls the optics temperature. For this reason each optic will be provided with two thermal baffles (internal and external) housing the heaters and thermistors for the thermal control and whose extremities are closed by a single kapton layer. From the phase A study of POLARIX it turned out, after thermal analysis, that the thermal philosophy adopted is indeed sufficient for maintaining the temperature within the requirements for either the spacecraft and the payload elements.

Table 10 Temperature requirements.

UNITS	Temperature Requirements			
	MIN OPER	MAX OPER	MIN NOT OPER	MAX NOT OPER
	[C]	[C]	[C]	[C]
TRSP	-10	50	-20	60
CDMU	-10	50	-20	60
GYRO	-20	55	-30	65
RWL	0	55	-10	65
PCDU	-10	50	-20	60
BATTERY	0	35	0	35
RFDN	-20	60	-30	70
BE	-10	50	-20	60
CE	-10	50	-20	60

5.14. Attitude and Control System

The Attitude Control Subsystem (ACS) manages the functions of attitude measurement and control during all phases of the mission. It is composed of dedicated sensors providing all necessary information on spacecraft attitude and rates, and actuators that provide torque capability to control the attitude. Control laws are implemented by dedicated software running on CDMU (Command & Data Management Unit). The ACS software shall be based on adaptations and/or minor customizations of already developed one, preferably based on PRIMA platform. A

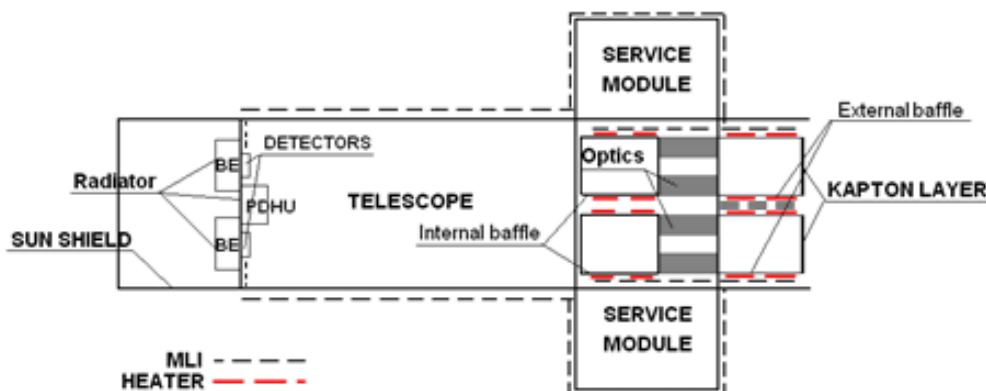


Figure 41 Sketch of the thermal philosophy.

Table 11 XIPE ACS satellite performance.

Description	Bus performance	Note
Accessible sky	all within $90^{\circ} \pm 30^{\circ}$ from Sun direction (corresponding to 1/2 of the sky)	Compliant with Req-Sci-080
Forbidden directions	None	Compliant with Req-Sci-081
Satellite Stabilization	Three-axis	
Absolute Pointing Error	1 arcmin	Compliant with Req-Mis-020
Absolute Pointing Drift	30 arcsec	Compliant with Req-Mis-030
Relative Pointing Error	30 arcsec	Compliant with Req-Mis-040
Absolute Measurement Accuracy	10 arcsec/5Hz	Compliant with Req-Mis-050
Observation	Stared (few hours to 20 days)	Compliant with Req-Mis-060
Number of pointing	150/year	Compliant with Req-Mis-070

multi-head attitude determination system (based on 3 optical heads, to reduce the possible operational impacts related to Earth and Moon) or classical two autonomous star-trackers only (nominal and redundant) have been considered for fine attitude determination taking into account the improvement in performances and reliability, permitting full gyro-less solution. ACS performance is given in Table 11.

5.15. Electrical Power System Architecture

The Electrical Power System (EPS) configuration is based on an Unregulated Bus Architecture with a Battery Bus in the range 24 – 34V and it is composed of the following elements: (1) Solar Array (SA), single fixed panel equipped with GaAs TJ solar cells able to deliver up to 1200 W (EOL) (2) Single Battery equipped with low capacity Li-Ion cells. (3) Power Conditioning and Distribution Unit (PCDU) that conditions the SA power, using a Maximum Power Point Tracking system (MPPT) with buck converters, controls the battery charge, supplies the satellite thermal control heaters, drives the on-board pyro-devices and distributes protected power lines to Platform users. The XIPE Solar Array shall be composed of **two body mounted panels installed in a fixed position** and they will be sized in accordance to the following main design drivers and conditions: (1) Cell type: RWE TJ GAGET 2; (2) Power Sized: BOL 1500W, EOL 1200W; (3) Maximum SAA 30° (4) 1 string in failure. The equipment heritage of the considered PCDU comes from the RADARSAT-2, COSMO-SkyMed and Gaia programmes. The battery is necessary to feed the system while sunlight is not available; i.e. during the Lift-off and the LEOP phase or during the eclipses. The fixed solar array allows XIPE to access the sky within $90^{\circ} \pm 30^{\circ}$ from the sun direction, which corresponds to 1/2 of the sky.

5.16. Data Handling Architecture

XIPE SVM On Board Data Handling (OBDH) architecture is based on a centralised computer for Satellite Service Management and Payload science, the SMU (Satellite Management Unit). The SMU has the task to: (1) Manage all Service Vehicle Module activities, including Nominal Mode and Safe Mode; (2) to reconfigure the satellite; (3) to receive telecommands and to decode them with the help of software or without software intervention (hardware decoded); (4) to store SVM telemetry and to transmit to ground via TT&C X-band link; (5) to collect payload data via 1553 enhanced Interface and to transmit to ground via TT&C X-band link; (6) to run thermal algorithm. The design of the SMU and the relevant interfaces are not a peculiarity of this program and for this reason a complete reuse of already available technologies is envisaged.

SMU architecture relies on a Leon processor that is located on the Processor Module Board. The processor capability is 34Mips at 40 MHz. On the same module, there is 1MB of Non volatile Memory, EEPROM, for storing the OBSW (On-Board Software) code and 2MB of volatile memory, the SRAM, for imaging and registering data storage and computation. The processor module is also allocated the communication via an enhanced 1553 Bus. The reconfigure module is the module devoted to FDIR purposes, which is the reconfiguration due to external or internal alarms. The Power Module provides the secondary voltages to each internal module to SMU.

The interfaces with the P/L is done via an enhanced 1553 Bus. Considering the nominal continuous data rate of 1Mbps, in case of Science Storage which is not considered a nominal situation, a total amount 54000 Mbit per Orbit has to be used. Consequently a Mass Memory of 10 Gbyte is foreseen, which covers all the different possibilities with a large margin.

5.17. Telecommunications Telecommanding and Tracking

The Telemetry Tracking and Command (TT&C) subsystem is in charge of: (1) the RF links with ground stations; (2) the Uplinks for satellite telecommands (TC); and (3) the downlinks for satellite telemetries (TM) and the ranging function to allow range measurements.

The Communication design drivers are: (1) omnidirectional RF coverage to ground; (2) best utilization of existing equipment; (3) identification and procurement of items compatible with the VEGA launcher; (4) Malindi ground station; (5) X-band for U/L (Up Link) and D/L (Down Link). (6) LEO (equatorial orbit at 550 km altitude beginning of mission). For using the X-band maintaining the compatibility with VEGA launcher interfaces, antenna lengths must be less than 20 cm. TM maximum high data rate is 10 Mbps (including Reed-Solomon coding), the maximum data volume downloadable is 72 Gbit/day. Based on the fact that the spacecraft will work as much as possible autonomously, it is not requested to establish the uplink before starting the TM data download: this avoids losing time in a very short duration contact with ground. The transponder transmitter shall be switched on by MTL before each contact and switched off after the data transmission by MTL as well. For this reason, the transmitter must be qualified for a very high number of on/off cycles.

Equipment composing the XIPE TT&C are: (1) 2 X-Band transponders, (2) 2 TWTA (Traveling Wave Tube Amplifiers), (3) 2 Low Gain Antennas. (4) RFDN (Radio Frequency Distribution Network). The transponder identified is designed to support uplink and downlink in X-band and to ensure cold redundancy in downlink and hot redundancy in uplink.

5.18. GPS

This system is to provide the CE and the Back-End Electronics with an accurate synchronization signal to implement an on-board time counter (OBT) able to time-tag the scientific events with the required accuracy of 10 μ s with respect to Universal Time (UT) (Req-Sci-051). The synchronization signal is a high accuracy (w.r.t. to UT) periodic signal to be used to update a local counter incremented by a standard oscillator. Usually this signal has a period of 1 second and it is called "Pulse Per Second": its signal edge shall have the required accuracy (i.e. 1-2 μ s). The simplest way to get such a signal is to use a GPS receiver, as done in other satellites that require an accurate time-tagging. We propose to use a similar unit also for the XIPE mission. A typical GPS receiver is made of the following items: (1) one or more RF antennas depending on their position on the spacecraft, satellite attitude and orbit; (2) a number of RF pre-amplifiers equal to the number of antennas and placed close to them (i.e. < 1 m); (3) a main unit able to carry-out the PPS signal according to the RF signals of the GPS constellation.

5.19. On Board Command and Control

The XIPE On-Board SW implements a set of capabilities relevant to the: (1) management of telecommands and telemetry; (2) management of the SW activity scheduling, on-board communications and on-board memories; (3) support the (central and local) failure management; (4) on-board end-items control.

5.20. Mechanical interfaces

The interface with the VEGA launcher adapter will be driven in accordance with the Launcher authority and as per the VEGA User's manual. The 937 interface is in accordance with the ARIANE availability to implement the corresponding adapter interface.

5.21. Ground Segment and Mission Operations concept

The XIPE Ground Segment (CS) shall be responsible for the following tasks: (1) performing the orbital verification and attitude determination during first mission phases (LEOP); (2) implementing the Observation Plan by translating it into a set of appropriate commands; (3) managing all the satellite operations and all real time contacts with the spacecraft and payload; (4) receiving all the TM data and provide their archiving for back-up safety; (5) forwarding all the scientific TM to the User Segment; (6) carrying out all the verification checks to assess the correct functioning of the XIPE spacecraft; (7) monitoring a set of payload parameters to be able to react in real time to critical anomalies. The XIPE Ground Segment main task is to govern and maintain in operational conditions the XIPE mission. The XIPE Ground Segment shall provide the following main functions: (1) Satellite Monitoring & Control; (2) Satellite Flight Dynamics to support control and mission operations; (3) Telemetry Tracking and Command (TT&C); (4) Mission Programming; (5) Ground Segment Network Communication; (6) Scientific data Ingestion, Archiving and Distribution to the User Segment. The User Segment is articulated as the Science operation Center (SOC) and Science Data Center (SDC), see Section 6.

5.22. Budgets

5.22.1. Power budget

	Functions	Design Maturity Margin	Total Power Avg (W)	Total Power Max (W)	Note
Bus	AOCS (gyro, RW, SAS, ST)	10%	125	124	
	TT&C (RX/TX S-Band, Antennas)	10%	26	69	
	DATA HANDLING	10%	52	52	
	EPS (PCU, Battery, SA)	10%	60	60	
	THERMAL CONTROL (heaters)	20%	50	100	Only for SVM
	Total Service Vehicle Module Power (W)			312	405
P/L	Mirrors Payload	20%	60	60	
	Detector Payload	20%	23	38	
	Control Electronics	20%	31	31	
	Total Payload Module Power (W)			114	129

Spacecraft	Service Vehicle Module (Max)		405	W
	Payload (Max)		129	W
	20 % System Margin		107	W
	Harness Loss		16	W
	PCDU Losses		37	W
	Total power with losses and system margin			694

5.22.2. Mass budget

	Functions	Basic Mass (kg)	Design Maturity Margin (DMM)	DMM (kg)	Current Mass (Kg)
Bus	AOCS (gyro, RW, SAS, ST)	58	8%	5	62
	TT&C (RX/TX S-Band, Antennas)	22	10%	2	24
	DATA HANDLING	26	10%	3	29
	EPS (PCU, Battery, SA)	133	11%	15	149
	STRUCTURE SUBSYSTEM (primary, secondary, TSS)	143	10%	14	157
	PROPULSION	13	10%	1	15
	THERMAL CONTROL (heaters+blanket)	26	20%	5	31
	Total Bus mass (kg)		421		46
P/L	MA (Mirror Assembly) (see	174	20%	35	210
	FPA (Focal Plane Assembly)	35	20%	7	47
	CE (Control Electronics)	11	20%	2	8
	Total Payload Mass (kg)		219		44

Spacecraft	Total Bus Mass (kg)		466
	Total P/L Mass (kg)		265
	System level margin (20%)		146
	Dry mass with margins		877
	Propellant (kg)		16
	Launcher Adapter (kg)		77
	Total Mass at launch (kg)		

5.22.1. ΔV budget for XIPE

Manoeuvre	Geometric ΔV (m/s)	Effective ΔV (m/s)	Margin (%)	Margin (m/s)	Overall ΔV (m/s)	System Margin 5% (m/s)	Total ΔV with margin (m/s)
Orbit Acquisition	14.00	14.29	10.00	1.43	15.71	0.79	16.50
Collision Avoidance	12.00	12.24	0.00	0.00	12.24	0.61	12.86
Total DV	26.00	26.53		1.43	28.0		
System margin (5%)					1.40		
Total DV with margin					29.36		29.36

6. Management scheme

6.1. Consortium organization

The Principal Investigator (P.I.) will be assisted by a project office through an industrial contract mixed with engineers and scientists to manage the interaction with ESA funded by the institutes. A Program Manager and a Project Scientist will be part of the P.I. team. A similar architecture is expected also for the main XIPE subsystems.

6.2. Procurement scheme

The XIPE mission takes advantage of already accomplished phase A studies performed by ASI (Costa et al. 2010, see also the POLARIX Phase A study report in the supporting documentation to the Proposal, Section 8.4) and development studies performed by ESA (XPOL on IXO) but with new mirror modules produced by means of a light-weight, high-performance, thin-shell technology. It relies on a procurement scheme with most critical parts of the payload and of the spacecraft from Europe. Each country will contribute on the basis of expertise and heritages. The procurement scheme is indicated in the product tree (see Figure 42).

We expect ESA to procure the VEGA launcher and the launch services. We, also, expect ESA to provide the MOC and the SOC. Part of the SDC activities will be under the responsibility of University of Geneva (Switzerland, see below) but ESA will have the responsibility of issuing and managing the Guest Observer Program, with XIPE operated as an observatory. We finally expect ESA to procure the Bus, including the Telescope Supporting Structure (TSS) and the Mirror Module Structure (MMS). The baseline Ground Station is Malindi (ASI) but with the option to use Kourou.

The payload (under the responsibility of Italy through the PI-ship) comprises: (1) the Mirror Assembly (MA), (2) the Focal Plane Assembly (FPA), and (3) the Control Electronics (CE). The MA, entirely procured by ESA, is composed of the Mirror Modules designed under the scientific responsibility of Italy (G. Tagliaferri of INAF/OABr, as part of the ASI contribution). The FPA is also under the responsibility of Italy (R. Bellazzini, INFN-Pi, as part of the ASI contribution) and is composed of three Detection Sets. Each Detector Set comprises a polarization sensitive Gas Pixel Detector (GPD) procured by INFN-Pi (R. Bellazzini, as part of the ASI contribution). However, part of the activity (baking, filling, mixture checking, sealing and GPD environmental tests) will be performed at OXFORD Instruments International-OY (Finland, with participation of the Finnish team), while the fine tuning of the mixture will be done by Tsinghua University (Hua Feng, as part of the CNSA contribution). INFN-Pi will also procure the Back End Electronics and the Peltier cooler for the GPD. The HVPS and the LVPS are procured by SRC-PAS (S. Gburek). KTH (M. Pearce, as part of the SNSB contribution) will procure a low mass anticoincidence system should it be motivated by studies of the GPD background, including

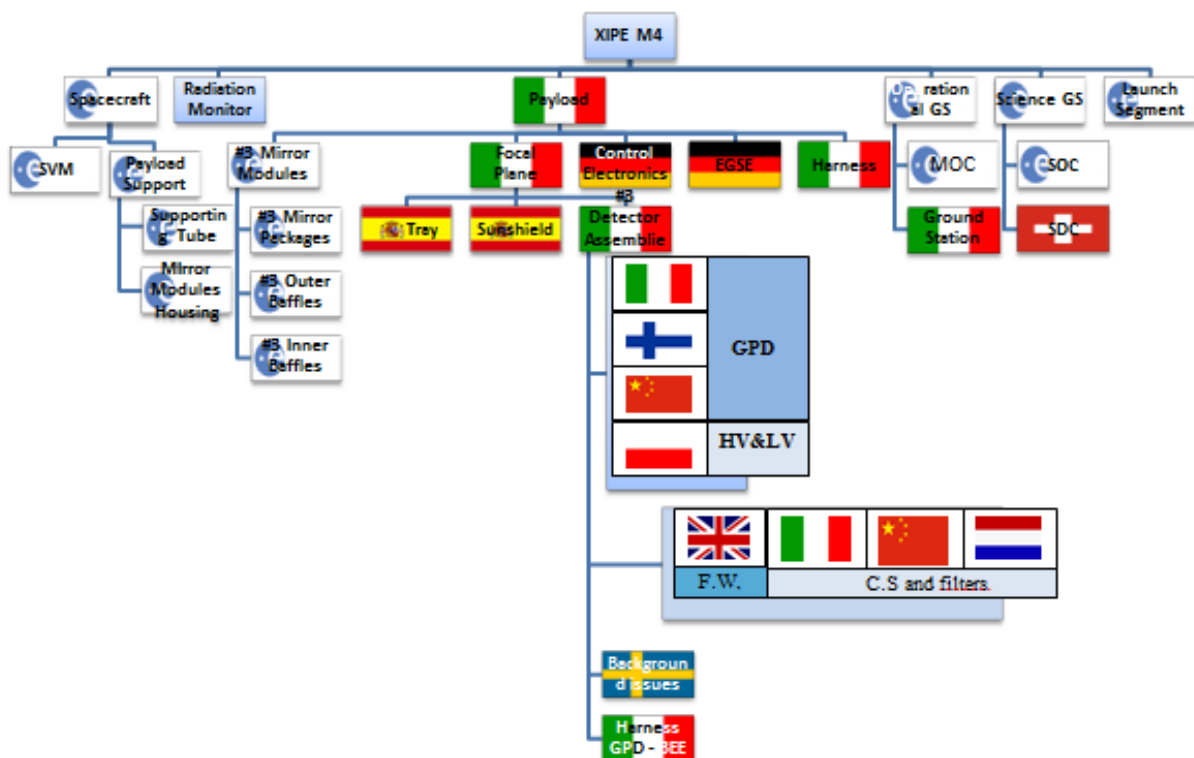


Figure 42 XIPE Product Tree.

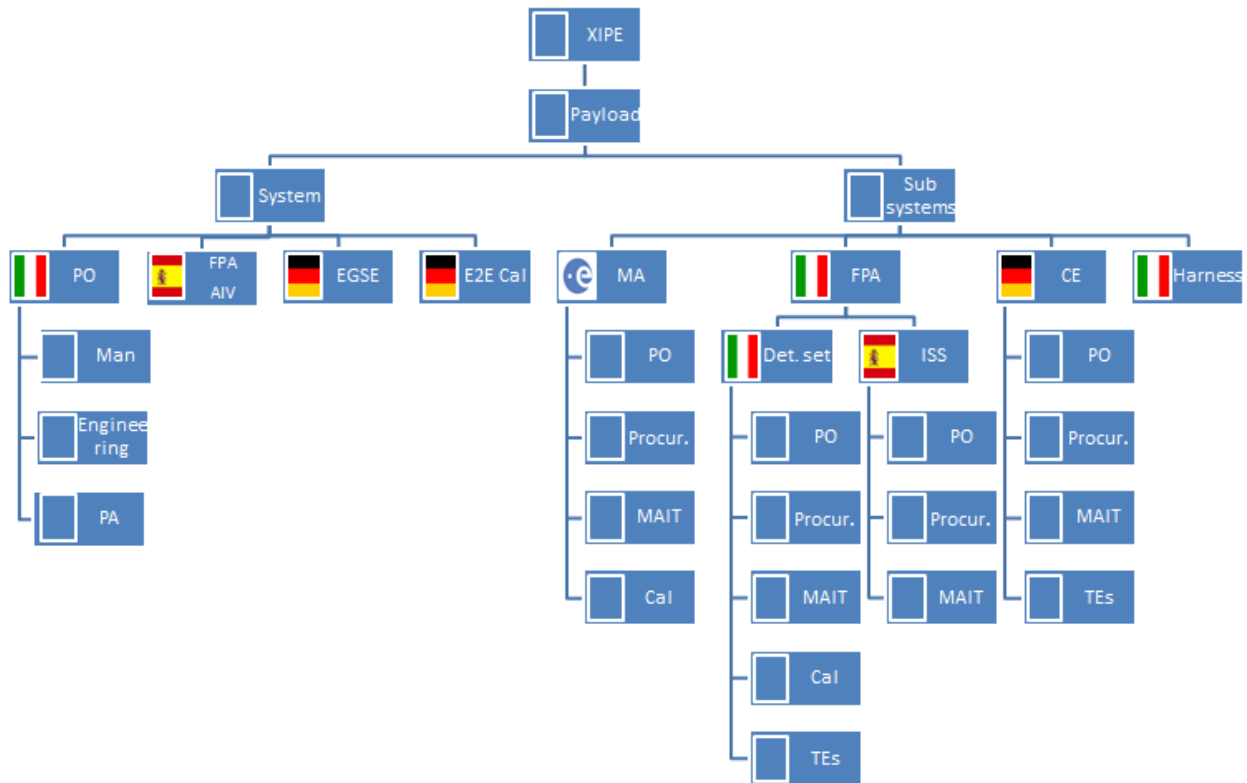


Figure 43 XIPE Work Break Down Structure

background rejection techniques and a possible high altitude balloon flight.

The calibration system includes a filter wheel (FW) designed and procured by MSSL (S. Zane, as UK SA contribution) and equipped with filters procured by Tsinghua University and with unpolarized and (Bragg-diffraction) polarized radioactive sources procured by IAPS/INAF (E. Del Monte, as part of the ASI contribution). However, the option to provide XIPE with a tagged source already developed by SRON (The Netherlands) as part of the payload of the JAXA satellite ASTRO-H and of ATHENA is under consideration (de Vries et al., 2012). This MXS (Modulated X-ray Source), placed on a fixed position, can, more efficiently, replace ^{55}Fe as a source for the Bragg polarizer and will be studied and customized for XIPE by Tsinghua University, as part of the CNSA contribution in collaboration with SRON.

The GPD cover box and the DS mechanical interface (for transport and AIV) is procured by IAPS/INAF (as part of ASI contribution).

The Control Electronics (CE), which manages the Payload, will be provided by University of Tuebingen (A. Santangelo, as part of DRL contribution), together with the Experiment Ground Support Equipment (EGSE). The science console will be procured by IAPS/INAF (Italy).

The focal plane mechanics (Instrument Support Structure, ISS and Sun Shield, SS) onto which the DSs are placed, is procured by University of Valencia (V. Reglero, as part of the CDTI/ES contribution).

6.3. Work Breakdown Structure

The payload WBS is shown in Figure 43. At Payload System level, the P.I. will assemble a Project Office (with both Industrial and institutes-funded engineers and scientists) for assuring the fulfilling of the scientific requirements within the timeline and cost cap of the M4 call. At Payload System level the AIV of the FPA will be done at INTA (M. D. Sabau for the CDTI/ES), the design, assembling and testing of the EGSE will be under the responsibility of University of Tuebingen for DRL/DE. The End-to-End Calibration, described in the P/L section, will be performed at the PANTER X-ray testing facility under responsibility of MPE. At the subsystem level, ESA will perform the MA activities with his PO (procurement, MAIT and stand-alone calibration), it will be advised in this task by the Telescope Advisory Group (TAG), led by G. Tagliaferri. The TAG will also have the capability to perform metrological and testing measurements on the mirrors developed to make sure that they meet the requirements. This was already done for XMM-Newton. The TAG will be also involved in the End-to-End calibration test at PANTER. FPA is under the responsibility of INFN-Pi including manufacturing the GPD and assembling the DSs. The GPD stand-alone calibration are performed at IAPS/INAF (F. Muleri). The ISS design procurement and MAIT will be performed by the University of Valencia and INTA. INFN-Pi will verify that the mechanical interface between ISS and DS are suitable for the AIV and the alignment with the Mirror Module. The

design, procurement and assembly of the CE which manages the different payload units will be done by the University of Tuebingen.

6.4. Payload Model Philosophy

The model philosophy and the relative levels of testing activities are different for each payload item.

(1) **Mirror Modules.** We foresee a Structural Thermal Model (STM), a Qualification Model (QM) with a subset of shells, three complete Flight Models (FMs) and one complete Flight Spare (FS). (2) MMS and TSS will have STM and Proto-flight models (PFMs). (3) **Detection Set.** For each GPD, BEE and FW we plan to produce a Structural Thermal Model, one QM, three FMs and one Flight Spare. **Control Electronics.** We foresee one STM, one Electrical Model (EM) and one PFM model. **ISS and Sun Shield.** We foresee one STM and one PFM model. We assume a STM and a proto-flight also for the SVM.

6.5. Environmental Tests

Environmental tests will include thermal, thermal cycling and vibration (sinusoidal and random) and acoustic tests. QMs will be tested at qualification level, while FMs and FSs will be tested at acceptance level. PFMs will be tested at a level typical for this model philosophy. We foresee to test each of these payload items separately. FPA will also be tested.

6.6. AIV

After the stand alone calibration of the GPDs at the IAPS/INAF polarized X-ray calibration facility and the provision of the FWs, the Detection Sets (DS) will be assembled and tested at the INFN-Pi facilities (where all the towers of FERMI/GLAST Large Area Telescopes were assembled). Each DS will be calibrated (End to-End) with the previously calibrated MM at PANTER. Then the DS will be integrated at INTA/Spain onto the ISS to make the FPA. The MM will be shipped to the ESA AIV facility. Finally, the CE will be integrated in the FPA. The FPA+CE will be subjected to environmental tests and then the whole assembly will be shipped to ESA. ESA will integrate the MM in the MMS to create the MA. Then the MA and the FPA will be integrated with the TSS (possibly designed by the company which provides the spacecraft, and therefore procured by ESA) and aligned to make the Payload Module (PM, see Figure 13). At this point the MA side of the PM will be accommodated into the ESA procured SVM by means of the MMS interface.

6.7. Schedule

XIPE is based on the heritage from many years of studies. Some of them were aimed at completing a phase A (POLARIX as ASI small mission) or an assessment phase (XPOL/IXO). The detectors are well known through years of testing and calibration activities. X-ray optics are designed based on well proven and controlled technologies. Therefore the study-phase (A/B1) for XIPE will be mostly spent to anticipate the implementation phase with a design activity which, using precedent studies, will be devoted to the optimization of some aspects of the mission (see Figure 44). Among these are the fine-tuning of the gas mixture, the evaluation of the option of using the MXS source in the filter wheel, and the assessing of the use of a low mass anticoincidence system to arrive at the required background rate needed for measuring the polarization of the most demanding sources, e.g. the extended faint molecular clouds in the crowded field of the Galactic Center. The requirements for the calibration facility (PANTER) and a preliminary calibration plan will be studied. The design of the DS will be an input for the design both of the ISS (mechanical) and of the CE (electrical). In turn the CE study will be an input for the study of the EGSE (both procured by DLR). The MMS and the ISS will be an input for the design of the TSS. Software requirements and a preliminary design for the final pipeline and for the inclusion of polarization in the standard software will be studied. The following phases (B2/C/D) will take advantage of the modularity, parallel development and construction of the MA, the FPA and the SVM included the TSS. The STM-EM need date is at K0+21 months. The End-to-End calibrations will last four months including the spare after that the FMs have been calibrated. The calibrated DSs will be sent to INTA/Spain for integration with the ISS and test (duration 3 months). The due date of the P/L FMs is at K0+57 months. The SVM integration, test and functional check will last 33 months. The Integration of the Payload Module with the Service Vehicle Module will take 1.5 months. At the end of phase B there will be the XIPE FM satellite thermal vacuum/thermal cycles at acceptance level.

6.8. Data managing

The scientific exploitation of XIPE data will be opened to the worldwide community and it will be conducted through a standard observatory management. XIPE observations will typically last from a fraction of a-day to one week. The total operative life of the mission will be three years.

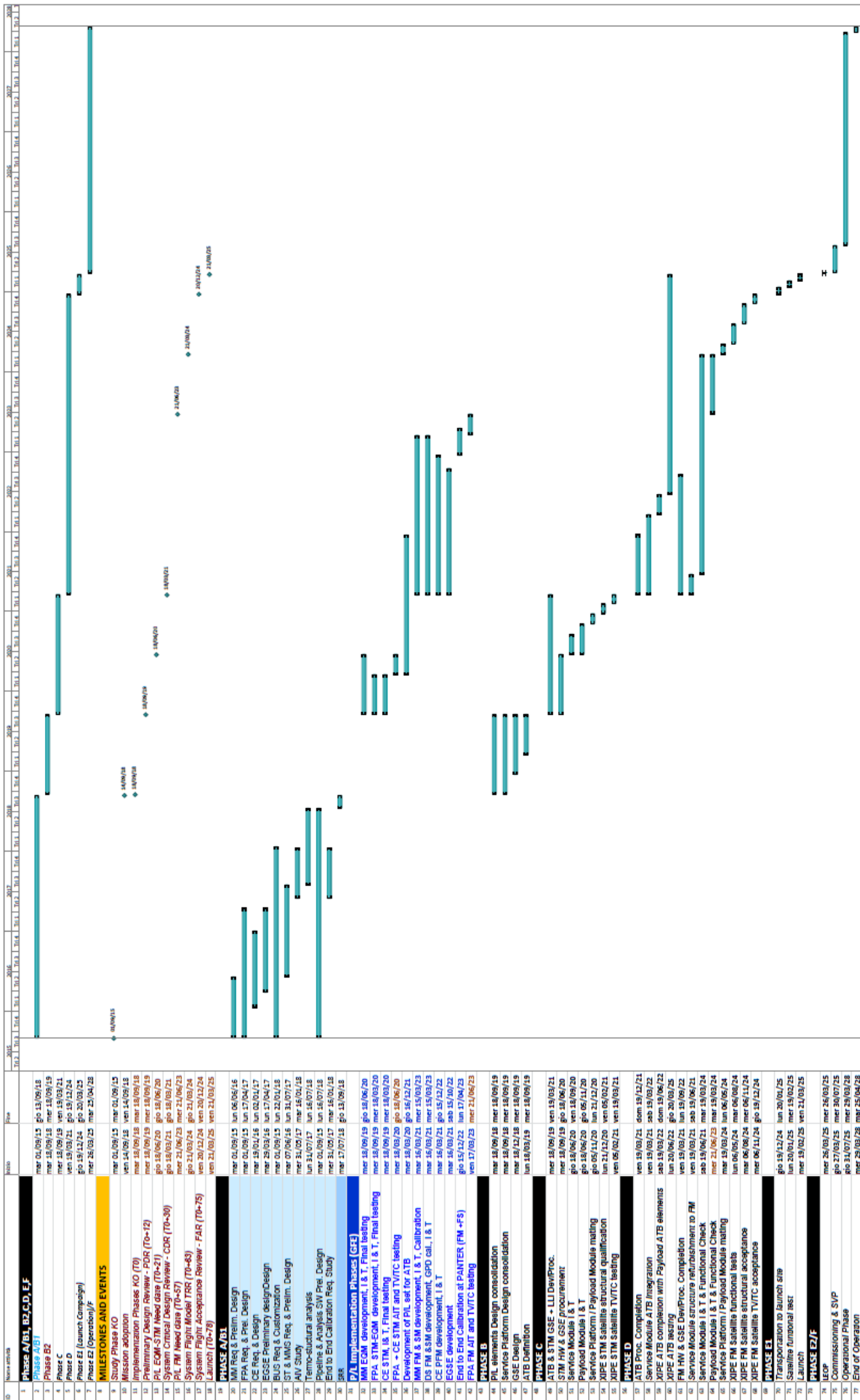


Figure 44 XIPe schedule.

After an initial Commissioning phase of one month, a Science Verification Phase (SVP) of three months will be followed by a Core Program (CP), planned by the team, which will cover about 3 months per year and by a Guest Observer Program (GOP) which will cover five months the first year and 9 months the following years. The GOP will be open worldwide on a competitive basis through an Announcement of Opportunity to be issued by ESA on yearly basis. Both the CP and GOP can include Target of Opportunity observations. A Guest Observer Handbook with documented software tools, based on open source, license-free codes and with all data needed for a full scientific exploitation will be made available to the Guest Observer (GO). CP data will be made public as soon as the on-flight calibrations will be released. GO data will remain proprietary for 1 year, before they will be put in an open access archive.

Table 12 Ground Segment & User Segment Funding Agencies.

Science Operation	Location	Funding Agency
Ground Station	Malindi	ASI/Italy
MOC	ESOC, Darmstadt/Germany	ESA
SOC	ESAC V. del Castillo/Spain	ESA
SDC	University of Geneva	SSO/Switzerland
Arch./GOP	c/o ESAC	ESA

The distributed data will be based on lists of qualified events including absorption point, time, energy and emission angle, plus the data on coverage, time windows and dead time. All the data, including those of the GOP, will undergo to Standard Scientific Analysis before their delivery to the observer. Standard Scientific Analysis (SSA) comprises: (1) pre-processing at ESOC; (2) Quick Look Analysis (QLA, orbital, daily-incremental, and complete observation) at ESAC; (3) Scientific Analysis (after the completion of a continuous observation of a given target, at ISDC); (4) archiving (ISDC) into the archive at ESAC, including products at their different steps (Telemetry, Level 1, Photon List, Products, the processing-log and the results of the QLA).

The data composed by the complete set of reduced data (photon list and auxiliary data) together with the other results of the SSA will then be made available to the owner of the data through a password-secured Web page for scientific exploitation and to the XIPE Team for QLA and calibration purposes only. After the period of proprietary data rights has expired, the SSA will be made publicly accessible through a Public Data Archive. The analysis of the tracks, the analysis of calibrations and the production of the response matrices of the instrument are the responsibility of the XIPE Team. The software required to reduce and analyze the XIPE data, including the QLA, will be developed and maintained by the XIPE team. ESAC/ESA will be responsible for the documentation and for distributing it to the Guest Observers. ESAC/ESA will also distribute to the GO a documented software-package that the GO will use under her/his own scientific responsibility to perform non-standard analysis (e.g. non-standard windowing of the data). The XIPE Off-line Scientific Analysis Software (XOSAS), based on the FTOOLS software and accessible by an open web interface, is developed, maintained and documented under the responsibility of the XIPE Team. New releases will be distributed periodically, together with the relevant calibration files. The data and the CALDB (Calibration Database) will be written and stored in the OGIP-FITS standard format and structure. The total amount of data expected to be archived is 60 terabyte. See Table 12 and Figure 45 for the organization of Ground Segment and User Segment.

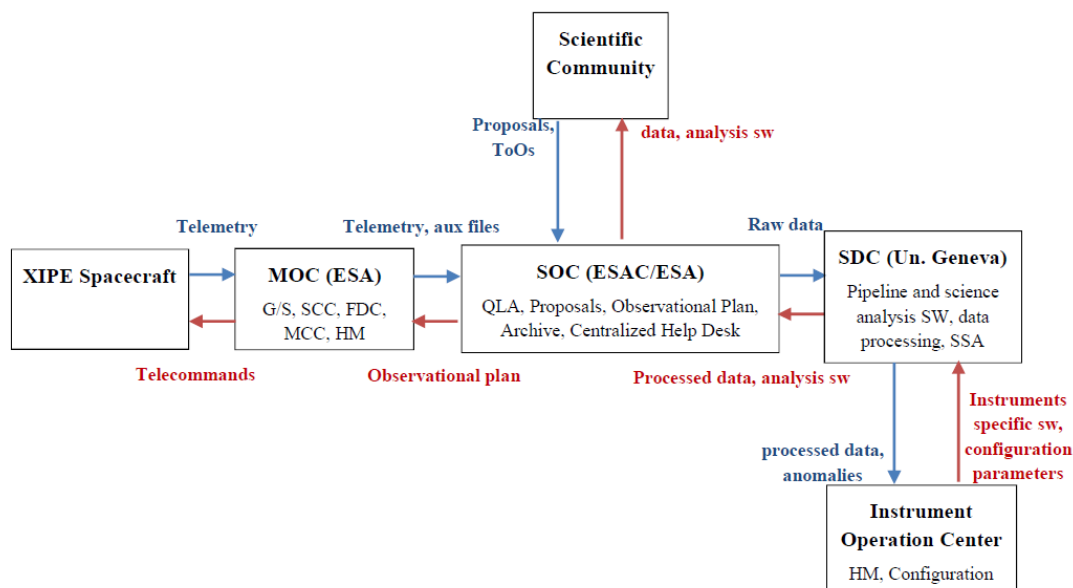


Figure 45 Block diagram of the Ground Segment and User Segment.

8. Annex

8.1. Bibliography

- Abdo A.A., et al. (2009) *Science*, 326, 1512.
- Agudo, I., et al. 2011, *ApJ*, 726, L13.
- Amato, E. (2014) *International Journal of Modern Physics D*, 23, 1430013.
- Antonucci, R. (1993), *ARA&A* 31, 473.
- Araya, M. & Cui W. (2010), *ApJ* 720, 20.
- Basso, S. et al., 2008, *Mem. S.A.It.* 79, 224.
- Basso, S. et al., 2011, *SPIE Proc.* 8147, 814709.
- Bellazzini, R., et al. (2006), *NIM Phys. Res. A* 566, 552.
- Bellazzini, R., et al. (2007), *NIM Phys. Res. A* 579, 853.
- Bellazzini, R., et al. (2010), in “X-ray polarimetry: A New Window in Astrophysics”, Cambridge University Press, 2010, pag. 269-274.
- Bleeker, J.A.M., et al. (2001) *A&A* 365, L225.
- Bucciantini, N. et al. (2005) *A&A* 443, 519.
- Bulgarelli A., et al. (2012) *A&A*, 238, 63.
- Bykov, A. M. et al (2009) *MNRAS*, 399, 1119.
- Bykov, A. M. et al (2011) *ApJ* 735:L40.
- Costa, E. et al. (2001) *Nature* 411,662.
- Costa, E. et al. (2010) *Exp Astron* 28:137.
- Celotti, A. & Matt, G. (1994), *MNRAS* 268, 451.
- Churazov et al. (2002), *MNRAS* 330, 817.
- Citterio et al.(1996), ‘Proc. of SPIE’, Vol. 2805, p. 56.
- Connors et al. (1980), *ApJ* 235, 224.
- Costa et al. (2001), *Nature* 411, 662.
- Costa et al. (2010, *Exp Astron* 28, 137.
- Cotroneo, V. et al., 2007, *SPIE Proc.* 6688, 66880U.
- de Vries, C. P. et al. 2012, *SPIE Proc.* 8443, 844353
- Dodson, R. et al. (2003) *MNRAS* 343, 116.
- Dovciak et al. (2008), *MNRAS* 391, 32.
- Emmanoulopoulos D. et al. (2014), *MNRAS*, 439, 3931.
- Eriksen, K. et al (2011) *ApJ*, 728, L28.
- Fabian A.C, et al. (2012), *MNRAS*, 419, 116.
- Fabiani, S. et al. (2012), *Proc. SPIE* 8443, 84431C.
- Fabiani, S. et al. (2014) *ApJSS* 212, 25.
- Fernandez, R. & Davis, S. W. (2011), *ApJ* 730, 131.
- Goosmann, R. & Matt, G. (2011), *MNRAS* 415, 3119.
- Götz D., et al., (2014) *MNRAS* 444, 2776.
- Gotthelf, E.V., et al. (2001) *ApJ* 552, L39.
- Haardt, F. & Matt, G. (1993), *MNRAS* 261, 346.
- Heisemberg, W. & Euler, H. (1936) *Z. Phys.* 98, 714
- Heyl, J. S. & Shaviv, N. J. (2000), *MNRAS* 311, 555.
- Hughes et al. (1984), *ApJ* 280, 255.
- Kaaret, P. (2004), *Nature* 427, 287.
- Koyama et al. (1996), *PASJ* 48, 249.
- Lai, D. & Ho, W. C. (2003), *Physical Review Letters* 91, 071101.
- Lazzarotto, F., et al. (2010), in “X-ray polarimetry: A New Window in Astrophysics”, Cambridge University Press, 2010, pag. 79-82.
- Long et al. (1979), *ApJ* 232, L107.
- Mc Namara, A.L. et al. (2008), *MNRAS* 386, 2167..
- Mc Namara, A.L., Kuncic, Z., & Wu, K. 2009, *MNRAS*, 395, 1507.
- Maccione et al. (2008), *Phys. Rev. D* 78(10), 103003.
- Marin, F. & Goosmann, R. W. (2011), *Proc. of the Annual meeting of the French Society of A&A*, p.597, arXiv:1204.0940.
- Marin, F. et al. 2012b, *MNRAS*, 426, L101.
- Marscher, A.P. & Gear W.K. (1984) *ApJ*, 298, 11.
- Marscher, A.P. et al. (2008) *Nature*, 452, 966.

Matt, G. (2004), A&A 423, 495..
Meszaros, et al. (1988), ApJ 324, 1056.
Mirabel, I. F. & Rodriguez, L. F. (1994), Nature 371, 46.
Muleri, F. et al. (2007), 'Proc. of SPIE', Vol. 6686, p. 668610.
Muleri, F. et al. (2008), NIM Phys. Res. A 584, 149.
Muleri, F. et al. (2010), NIM Phys. Res. A 620, 285–293.
Muleri, F. et al. (2012), Proc. of SPIE, 8843, 88430L.
Murakami et al.(2001), ApJ 550, 297.
Nakamura, Y. & Shibata, S. (2007), MNRAS 381, 1489.
Pareschi, G. et al., 2004, SPIE Proc. 5488.
Parker M., et al. (2014), MNRAS, 443, 1723.
Perna, R. et al. (2014), ApJ, 748, 116.
Ponti, G., et al. (2013), ASSP, 34, 331.
Porth, O. et al. (2014), MNRAS, 438, 278.
Poutanen, J. (1994), ApJS 92, 607.
Poutanen, J. & Vilhu, O. (1993), A&A 275, 337.
Reis R.C. & Miller J.M, (2013), ApJ, 769, L7.
Reynoso, et al. (2013) Astron. J. 145, 1.
Ryu et al. (2009) PASJ 61, 751.
Ryu et al. (2013) PASJ 65, 33.
Sanchez Almeida, J. & Martinez Pillet, V. (1993), Appl. Opt. 32, 4231.
Schnittman, J. D. & Krolik, J. H. (2010), ApJ 712, 908.
Seward, F.D. (1990) ApJS 73, 781.
Soffitta, P. et al. (2012), Proc. of SPIE 8443, 84431F
Soffitta, P. et al. (2013), NIMPA 700, 99.
Spiga, D. et al (2010), *X-ray tests at PANTER on the TDM2 optic prototype for the New Hard X-ray Mission*, INAF/OAB internal report 2010/06.
Spiga, D. et al. (2014), Exp. Astron. 37, 37
Spiga, D. 2011, A&A, 529, A18.
Stark, R. F. & Connors, P. A. (1977), Nature 266, 429.
Sunyaev et al. (1993),ApJ 407, 606.
Tamagawa, T. et al. NIMPA 608, 390.
Taverna, R. et al. (2014) MNRAS 438, 1686.
van Adelsberg & M., Lai, D. 2006, MNRAS 373, 1495.
Viironen, K. & Poutanen, J. (2004), A&A 426, 985.
Vink, J. (2012) A&A Rev. 20, 49.
Volpi et al. (2008), in 'Polarimetry days in Rome: Crab status, theory and prospects'.
Warner, B. (1995), Ap&SS 226, 187–211.
Weisskopf M.C., et al. (1977) ApJ, 215, L65.
Weisskopf et al. (1978), ApJ 220, L117.
Weisskopf et al. (2000), ApJ 536, L81.
Weisskopf et al. (2010), in Proceedings of the SPIE, 7732, 77320E.
Yonetoku et al. (2011), ApJ 743, L30.
Zajczyk, A. et al. (2012) A&A 542, 12.

8.5. List of acronyms

ACS	Attitude Control Subsystem
AGN	Active Galactic Nucleus
AIV	Assembly Integration and Verification
AIV&T	Assembly Integration, Verification and Test
ALP	Axion-like particles
AMA	Absolute Measurement Accuracy
aMSPs	Accretion-powered millisecond pulsars
AOO	Announcement Of Opportunity
APD	Absolute Pointing Drift
APE	Absolute Pointing Error
ASI	Agenzia Spaziale Italiana – Italian Space Agency
ASIC	Application Specific Integrated Circuit
AVUM	Attitude & Vernier Upper Module
AXP	Anomalous X-ray Pulsar
BEE	Back End Electronics
BH	Black Hole
BOL	Beginning of Life
CALDB	Calibration Database
CCD	Charge Coupled Device
CDMU	Command & Data Management Unit
CE	Control Electronics
CMOS	Complementary metal–oxide–semiconductor
COP	Commissioning Phase
CP	Core Program
CR	Compton Reflection
CS	Calibration Source
DFAC	Drag Free and Altitude Control
D/L	Down Link
DME	Dimethyl ether
DMM	Design Maturity Margin
DS	Detection Set
DSA	Diffusive shock acceleration
DSMI	Detection Set Mounting Interface
EGSE	Electrical Ground Support Equipment
EM	Electrical Model
EOP	End of Mission Phase
EOL	End of Life
EPS	Electrical Power System
EQM	Engineering Qualification Model
ESA	European Space Agency
FDIR	Fault Detection Isolation and Recovery
FEE	Front End Electronics
FEM	Finite Element Method
FM	Flight Models
FOV	Field of View
FPA	Focal Plane Assembly
FS	Flight Spare
FW	Filter Wheel
GEM	Gas Electron Multiplier
GEVS	General Environmental Verification and Standard
GO	Guest Observer
GOP	Guest Observer Program
GPD	Gas Pixel Detector
GPS	Global Positioning System
GR	General Relativity
GRB	Gamma-Ray Burst
G/S	Ground Station

HEW	Half Energy Width
HIMAC	Heavy Ions Medical Accelerator in Chiba
HK	House Keeping
HPTM	High priority telemetry
HV	High Voltage
HVPS	High Voltage Power Supply
IC	Inverse Compton
IR	Infrared
ISS	Instruments Supporting Structure
LEO	Low-Earth Orbit
LEOP	Launch and Early Orbit Operations
LOS	Line Of Sight
LV	Launch Vehicle
LVPS	Low Voltage Power Supply
MA	Mirror Assembly
MAIT	Manufacturing Assembly Integration and Test
mCV	Magnetic cataclysmic variable
MDP	Minimum Detectable Polarization
MFA	Magnetic Field Amplification
MHD	Magnetohydrodynamics
MM	Mirror Module
MMS	Mirror Mounting Structure
MOC	Mission Operations Center
MOP	Measurement Phase
MPPT	Maximum Power Point Tracking system
μ QSO	Microquasars
MSA	Member State Agency
MTL	Mission TimeLine
MXS	Modulated X-ray Source
NL-DSA	Non-Linear Diffusive Shock Acceleration
NS	Neutron Star
OBDH	On Board Data Handling
OBMF	Board Monitoring Function
OBSW	On-Board Software
OBT	On-board time counter
PCDU	Power Conditioning and Distribution Unit
PFM	Proto-flight model
PI	Principal Investigator
P/L	Payload
PM	Payload Module
PO	Project Office
POP	Payload Calibration
PSF	Point Spread Function
PWN	Pulsar Wind Nebulae
QED	Quantum-electrodynamic
QLA	Quick Look Analysis
QM	Qualification Model
RCS	Resonant cyclotron (up-)scattering
RF	Radio Frequency
RFDN	Radio Frequency Distribution Network.
ROI	Region of Interest
RPE	Relative Pointing Error
SA	Solar Array
SAA	South Atlantic Anomaly
S/C	Spacecraft
SDC	Science Data Center
SED	Spectral Energy Distribution
SGR	Soft-Gamma Repeater
SMU	Satellite Management Unit

SNR	Supernova Remnant
SOC	Science Operation Center
SP	Solar Panels
SS	Sun Shield
S/S	Space Segment
SSA	Standard Scientific Analysis
SSC	Synchrotron Self-Compton
STM	Structural Thermal Model
SVM	Service Vehicle Module
SVP	Science Verification Phase
SW	Software
TAG	Telescope Advisory Group
TC	Telecommand
TM	Telemetry
TOO	Target of Opportunity
TRL	Technology Readiness Level
TSS	Telescope Support Structure
TT&C	Telemetry Tracking and Command
TWTA	Traveling Wave Tube Amplifiers
UART	Universal Asynchronous Receiver/Transmitter
U/L	Up Link
UT	Universal Time
UV	Ultraviolet
WBS	Work Breakdown Structure
WD	White Dwarf
XOSAS	XIPE Off-line Scientific Analysis Software
XRN	X-ray reflection nebulae



QUOTATION

Quote # ML-QT-022/14
Issue 2

Page 1 of 5

Media Lario Technologies
Località Pascolo
23842 Bosisio Parini (LC) – Italy

Tel.: +39.031.867139/111
Fax: +39.031.876595
E-mail: sales@media-lario.com

C.F./P.I.: IT01956450132
Reg. Imp. Lecco: 29896
R.E.A. Lecco: 230.070
Cap. Soc.: 260.000,00 Euro i.v.

Quote Number:	ML-QT-022/14 – issue 2
Quote date:	December 29, 2014
Quote Expiration date:	January 31, 2015
Quote originator:	Mara Bello
Customer:	INAF - OAB
Delivery:	To be agreed with the customer
Payment terms:	To be agreed with the customer
Shipped via:	To be agreed with the customer
Delivery terms:	Ex works (Bosisio Parini, Italy)
Terms quoted are based on Inco Terms 2000 Edition	

To the attention of Prof. G. Tagliaferri
cc: Giuseppe Valsecchi, Giovanni Bianucci (Media Lario Technologies)

With reference to your inquiry dated November 4, 2014 and following verbal agreements with Giuseppe Valsecchi, we are pleased to provide you with the ROM quotation for the manufacturing of 1 EQM and 4 Mirror Modules for a ESA mission of X polarimetry.

Each Mirror Module will consists of 27 Wolter I grazing-incidence mirrors which will be nested in a coaxial and cofocal configuration and will be bonded both on the entrance and exit aperture on two spiders. The mirrors will be produced via Nickel eforming process while the optical surface will be coated with Ir/C.

The HEW for each Mirror Module will be of 20 arcsec in the whole range 2-10 keV with the goal of 15 arcsec at 3 keV.

The EQM will be composed of 5 flight quality mirror shells and 22 dummy shells.

Item No.	Qty.	Description	Unit ROM Price (Euro)	Extended ROM Price (Euro)
1	1	EQM and 4 Mirror Modules for X polarimetry: <ul style="list-style-type: none"> – Manufacturing of the mandrels required for the manufacturing of the mirror shells; – Manufacturing of the required jigs and tools for the production of the mirrors, handling and integration; – Upgrading of the facilities required for the production and integration of the mirror modules; – Production of 1 EQM with relevant transport container; – Optical tests on EQM performed at the Optical Bench at our premises – Thermal-vacuum and vibration tests on EQM; – Production of 4 Flight Mirror Modules with relevant transport containers; – Optical tests on each Mirror Module performed at the Optical Bench at our premises – Thermal-vacuum and vibration tests on each Mirror Module – Project documentation 	7,200,000.00	7,200,000.00
Total				7,200,000.00

Type of Price:

- All the prices included in this document are ROM Prices, VAT excluded.



QUOTATION

Quote # ML-QT-022/14
Issue 2

Page 2 of 5

Delivery date and terms:

- Delivery date: to be agreed with the customer.
- Delivery terms: Ex-works, Bosisio Parini, Italy.

We trust that our quotation meets your expectations. Do not hesitate to contact us for any clarifications you may require.

Kind regards,

A handwritten signature in blue ink that reads 'Mara Bello'.

Mara Bello
Marketing

Media Lario S.r.l.
e-mail: mara.bello@media-lario.com
Telephone: +39.031.867126
Mobile: +39.347.1141804



QUOTATION

Quote # ML-QT-022/14
Issue 2

Page 4 of 5

5. SHIPPING. Unless otherwise agreed to in writing by Seller, delivery shall be EXW. Seller's Factory.
In all cases, title and risk of loss or damage shall pass to Buyer on Seller's delivery of the Goods in good condition to a carrier at Seller's factory. It shall be Buyer's responsibility to obtain proper insurance coverage and to file any claims therefore with the carrier.
6. DELIVERY DATE: EXCUSABLE DELAY. Shipping dates are approximate only and are subject to change. Seller shall not be liable for delays in delivery or failure to manufacture or deliver the Goods due to acts of God, acts of Buyer, acts of civil or military authorities, judicial orders, embargoes, fires, floods, accidents, epidemics, wars, insurrections, riots, strikes, delays in transportation or other causes beyond Seller's reasonable control, including but not limited to, the inability to obtain necessary labor, materials, component parts, or manufacturing facilities.
7. CUSTOMER CHANGES, TERMINATION, DELAYS AND RETURNS. Orders for Goods or Services may be changed or terminated by Buyer only with the specific approval of Seller, and shall be subject to change or termination charges which shall include, among other things, compensation for specific expenses and commitments already incurred or made in connection with the orders and a reasonable allowance for overhead, general and administrative expenses and profit, determined in accordance with Seller's standard accounting practices. The following minimum cancellation charges will apply to system orders cancelled prior to their scheduled shipment date: (1.) ninety percent (90%) prior to 120 days of the originally scheduled ship date; (2.) ten percent (10%) beyond 120 days of the originally scheduled ship date. Change orders may also necessitate a revision in shipment dates and create additional costs to Seller for which such compensation will be due to Seller.
If Buyer causes a delay in contract completion or requests that shipment be delayed, Seller shall have the right to submit invoices for Goods after giving notice to Buyer that work has been performed and parts for use in completion of the contract have been purchased and/or commitments made. Such invoices shall be due and payable within thirty (30) days from invoice date. Risk of loss or damage shall pass to Buyer on the date such notice is given, and Buyer shall pay all necessary storage charges incurred thereafter. Seller shall be equitably compensated for any additional costs it may incur by reason of such delay.
Returns of "unused" purchased spare parts for credit are allowed only within 30 calendar days of shipment; and upon receiving prior approval by Media Lario S.r.l. as evidenced by a valid Return Materials Authorization Number. Spare parts returns are subject 20 % restocking fee.
Any payments made by Buyer to Seller upon acceptance of an order by Seller may be applied by Seller to the cancellation charges payable by Buyer.
Buyer understands and agrees that the cancellation charges are reasonable in light of the anticipated or actual harm to Seller, the difficulties of proof of loss and the inconvenience to Seller of otherwise being reasonably compensated for its efforts as a result of cancellation of any purchase order for Goods. Seller acknowledges and agrees that any cancellation charges paid by Buyer will be Seller's sole and exclusive remedy for cancellation of a purchase order.
8. PATENT INFRINGEMENT – INDEMNIFICATION. Seller's liability for Patent infringement is limited to the Purchase price of the infringing product.
9. PACKAGING. Seller will provide commercial packaging adequate under normal conditions to protect the Goods in shipment and to identify the contents. Should Buyer request special packaging; it shall be at Buyer's expense.
10. MATERIAL FURNISHED BY BUYER. Seller assumes no responsibility for parts and subassemblies furnished by Buyer or its agents.
11. INSTALLATION. Buyer shall accept delivery and will, at Buyer's sole expense, provide facilities for installation of the Goods which comply in all respects with Seller's instructions, all governmental laws, codes, regulations, orders and the like and with all agreements and understandings with labor unions.
12. LIMITED WARRANTY. See Quote text. The warranties of seller set forth in this paragraph 12 are in lieu of, and buyer hereby waives, the implied warranties of merchantability and fitness for a particular purpose and all other warranties of seller, express, statutory or implied, arising out of or in connection with the sale, resale, and purchase of seller's goods, or the use, repair or performance thereof, or the course of dealing or performance under any agreement between buyer and seller to which these terms and conditions apply.
13. LIMITATION OF LIABILITY. Seller's liability for any claim of any kind, including negligence, for loss or damages arising out of, in connection with or resulting from the manufacture, sale, delivery, resale, repair or use of any Goods or Services covered by or furnished under these Terms and Conditions, or Seller's breach of any of these Terms and Conditions, shall in no case exceed the lesser of: (i) the cost of correcting any non-conformities in the Goods or Services, or (ii) the cost of replacing any non-conforming Goods with conforming ones. In the event Seller fails to manufacture or deliver the Goods or Services subject to these Terms and Conditions, Seller's exclusive liability and Buyer's exclusive remedy shall be release of Buyer from the obligation to pay the applicable purchase price for such Goods or Services. Except as provided expressly in paragraphs 8, 12 and 13 hereof, seller shall not be liable to buyer, to buyer's customers or to any other person. Buyer acknowledges and agrees that the amounts which seller charges for the goods and services do not include any consideration for assumption by seller of the risk of consequential or incidental damages which may arise in connection with the use of seller's goods by buyer or buyer's customers. Buyer agrees that seller shall not in any event be liable for any incidental, special, indirect, or consequential damages, including without limitation personal injury or loss of profit, plant, equipment, information, property or production, arising from the manufacture, sale, purchase, resale, repair or use of seller's goods and from any promise or offer to sell, purchase or repair such goods, regardless of whether seller has been informed of the possibility of such damages. This limitation of liability will apply regardless of the form of action, whether in contract or tort, including negligence. Buyer agrees that this limitation of damages is reasonable and will not cause it to lose any expected benefits, rights or remedies under any agreement for the sale of goods.
14. INDEMNIFICATION OF BUYER. Seller agrees to indemnify Buyer against any claims against Buyer for loss, liability or damages in respect to personal injury or loss of or damage to tangible property, but not otherwise, up to the limits of Seller's insurance policy as a result of any negligent act or omission of Seller's employees during any work at Buyer's facilities. Seller's indemnification obligations under this Paragraph 14 shall apply only if Buyer has provided notice to Seller, in writing, of any such claims within ten (10) calendar days after the date on which Buyer first receives any notice, written or oral, that such claims may be asserted against Buyer. Upon receipt of any such written notice from Buyer, Seller or its representative shall have the right to defend any such claims and/or to participate in any discussion or agreements entered into by Buyer to settle same. Seller shall have the right to refuse to settle or compromise any such claims, or in its sole judgment, to defend Buyer against any lawsuit at Seller's expense. Seller shall not be bound by any judgments or settlement agreements to which it



QUOTATION

Quote # ML-QT-022/14
Issue 2

Page 5 of 5

has not been a party or to which it has not consented in writing. The above constitutes the full extent of Seller's indemnification obligation, express or implied, to Buyer.

15. INDEMNIFICATION OF SELLER IN CONNECTION WITH BUYER'S ACCEPTANCE AT SELLER'S FACTORY. Buyer shall take such steps as may be reasonably necessary to prevent personal injury or property damage during any activity hereunder that may be performed by any employees, agents, or subcontractors of Buyer during Buyer's visits to Seller's factory. Buyer shall indemnify and hold harmless Seller from and against all claims for loss, liability, and damages arising from or caused directly or indirectly by any negligent act or omission of such agents, employees, or subcontractors of Buyer, and Buyer shall maintain insurance against public liability and personal injury or property damage and for employee's liability and compensation such as will protect Seller against the aforementioned risks and against any claims under any Worker's Compensation and Occupational Health and Safety Acts.
16. PROPRIETARY RIGHTS. Buyer agrees that Seller retains proprietary rights in and to all product specifications, designs, engineering details, discoveries, inventions, patents, copyrights, trademarks, trade secrets and other proprietary rights relating to the Goods (other than software marketed by Seller under a licensing agreement with its owner or permitted licensor). The Goods are offered for sale and are sold by Seller subject in every case to the condition that such sale does not convey any license, expressly or by implication, estoppel or otherwise, to manufacture, duplicate or otherwise copy or reproduce any of the Goods.
17. ASSIGNMENT. Except as herein expressly provided to the contrary, the sale of Goods and Services is to Buyer and not for the benefit of any other party. Any attempted assignment by Buyer of Buyer's purchase agreement or of any rights arising under these Terms and Conditions without the written consent of Seller shall be void and of no effect whatsoever.
18. DATA. In the event data is supplied by Seller, it shall be conclusively presumed to pertain to products, components, or processes developed at Seller's own expense and no rights in such data or in any inventions, patents, or copyrights related thereto shall pass to Buyer. If Buyer furnishes data, no rights therein will pass to Seller, provided, however, that Seller may copy and use such data to the extent necessary to furnish the Goods or Services called for hereunder.
19. INVALIDITY OF PROVISIONS. If any, all, or any portion of one or more of these Terms and Conditions shall be declared invalid by any court of law, such part of such term or terms shall be considered deleted from the contract for the sale of Goods or Services and the remaining portion shall be unaffected and shall remain in full force and effect.
20. GOVERNING LAW. Any agreement to which these Terms and Conditions apply shall be governed by, and construed in accordance with, the substantive laws of Italy, without giving effect to the rules of conflicts of law. The United Nations Convention on Contracts for the International Sale of Goods shall not apply in any manner to any such agreement. Any claim, action or legal proceeding arising under this Agreement shall be brought only in a court of competent jurisdiction in Milan and the parties hereby consent to the exclusive jurisdiction and venue of such courts
21. DISPUTES. Any dispute which arises with respect to the sale of Goods or Services or under these Terms and Conditions which is not resolved by the parties within ninety (90) days after the original written notice of dispute is first given shall thereafter be resolved exclusively by binding arbitration in Italy in accordance with the Commercial Rules of the American Arbitration Association, and judgment upon the award entered by the arbitrators may be entered in any court having jurisdiction thereof. Each party shall bear its own costs and expenses in any such arbitration proceeding. If any judicial proceedings shall be commenced to enforce any arbitral award issued pursuant to this Paragraph 21, the prevailing party in such proceeding shall be entitled to recover from the other party the reasonable attorneys' fees, costs and expenses incurred by the prevailing party in connection with such proceedings.
22. NO WAIVER. No waiver of these Terms and Conditions shall be effective unless made in writing. No waiver of any breach of these Terms and Conditions shall constitute a waiver of any subsequent breach of the same or of any other provision of these Terms and Conditions.
23. EXPORT. Seller shall disclose information to be disclosed to Buyer and deliver materials to be delivered to Buyer only in compliance with the export control laws and regulations of the exporting country in effect from time to time. Buyer agrees to abide by any limitation of disclosure placed on information revealed to it, and by any limitation of material deliveries that may be placed thereon as a result of such regulations. Buyer shall provide Seller with all documentation and data necessary or desirable for compliance with all such laws and regulations. In particular, before Buyer purchases Goods that Buyer intends to export, Buyer will so notify Seller and will identify the country (ies) of intended destination. Buyer agrees to hold Seller harmless from any liability arising from the failure of Buyer to comply with such laws and regulations, or with the provisions of this paragraph.
24. COMPLIANCE WITH LAWS. Unless specifically stated in Seller's quotation or acceptance of Buyer's purchase order, Seller does not represent that the Goods and Services meet any state or laws of any country, ordinances, regulations, and the like. Compliance with such requirements is the responsibility of Buyer.